Master's Thesis

Bistable SiC MEMS membranes: The potential for medical applications

to obtain the degree
Master of Science (Diplom Ingenieur)
at the Institute of Sensor- und Actuator Systems
and the Institute of Solid State Physics
at the TU Wien, Vienna

under the supervision of:

Univ.Prof. Dipl.-Phys. Dr.rer.nat. Ulrich SCHMID
Institute for Sensor- und Actuator Systems, TU Wien

and co-supervised by:

Univ.Ass. DI Dr.techn. Georg PFUSTERSCHMIED
Institute for Sensor- und Actuator Systems, TU Wien

Ao.Univ.Prof. DI Dr. Heinz WANZENBÖCK
Institute of Solid State Physics, TU Wien

Univ.Ass. Dipl.-Phys. Dr.techn. Michael SCHNEIDER
Institute for Sensor- und Actuator Systems, TU Wien

by

Philipp Moll, BSc
Matr.-Nr.: 01225247

Vienna, January, 2020

Danksagung

Ich möchte an dieser Stelle die Gelegenheit nutzen, mich mit den folgenden Zeilen bei all jenen zu bedanken, die es mir ermöglicht haben, mein Studium mit dieser Masterarbeit abzuschließen.

Neben der emotionalen und finanziellen Unterstützung durch meine Familie und Freunde, gilt ganz besonderer Dank meinen Eltern. Die beiden haben mich immer mit großer Zuversicht auf meinem akademischen Werdegang begleitet und mir durch einen gestärkten Rücken das Studium maßgeblich erleichtert.

Nach über einem Jahr Zusammenarbeit möchte ich Dr. Georg Pfusterschmied für seine hervorragende Betreuung der Diplomarbeit meinen Dank aussprechen. Nicht nur das fachliche Know-how ist zu erwähnen, sondern auch besonders seine Geduld, sein Engagement zum Thema und die Bereitschaft die Arbeit inhaltlich durch eigene Gedanken immer weiter zu verbessern. Danke Georg!

Einen weiteren wichtigen Beitrag leistete Dr. Heinz Wanzenböck mit der Betreuung des Zellexperiments, welches ohne die Räumlichkeiten, die richtige Methodik und die fachliche Kompetenz des Festkörperinstituts, so hätte nicht stattfinden können. Auch Sebastian Knafl soll hier erwähnt werden. Durch seine Beratung und Begleitung durch das Zellexperiment, konnten tolle Ergebnisse generiert werden.

Das gilt auch für Dr. Michael Schneider und DI Manuel Dorfmeister die mir bei persönlichen und fachlichen Fragen immer zur Seite gestanden sind und mit kritischen Kommentaren neue Perspektiven zur Thematik offenbart haben. Besonders Dr. Schneider konnte mir dabei helfen aus den oft unüberschaubaren Teilgebieten und Fragestellungen, welche die Masterarbeit mit sich brachte, einen besseren Überblick zu verschaffen und die zentralen Fragestellungen der Arbeit zu identifizieren.

Zu guter Letzt darf ich auch dem Institut für Sensor- und Aktuatorsysteme meinen Dank aussprechen. Durch die Mithilfe der ISAS Techniker und die organisatorische Unterstützung und reibungslose Abwicklung durch das Sekretariat, konnte ich mich voll und ganz auf die Umsetzung meiner Aufgaben konzentrieren.
Selbstverständlich darf an dieser Stelle Univ.Prof. Dr. Ulrich Schmid nicht vergessen werden. Dr. Schmid, als Kopf des MST Teams und Institutsvorstand, hat es mir ermöglicht meine eigenen Ideen im Rahmen einer Diplomarbeit zu erforschen und umzusetzen. In immer wieder sattfindenden Treffen hat sich Dr. Schmid die Zeit genommen auf meine bisherige Arbeit und Ergebnisse einzugehen und den weiteren Verlauf maßgeblich mit Ideen und Gedanken positiv zu beeinflussen. Diese Treffen sind in meinen Augen keineswegs selbstverständlich, weshalb ich mich hier ganz besonders bedanken will.

Abstract

The aim of this thesis is to fabricate and characterize silicon carbide coated and hence, biocompatible, bistable membranes, which are controlled by integrated piezoelectric thin film actuators. Due to different membrane configurations and electrical excitation signals it is possible to switch the buckled membrane from one stable state to the other and *vice versa*.

The first part of this work concentrates on the stress behaviour of a-SiC:H thin layers. By coating the top surface of the membranes, biocompatibility to any human tissue is ensured with an electrically insulating material. Silicon carbide as thin layer can be deposited by PECVD in different compositions of silicon and carbon, which has a huge impact on the thickness and layer stress of the resulting thin layer. However, not only the stress behaviour of a-SiC:H layers will be characterised, but also its biocompatibility and the likeliness of CaCo-2 cells attaching to the substrate's surface. Epithelial cells of the small intestine were used to characterise the adhesiveness and proliferation on a-SiC:H layers, deposited with different gas flow ratios of silane and methane. Silicon is known as a hydrophile material, while SiC with an increasing amount of carbon gets more hydrophobic, which tends to directly influence the attachment behaviour of cells. The more hydrophile a surface is, the more likely is the attachment of a cell. Living mammalian cells adhere especially well to surfaces, whose electrochemical potential is similar to their own. Since carbon fits this aspect very well, carbon-rich surfaces are preferred with respect to the attachment behaviour of such cells, which stands in contradiction with the hydrophobicity of SiC substrates with high contents of carbon.
This work found a balanced composition of silicon and carbon in an a-SiC:H thin layer, where cells adhere best, and compares the stress behaviour of different SiC composed layers with the proliferation and adhesiveness of cells. For this purpose, 50.000 CaCo-2 cells were placed on 13 different processed 6 x 6 mm^2 a-SiC:H coated silicon samples. To get a broader result, each of the 13 samples was produced six times, whereby every sample was either pre-treated in an O_2-plasma or additionally coated with collagen or Poly-D-Lysine in order to create different growing surroundings, while the same procedures for cell planting, feeding, growing and measuring were applied.

After finding the right deposition conditions for a preferably low stress state, the SiC layer got deposited on several different diaphragms, which were produced with diameters from 600 – 800 µm. The fabrication process starts with an SOI-wafer as base material, where different thin film layers were subsequently deposited. These layers were treated with several etching steps, until the final structure of the membrane was created. Through a careful adjustment of the layer stress of all other thin films involved, the diaphragm buckled randomly in one of its two stable states. As piezoelectric layer aluminium nitride (AlN) was used as the material of choice.
Secondly, the vibrational behaviour of bistable membranes under the load of an electrical signal was measured, as well as the directly related characteristic resonance frequencies, to predict the switching behaviour of such biocompatible diaphragms in air and different fluids. These measurements were conducted with a Laser-Doppler-Vibrometer, a White-Light-Interferometer, wafer-bow-measurements, contact angle measurements and an oscilloscope.

In this thesis, the fabrication process, the measurements approach as well as the results of the switching behaviour of bistable membranes in both air and fluids are described and discussed. Finally, the correlation of living cells growing on substrates of different Si-C compositions and its correlation to the mechanical stress state will be presented.

Zusammenfassung

Die folgende Arbeit beschreibt die Herstellung und Charakterisierung von biokompatiblen bistabilen Membranen, deren Schwingungs- und Schaltverhalten durch integrierte, piezoelektrische Dünnschichtaktuatoren kontrolliert werden kann. Mit verschiedenen Membrankonfigurationen und Anregesignalen soll es möglich sein die gebeulte Membran von einem Grundzustand in den anderen umzuschalten.

Der erste Teil der Arbeit befasst sich mit dem Stressverhalten von a-SiC:H-Dünnschichten, welche mit den richtigen Abscheideparametern als stabile Verkapselung zu jeder menschlichen Gewebsart fungiert. Eine a-SiC:H Schicht kann durch variieren des Methan und Silan Anteils in verschiedenen Schichtdicken und Stressvariationen mittels des PECVD Verfahren hergestellt werden, wobei nicht nur die entstehende Schichtcharakteristik bestimmt wird, sondern auch das damit zusammenhängende Aufwachsverhalten von CaCo-2 Zellen. Je nach Anhaftung und Proliferation dieser Dünndarmwandzellen kann die Biokompatibilität der entsprechenden Schicht eingestuft werden. Da Silizium als hydrophil gilt und SiC mit steigendem Kohlenstoffanteil immer hydrophober wird, kann diese Eigenschaft das Aufwachsverhalten der Zellen direkt beeinflussen, da hydrophile Oberflächen bevorzugt werden. Auf der anderen Seite wachsen Zellen gerne in einer Umgebung auf, welche dem eigenen elektrochemischen Potential entspricht. Dies wird durch den Kohlenstoffanteil im Siliziumcarbid begünstigt, was im Widerspruch zur gesteigerten Hydrophobie steht.
Im Zuge dieser Arbeit wird ein Gleichgewicht dieser Eigenschaften gefunden, auf dem CaCo-2 besonders gut aufwachsen. Dazu werden 50.000 Zellen auf 13 verschieden kombinierten SiC Substraten ausgesät und an drei aufeinanderfolgenden Tagen ausgezählt. Um einen besseren Einblick auf das Zellwachstum zu erhalten, werden sechs verschiedene Kombinationen untersucht. Sie umfassen eine Sauerstoffplasmabehandlung und zwei verschiedenen organischen Beschichtungen dieser 13 SiC Proben für das Zellexperiment.

Nachdem die Parameter für die Herstellung einer a-SiC:H -Schicht mit möglichst geringem mechanischem Stress gefunden wurden, konnten verschiedene Membranen mit einem Durchmesser von 600 – 800 µm damit beschichtet werden. Der beginnt mit einem SOI-Wafer, wobei hintereinander aufgetragene Schichten und Ätzvorgange es ermöglichen, eine bereits zufällig in einen der beiden Grundzustände gebuckelte Membran zu realisieren. Die benötigte Kraft, um die Membran in Schwingung zu versetzen oder umzuschalten, liefert das piezoelektrische Material Aluminiumnitrid (AlN).
Das charakteristische Schwing- und Umschaltverhalten der Membranen in Luft und verschieden viskosen Flüssigkeiten soll Mithilfe einiger Messungen bestimmt und dadurch maßgeblich vorhergesagt werden. Die dazu notwendigen Messungen wurden mithilfe der Laser-Doppler-Vibrometrie, Weißlichtinterferometrie, Waferbow- und Kontaktwinkel-Messungen und eines Oszilloskops durchgeführt.

Der Herstellungsprozess, sowie die Interpretation der Messdaten von bistabilen und biokompatiblen Membranen in Luft und Flüssigkeiten werden ausführlich beschrieben und diskutiert. Abschließend soll auch das Aufwachsverhalten von CaCo-2 Zellen mit dem intrinsischen, mechanischen Stresszustand in a-SiC:H Dünnschichten in Relation gesetzt und ein Ausblick für verschiedenen entsprechende Anwendbarkeiten gegeben werden.

List of abbreviations and symbols

SOI	Silicon On Insulator
SiC	Silicon Carbide
a-SiC:H	Amorphous Hydrogenated SiC
AlN	Aluminium Nitride
BOX	Buried Oxide Layer
MEMS	Micro Electromechanical Systems
ECM	Extra Cellular Matrix
PCI	Percutaneous Cardiac Intervention
CTE	Coefficient of Thermal Expansion
CVD	Chemical Vapor Deposition
PVD	Physical Vapor Deposition
CCP	Capacitively Coupled
ICP	Inductively Coupled
PECVD	Plasma Enhanced Chemical Vapor Deposition
RF	Radio Frequency
DRIE	Deep Reactive Ion Etching
HF	Hydrofluoric Acid
C_4F_8	Octafluorocyclobutan
PFC	Perfluorocarbon
PZT	Lead-Zirconate-Titanate
IR	Image Reversal
PFC	Perfluorocarbon
LDV	Laser-Doppler-Vibrometer

WLI	Wight-Light-Interferometry
MEM	Minimum Essential Medium
FBS	Foetal Bovine Serum
FDA	Fluorescein Diacetate
PI	Propidium Iodide
HMDS	Hexamethyldisilane
PFA	Paraformaldehyde
GA	Glutaraldehyde

Contents

1 Introduction

1.1 Motivation

Medical devices exist for thousands of years and since then they are still improving. They get smaller and more effective and formerly externally worn devices get more and more integrated in the human body. The research of such technologies had a big influence in medical procedures and operation. It is known that 2000 years ago the life expectancy of an average human was around 40 – 50 years. From the beginning of the 20th century until now the life expectancy increased from 50 to astonishing 80 years, through better lifestyle choices, like healthier food or less sugar, more sport-activities and especially because of a huge improvement of medical research. A major number in lowering the death rate is the decreased death rate after a heart disease in the US from 1960 – 2015 from 2.7 % to 0.9 %. Though, the curve of medical improvements and curing different major diseases, like as already mentioned heart diseases, but also strokes or cancer, has flattened over the past ten years. [9]

The invention and development of new devices, but also the miniaturization of already existing medical devices are still one of the most important fields of biomedical engineering. These medical improvements helped a lot to gain huge impacts on the increased life expectation of people around the world [9]. The probably best-known devices are pacemakers, cochlea implants and valves. The main purpose of a pacemaker is to monitor the cardiac cycle and intervene in case of a harmful detection, while cochlea implants stimulate nerve endings inside the inner ear with electrical signals, generated from acoustic waves. Valves are commonly used to keep various types of lumen either open or shut. The obvious disadvantage of a cardiac pacemaker or a cochlea implant is the requirement of batteries, cables and a housing. But there are also non-electrical devices, which have great influence to human bodies. One example are stents, which reduced the mortality over five years after a PCI (Percutaneous Cardiac Intervention) by 90 %, with almost 50 % of noncardiovascular caused deaths. [10]

Especially self-powered valves produced within a macroscopic range and used *e.g.* in the field of drug administration outside the body are too big to get implanted. The application of a bistable membrane as an actuator in a microfluidic valve has great potential in biomedical engineering, as cables or batteries can be avoided, which facilitates miniaturization and implantation. The idea of using such microvalves is not new [63], though the mechanism of making them actually work, is. The usage in the human body is a huge field of applications and already existing devices would be replaced by a miniaturized version. Biocompatible microfluidic MEMS (Micro Electromechanical Systems) valves could be used inside the body for example after surgeries to drain superfluous body liquids on demand, which would otherwise stream out constantly. This could provide more flexibility after a surgery. Another application could be in the field of drug administration amounts. A microvalve housed inside the body, which can be controlled from outside and differentiates between two different drug amounts, dispensed depending on the current needs of a patient, can increase the comfort of wearing such devices. Even though medicine and the research of biomedical engineers has come so far, such a mechanism has not been invented yet.

1.2 State of the art

Microfluidic valves already exist in many variations and can be actuated through different mechanisms. While magnetic stamps provide contactless opening and closing of a valve, other actuators require more complex systems including cables and different power sources. A common building block in microvalves are MEMS membranes, which can be manufactured either mono- or bistable and are distinguishable from each other by the number of ground states. While monostable membranes feature only one stable state, a bistable diaphragm can be switched from one stable ground state into a second one and consumes only energy during the short time of switching. Both types of these membranes can be introduced into a valve to open or close one or even more channels. Several mechanisms can be used to actuate microvalves with membranes, as heating a cavity and using the rising pressure as actuating power [36] or using a pneumatic system, which uses the increasing air pressure as driving source of power for a switching procedure [30]. One main disadvantage of most actuation principles is the requirement of an acting chamber on one side of the membrane, which is the reason why corresponding valves are just single channelled.
Another most promising approach to switch a bistable membrane is the exploitation of the inverse piezoelectric effect. An electrical signal applied to a piezoelectric material sandwiched between two electrodes and integrated on the membrane, makes it possible to create enough movement of the diaphragm, whereby it switches from one stable state to the other. To use a bistable MEMS-diaphragm excited by integrated, piezoelectric thin film actuators is a novel approach. This could guarantee not just closing a small pipe or reopen it, but also create the ability of choosing between two channels, where liquids can run through, since no acting chamber is necessary anymore. [11]

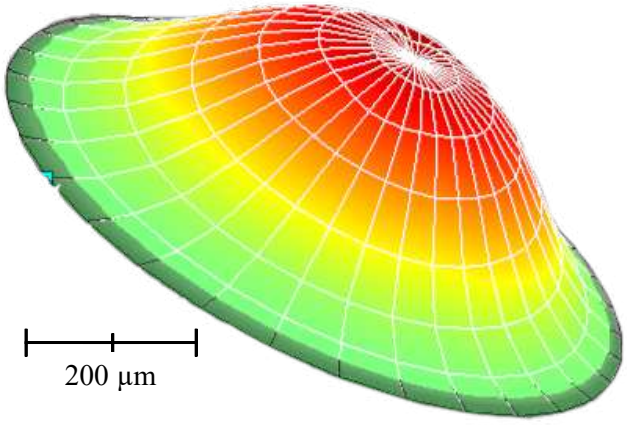

Figure 1.1: Typical 3D view of a round, buckled membrane in its upper stable ground state, with a diameter of 800 µm and a maximum deflection of 5 µm in the centre.

To switch a membrane, no matter if they are mono- or bistable, a compressive stress level is required. The necessary, compressive stress level is created by the deposition of specific thin layers and needs to be high enough to cause buckling. Therefore, an SOI-wafer serves as starting material, where two gold layers are deposited serving as electrodes, which are separated through a piezoelectric aluminium nitride thin film layer, acting as functional material. A piezoelectric layer of Scandium AlN ($Sc_xAl_{1-x}N$, for $x = 27\,\%$) would have also been possible and would have needed 20 – 23 % less voltage to switch between the two stable states [11], though this material was not investigated in the scope of this work, because of the low availability and high costs of the material. The arrangement of these layers will reach a specific cumulated stress level and the membrane finally buckles after completion (Figure 1.1).

Amorphous hydrogenated silicon carbide is used in many cases as the biomaterial of choice, because of its outstanding mechanical and electrical properties, as well as for its chemical inertness [7]. Those properties made the material promising for the implementation into MEMS technologies. SiC is declared as a high biocompatible material for a wide range of different cells, also including mammalian cells [2]. Devices coated with a continuous layer of SiC can also be classified as biocompatible and used in the field of medical applications. Depending on the composition of silicon and carbon, different stages of biocompatibility can be accomplished. The higher the hydrophilicity of a surface is, the more likely mammalian cells will adhere, however cell adhesion proteins adhere better on surfaces of materials which, are more hydrophobic [5|. It is also known that cells adhere especially well on surfaces with an electrochemical potential close to one of living cells [8]. Carbon has an electrochemical potential close to the one of living cells, but is also classified as a hydrophobic material. Since silicon is a hydrophilic material, a competing behaviour between hydrophilicity and electrochemical potential can be noted by changing the carbon content of silicon carbide [2]. Therefore, the overall biocompatibility of different SiC surfaces will be investigated. It should also be mentioned that the different compositions of silicon and carbon have a direct impact on the resulting stress level of a-SiC:H thin films [7].

1.3 Overview

The following thesis will discuss the term biocompatibility, including measurements and standards to declare materials in terms of acceptance and interaction with living cells. Common procedures used in this work to deposit cells on surfaces to establish the theory of silicon carbide used as a biocompatible material, will be described. Furthermore, the concept of bistable membranes will be presented. This includes the origin of intrinsic mechanical stress in thin film layers, different mechanisms to switch from one stable ground state into the second and the necessary background knowledge of piezoelectric materials to achieve this switching, especially with an electrical signal. Chapter 2 will provide an overview of procedures and equipment, which are required to complete a production cycle for manufacturing a bistable and biocompatible membrane. Information about the instruments used to measure the static and dynamic mechanical behaviour of the diaphragms will be provided, as well as the exact parameters used in the production cycle, whereby the biocompatible a-SiC:H layer will be described in Chapter 3. Chapter 4 will treat the investigation of living cells, interacting with surfaces of different a-SiC:H concentrations, whereby the wettability and proliferation is measured to receive information of the grade of biocompatibility, compared to the SiC composition and stress levels of a-SiC:H layers. A brief description of the corresponding results will also be provided. In Chapter 5 the setup for the measurements of the membranes in air and fluids of different viscosities will be described. Those measurements provide information about thickness, cumulated stress level and the mechanical behaviour of the diaphragms under load. The results will be presented, discussed and summed up in Chapter 5, describing the switching behaviour depending on properties like layer thickness, diameter and the characteristic resonance spectrum, respectively. Finally, this work will provide a conclusion and outlook, if biocompatible bistable membranes will achieve the potential to be used in medicine for the first time.

2 Theory

2.1 Biocompatibility

The term biocompatibility is often used in the field of medicine, but less understood. This subchapter will declare and explain what a material needs to get accepted as biocompatible. A biomaterial is *per definition* a material which is intended to interact with any tissue of the body, evaluate, treat or replace any organs or function. Since materials get placed inside the body and get in contact with tissue, it is absolutely necessary to be aware of the possible upcoming interactions between tissue and material. [1]

The most important part is to understand that there are different stages of biocompatibility, which will be described briefly below [64-66].

Toxic
The reaction of the contacting tissue with the material leads to a necrosis. Body cells die due to the interaction with the material.

Inert
Cells are not interacting with the implant and form a capsular around it. In this case no cells die, nor is any change of the material itself noticeable.

Bioactive
A material declared as bioactive adheres with its surrounding, without any alternation of the tissue or material.

Degradable
Surrounding tissue degrades the implant and replaces it over time with own body cells. After that process nothing of the original material will be left.

These properties are not sharply separated, but depend strongly on many factors, for example a patient's properties like sex, age or allergies.

Within the scope of this thesis hydrogenated amorphous silicon carbide was chosen in the first place, because it is already known as a biocompatible material. Another reason was that the thin film properties as layer stress or hydrophilicity can be changed by altering the chemical composition and the material is well established in MEMS-technologies. These properties made a-SiC:H a good choice for the development of a device which may reach the point of getting tested for medical purposes [2-4]. Furthermore, it is known that cells adhere especially well on surfaces of materials, whose electrochemical potential is close to the one of the cells. [8]

2.1.1 Measurements

To guarantee safety by not causing any harm, if a foreign material is implanted in the body there are several tests, which declare a material as biocompatible. The ISO 10993 contains many recognized standard tests for biocompatibility. It involves animal and benchtop tests which always have to be completed in the first place, before implanting a material in a human body. Also, chemical tests are part of the ISO 10993 which checks for any chemicals that could potentially leach from the material into its surrounding inside the human body.
Wear debris is another mentionable factor of materials, since every two materials under load experience wear through adhesive, abrasive or fatigue mechanisms. In the period of a lifetime circle of a device it is important to know if and how much wear debris will be generated. Such wear tests are performed mechanically in vitro with two materials under load and in vivo over some time in animals to evaluate the biological response. [1]

One specific way to test the biocompatible response of in this work used silicon carbide (SiC) is to directly cultivate different mammalian cell cultures on the surface of this compound substrate. The response, cell proliferation and adhesion-quality can be tested by using FDA (Fluorescein Diacetate Assays) and be obtained under a fluorescence microscope. Since a maximization of the contact area with the substrate indicates a good biocompatibility and in general the obtained cells appear flattened and similar to control cells, SiC can be declared as a good biocompatible material under the aspect of this test. [2]

Another indicator for different characteristics of biocompatibility of a material is the wettability of the surface, since cell adhesion proteins adhere better on hydrophobic surfaces, but mammalian cells would prefer hydrophilic surfaces [5]. The wettability can be determined by contact angle measurements. There can be no decisive differences found in different polytypes of SiC (proven in [2] with 3C-SiC, 4S-SiC and 6H-SiC), though there is a significant change of the wettability due to different cleaning cycles of the substrate as RCA or the piranha treatment. This should get directly reflected in cell adhesion and further on in the type of biocompatibility as mentioned in 2.1. The piranha treatment of a cleaning cycle affects the properties of the SiC surface the most. Surfaces treated with a standard RCA-procedure show less hydrophilicity than surfaces, which went under the piranha treatment. [2]

2.1.2 Cell adhesion on surfaces

The in vitro treatment of cells is an important step before a medical product gets in the phase of in vivo treatment or human experiments. Thus, cell adhesion is essential to control the interaction with different surfaces. The mechanical response of cell structures to their extra cellular matrix (ECM) is of fundamental importance in the development of tissue and monitoring of behaviour and function. The investigation of cell adhesion is a wide field used in cellular biology and biomedical engineering, in order to understand cell signalling pathways, the response of implantable biosensors, artificial bone or tooth replacement and gaining of knowledge about tissue-on-a-chip or organ-on-a-chip microsystems. [15]

The terminus cell adhesion stands for the ability of single cells to stick to other surrounding cells or the ECM of foreign surfaces. Most mammalian cells placed in vitro on a surface are anchorage-depending and will attach firmly [13]. It is important to understand that cells demand different requirements for adhesion for various types of applications, for example medical devices which are forced to interact with blood cells, like artificial heart valves or blood vessels

are required not to be adherent to cells or plasma proteins, because otherwise unwanted cell adhesion could cause major diseases through the formation of thrombosis and further embolisms. On the other hand, materials used in scaffolds for tissue generation are postulated to support cell adhesion, subsequent proliferation and biosynthesis. [14]

2.1.2.1 Passive in vitro cell culture

Placing a single cell on a surface transmits extracellular or intracellular forces to the adhesion sites, which are formed by transmembrane proteins called *integrins* [16]. Integrins are responsible for the attachment to ECMs and the adhesion molecules of other cells, while the quality of sticking is depending on the quantity of numbers of chemical bonds on a cell´s surface [17-18]. This way of placing cells on static substrates, *e.g.* culture flasks or petri dishes, is described as passive in vitro cell culture. During the attachment process, the cell undergoes morphologic alternations driven by passive deformation and active reorganization within the cell's cytoskeleton. [15]

The procedure of a cell attaching to the ECM of a substrate can be separated and characterized in three parts. The first stage is the initial attachment of the cell body to its substrate, caused by electrostatic interactions. Secondly, the cell's integrins will start to form single receptor-ligand pairs driven by the specific integrin mediated adhesion [19]. Those bindings enhance quickly and result in total adhesion strength. In this state the cells' structures changed from their initial shape to a more flattened one. By increasing time, cells will spread and flatten out over the substrate resulting in a decreased height and bigger contact surface. Phase three is the ongoing process of spreading and flattening until a final state, where contact area and adhesion strength are maxed out. [15]

2.1.2.2 Cell attachment measurements

In general, one can divide between single cell or cell population attachment. While single cell approaches give information about the molecular bonds between the cell and the ECM, the resulting bonding forces, changes of the morphology and the cell's migration, cell population studies play a bigger role for attachment events for bigger number of cells. This provides knowledge about the adhesion kinetics and determination of biocompatibility of materials for medical devices and applications in the field of tissue engineering. [15]

A qualitative way to determine the fraction of cells remaining adhered to an ECM-coated medium is a wash assay [20]. This measurement can be divided into static and dynamic cell culture, depending if the medium is stagnant during the time of incubation or not. First, cells get cultured inside petri dishes, microwell plates or culture flasks, followed by adhesion analysis like cell count, protein/DNA count or antibody binding after the distinguishing additional step of cell washing was carried out [21].

2.2 Thermal and intrinsic stress in thin films

Through the deposition of different materials onto a substrate it is possible that inside the resulting layer a mechanical strain arises. By introducing Hook's law the strain results either into tensile or compressive stress, depending on the material's Young's modulus E. It is important to gather information about the stress in each deposited layer, in order to receive knowledge over its behaviour in real applied fields as well as the ability to control the layer stress by changing deposition. [23]
Basically, two different kinds of stress are distinguishable from each other. While thermally induced layer stress depends on different values of diverging CTEs (Coefficient of thermal expansion) of different materials, intrinsic stress might have several reasons at once, which are listed and explained in this section. Both stress variations have in common, that depending on material and kind of procedure the resulting layer behaviour could manifest itself as tensile or compressive stress (Figure 2.1).

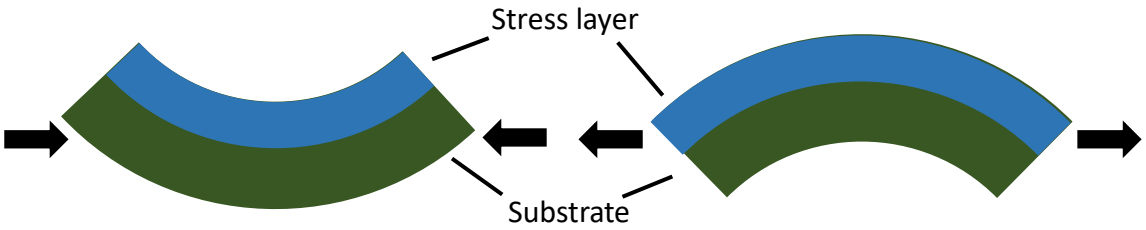

Figure 2.1: Schematically representation of compressive (left) and tensile (right) stress, caused by a deposited material on a substrate

2.2.1 Thermal stress

Thermal stress is the result of a material with a specific CTE, which changes its temperature. Assuming a thin film has the initial length l_0, the Young's modulus E and a linear CTE α, the measurements of the thin film will change around the value of Δl, if the material's temperature is altered from T_0 to T (Equation 2.1).

$$\Delta l = \alpha(T_0 - T)l_0 \tag{2.1}$$

If two materials have different CTEs, Equation 2.1 will result in two different changed lengths for each material, but since the thin film assumingly adheres very strong to the substrate, both will still have the same lateral size. This results in a contest of strength between both materials, whereby the stronger material will lead the softer or thinner material to follow its own expansion (or shrinking). If the substrate shrinks less while cooling down as the deposited thin layer, a tensile force arises between the materials, expressed by a strain ε of

$$\varepsilon = \frac{\Delta l}{l_0}. \tag{2.2}$$

Introducing Hooke's law

$$\sigma = \varepsilon E \tag{2.3}$$

into the Equation 2.2 results directly in an expression for the thermal stress σ_{th}, depending on the temperature change of a material

$$\sigma_{th} = E\alpha(T_0 - T). \quad (2.4)$$

Thereby, the coefficients α and $(T_0 - T)$ each individually are positive or negative and the stress of the thin film is of tensile or compressive behaviour. [23-24]

2.2.2 Intrinsic stress

The origin of intrinsic stress is a misplacement of atoms leading to defects inside the thin film's microstructure. Such defects may arise by depositing different materials onto a substrate, though they are often created on porpoise and being taken advantage for applications, where layer stress is necessary. In general, three different kinds of intrinsic stress are distinguishable from each other.

2.2.2.1 Zero dimensional defects

Zero dimension defects, also called point defects or vacancies, are the result of thermal lattice vibrations, which exist in every material over a total temperature of $T > 0K$. Because of the vibrations it is possible for an atom to leave its interior place in the lattice structure and settle down on the surface. Depending on the amount and size of misplaced atoms in the lattice structure an associated perturbation will lead to a specific value of intrinsic stress σ_i. The amount of point defects is calculatable with

$$n = Ne^{\frac{-E_f}{k_B T}}, \quad (2.5)$$

whereby N is the number of lattice sites, E_f the necessary energy to resolve an atom out of its initial lattice position, k_B the Boltzmann constant and T the temperature. It should be mentioned that E_f is typically 1 eV per atom and therefore the term $e^{\frac{-E_f}{k_B T}}$ gives a value of 10^{-5} for $T = 1000\ K$. [23]
Another source of zero dimensional defect is the insertion of excess atoms, which is one of two assumed possibilities, in which way atoms can be inserted during a film growth. In this case the resulting compressive stress is the consequence of the incorporation of excess atoms into the grain boundaries (Figure 2.2) [25].

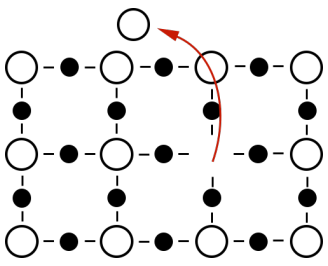

Figure 2.2: Displaced atom from a fixed lattice structure, by the implementation of an external energy E_f.

2.2.2.2 One dimensional defects

Line or one dimensional defects arise under the load of *e.g.* external pressure leading to plastic deformation. They can be separated into edge and screw dislocations, the latter appears through the presence of shear stress. [23]

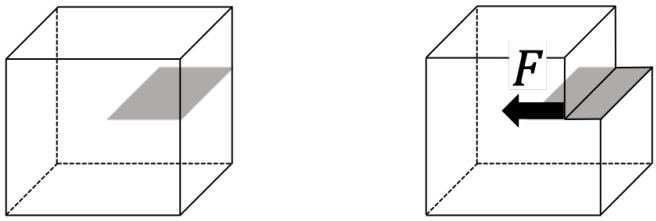

Figure 2.3: Edge dislocation along a horizontal cut, by an external force.

Edge dislocations, causing a line defect origins through a linear deformation or the wedging of an additional atomic layer into a perfect lattice structure. For example, Figure 2.3 shows a solid material, whose upper part was compressed by an external force. By contrast, screw dislocations arises, if shear stress acts parallel to the material's surface, which most commonly changes the angles in an object (Figure 2.4). Shear stress τ is calculated as force F per area A. Both varieties of line defects tend to occur in nature in a combined way. [23]

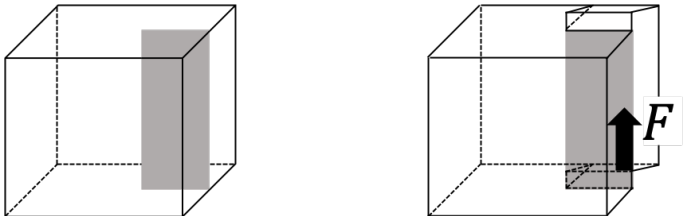

Figure 2.4: Screw dislocation along a vertical cut, by a shear force F acting parallel to the materials surface.

2.2.2.3 Two dimensional defects

Two dimensional defects affect whole areas of a thin film and are therefore often called area defects. The two most common reasons are the coalescence of grain boundaries and the mismatch of a substrate and a deposited thin film with different lattice constant, leading to misfit stress [27]. Grain boundaries develop in the early stage of a growing thin film, where first small grain island originate and grow until they make contact to adjacent islands. Since the surface energy of single islands is higher than the energy between the grain interfaces and cohesion develops. While closing the gaps between the grain islands the participating islands become elastically strained and a tensile stress is generated (Figure 2.5) [26].

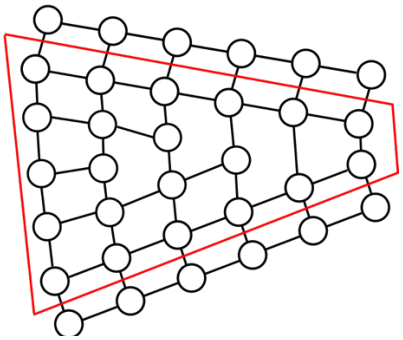

Figure 2.5: The red framed area represents a grain boundary.

A microscopic view reveals a mechanism, where interatomic interactions try to close the gaps, which leads to different lattice distances of involved atoms and as already mentioned tensile stress σ_{gb} calculated by the formula

$$\sigma_{gb} = \frac{E}{1-v}\frac{d}{D}, \tag{2.6}$$

whereby E is the elastic modulo, v the Poisson's ratio, d stands for the average relaxations distance and D is the average grain size [33]. Following Equation 2.6 the stress is inversely proportional to the crystalline dimensions of a material and therefore higher for materials with smaller grain sizes. [28-29]

The second mechanism creating area defects in thin films originates in the initial phase of depositing a material. Since most commonly the thin film material and the substrate have different lattice constants and since during deposition both materials are forced to line up perfectly, either a tensile or a compressive stress arises on the boarder of both materials, depending on the lattice constants of the thin film a_{film} and the substrate a_{sub} (Figure 2.6) [32]. The resulting lattice misfit m is calculated by

$$m = \frac{a_{film} - a_{sub}}{a_{sub}}. \tag{2.7}$$

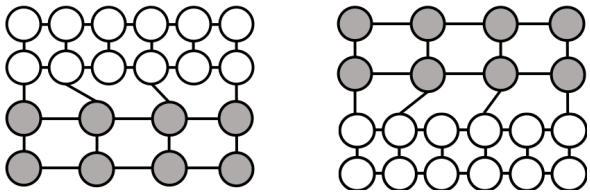

Figure 2.6: Lattice distortion caused by different lattice constants. Left: lattice constant of the film is smaller than the substrate's one. Right: lattice constant of the substrate is smaller.

As long as the film thickness is small enough, the thin film will tend to take over the lattice constant of the substrate and grow with an increasing tensile or compressive stress. If the thickness of the deposited material exceeds a critical thickness d_{crit}, relaxation processes will reduce the residual stress of the thin layer, because of its inner growing accumulated energy. Materials deposited above the critical thickness d_{crit} will grow with its own lattice constant. The value for d_{crit} can be expressed for relatively small lattice misfits m after the model of Matthews and Blakeslee.

$$d_{crit} = \frac{b(1 - v\cos^2(\theta))}{4\pi m(1+v)\sin(\theta)\cos(\lambda)} ln\left(\alpha \frac{d}{b}\right) \quad (2.8)$$

In this equation b stand for the length of the Burger's vector describing the magnitude of lattice distortion, v again the Poisson's ratio, θ and λ the angles of the dislocation and α describes the dislocation core parameter.
To make a complete statement, it should be mentioned, that there are also three dimensional defects. Such defects describe whole volumes inside a material, where completely different lattice structures predominate. [30-31]

2.2.3 Buckled membranes

This section of the thesis will briefly describe the origin of buckled MEMS membranes, also a mathematical model will be introduced to declare membranes in their stable states. Since only some thinlayers with undefined stress state on top of each other would not generate a buckling behaviour, information about a necessary compressive stress level for buckled membranes will be provided.

MEMS membranes can be processed in all kind of compositions of different thinlayers, with different thicknesses, different forms like circle- or square shaped and a wide range of diameters. The lower limit of the thickness of such diaphragms are a few nano meters restricted by the production itself, while the upper limit of 500 µm is set by the definition MEMS, since higher values would not be covered by this term anymore. In general, one can distinguish between thick and thin membranes (Figure 2.7), although the boarder of the definition of thick and thin membranes alters strongly. Dependent on the thickness, thin membranes will have a higher vibrating amplitude $\omega(r)$ under load compared to thick ones. [30][34]

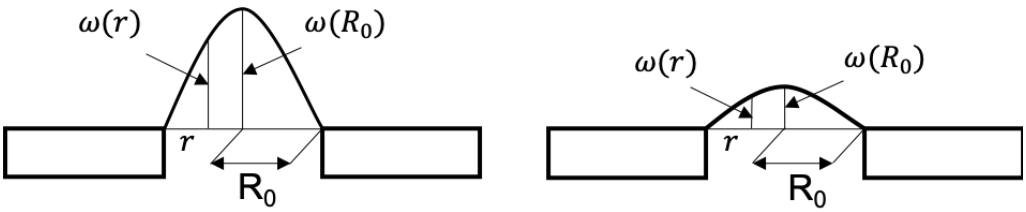

Figure 2.7: Schematic comparison of thin (left) and thick (right) membranes

The displacement ω of the bending shape at r of *thick* diaphragms is calculated according to

$$\omega(r) = \omega_0 \cdot \left(\frac{r^2}{{R_0}^2}\right)^2, \quad (2.9)$$

the one of *thin* diaphragms with

$$\omega(r) = \omega_0 \cdot \left(\frac{r^2}{R_0^2}\right), \quad (2.10)$$

whereby ω_0 is the deflection from its stable state, r the radial position of interest and R_0 the radius of the diaphragm. [30][34]

Generally, a buckled membrane originates through depositing one or several thinlayers on top of each other creating enough cumulated compressive stress to exceed a specific critical stress level, which can be calculated after the model of Timoshenko [24] and Schomburg [22]. The base for the model is the potential energy V_p of a membrane with a radius R_M, the deflection ω, the biaxial Young's modulus E_M, with a thickness of t_M, the Poisson's ration v_M, the radial stress σ_r, tangential stress σ_φ, which is zero due to the axial symmetry and the differential pressure of Δp between the upper and bottom side of the membrane, represented through following equation.

$$V_p = \int_0^{2\pi} \int_0^{R_M} \left[\frac{E_M t_M^3}{24(1-v_M^2)} \left(\frac{\partial^2 \omega}{\partial r} + \frac{1}{r}\frac{\partial \omega}{\partial r} + \frac{1}{r^2}\frac{\partial^2 \omega}{\partial \varphi^2} \right)^2 + \frac{t_M}{2} \left(\sigma_r \left\{ \frac{\partial \omega}{\partial r} \right\}^2 + \frac{\sigma_\varphi}{r^2} \left\{ \frac{\partial \omega}{\partial \varphi} \right\}^2 \right) \frac{t_M}{8} \frac{E_M}{1-v_M^2} \left(\frac{\partial \omega}{\partial r} \right)^4 - \omega \Delta p \right] r dr d\varphi \quad (2.11)$$

Equation 2.11 is the result of the equilibrium of forces on the frame, where the total force is the pressure difference Δp times the area which is balanced by the frame fixing force F_f. Lateral components were not taken into account, because there is no movement of the diaphragm in such directions. The output is a differential equation of the fourth order, which demands an Ansatz of also fourth order to get a solution. In the case of membrane theory, the characteristic shape of static deflection is described by

$$\omega(r) = \omega_0 \left(a_0 + a_1 \frac{r}{R_M} + a_2 \left(\frac{r}{R_M} \right)^2 + a_3 \left(\frac{r}{R_M} \right)^3 + a_4 \left(\frac{r}{R_M} \right)^4 \right) \quad (2.12)$$

and used as Ansatz. The four free parameters a_0 - a_4 can be received through the boundary conditions of such a membrane. Starting in the centre at $r = 0$, the initial deflection is ω_0 (Eq. 2.13) and because of the assumed ideal shape of the diaphragm the derivation of the deflection at $r = 0$ (Eq. 2.14) and $r = R_M$ (Eq. 2.15) is zero. The fourth boundary condition results from the fact, that the membrane is fixed at the edge, leading to a deflection at $r = R_M$ of zero (Eq. 2.15).

$$\omega(r) = \omega_0 \,|_{r=0} \quad (2.13)$$

$$\frac{\partial \omega(r)}{\partial r} = 0 \,|_{r=0} \quad (2.14)$$

$$\frac{\partial \omega(r)}{\partial r} = 0 \,|_{r=R_M} \quad (2.15)$$

$$\omega(r) = 0 \,|_{r=R_M} \quad (2.16)$$

Combining the Equations (2.13) and (2.14) with Equation (2.12) gives the values for $a_0 = 1$ and $a_1 = 0$ and doing the same with Equations (2.15) and (2.16) results in $a_2 = a_4 - 3$ and $a_3 = 2 - 2a_4$. Putting the outcome for the parameters a_0 - a_3 back into Equation (2.12) gives

$$\omega(r) = \omega_0 \left(1 + (a_4 - 3)\left(\frac{r}{R_M}\right)^2 + (2 - 2a_4)\left(\frac{r}{R_M}\right)^3 + a_4\left(\frac{r}{R_M}\right)^4\right) \quad (2.17)$$

with a single dependency of the last free parameter a_4. From literature one can determine a_4 as the parameter for the shape of the deflected membrane and fits the model best with a value of $a_4 = 1$ [22][24]. This was experimentally proven in [40], with a 2.05 µm thin membrane with a diameter of 800 µm. The deflection curve measured with a WLI was almost coherent to the model's curve, calculated with Equation (2.17) for $a_4 = 1$. The mathematical result is the equation for ideal plate behaviour Equation (2.18) [24].

$$\omega(r) = \omega_0 \left(1 - \frac{r^2}{{R_M}^2}\right)^2 \quad (2.18)$$

Inserting the solved ansatz (2.18) back into the initial Equation (2.11) and determining the extremal values with respect to ω_0, gives an equation for the origination of the force F_M in the diaphragm, which is no longer dependent from the tangential stress σ_φ.

$$F_M = -\frac{\partial V_p}{\partial \omega_0} = -\frac{2\pi}{3}\left(\frac{8}{3}\frac{E_M t_M^3}{1 - v_M^2}\frac{\omega_0}{R_M^2} + 2t_m\sigma_r\omega_0 + \frac{128}{105}\frac{E_M t_M}{1 - v_M^2}\frac{\omega_0^3}{R_M^2} - \frac{1}{2}\Delta p R_M^2\right) = 0 \quad (2.19)$$

This is in good agreement with the literature, which predicted the negligibility of the tangential stress component, because of the symmetry as already mentioned before. After a rearrangement of Equation (2.19) to change the subject to the pressure difference Δp, the following equation results. [36][40]

$$\Delta p = \frac{4t_M\omega_0}{R_M^2}\left(\frac{4}{3}\frac{E_M}{1 - v_M^2}\frac{t_M^2}{R_M^2} + \sigma_r + \frac{64}{105}\frac{E_M}{1 - v_M^2}\frac{\omega_0^2}{R_M^2}\right). \quad (2.20)$$

Without any pressure load $\Delta p = 0$ on the diaphragm, the initial buckling height of the membrane ω_0, only dependent of the radial stress component σ_r, can be calculated with Equation (2.21).

$$\omega_0 = \pm\frac{\sqrt{135}}{4} t_M \sqrt{\sigma_r \frac{1}{\frac{4}{3}\left(\frac{t_M}{R_m}\right)^2 \frac{E_M}{1 - v_M^2}} - 1} \quad (2.21)$$

It can be clearly seen, that the term in the square root of Equation (2.21) must be a positive number to get an initial deflection ω_0. This specifically needed stress level is called critical stress σ_{crit} and quantifiable through

$$\sigma_{crit} = -\frac{4}{3}\left(\frac{t_M}{R_m}\right)^2 \frac{E_M}{1 - v_M^2}. \quad (2.22)$$

Mathematically, the same result is achieved by calculating the first derivation of Δp in Equation (2.20), with respect to ω_0, zeroed and for $\omega_0 = 0$. [22][24]

$$\frac{\partial \Delta p}{\partial \omega_0} = 0\,|_{\omega_0=0} \qquad (2.23)$$

A buckling behaviour of a membrane can be monitored, if the initial stress σ_0[1] exceeds the critical stress σ_{crit} of Equation (2.22), which obviously can be seen is strongly dependent on the membrane's properties. Furthermore, if the initial deflection is known and because of the strong dependency of the stress in the membrane, σ_0 can be calculated from Equation (2.21) with

$$\sigma_0 = \sigma_{crit}\left(1 + \frac{16}{35}\frac{{\omega_0}^2}{{t_M}^2}\right). \qquad (2.24)$$

The Equations (2.20) and (2.21) represent a good approximation for the conceptual design of a membrane, like the estimation of the switching pressure or the initial deflection height ω_0. In this work membranes will be presented, which are based on a multi-layer concept. Thus, the calculation for the intrinsic stress must be adjusted and effective values need to be introduced. In case of a N-layer membrane the stress for each layer and its dimensions must be known to calculate the total effective stress σ_{total} with

$$\sigma_{total} = \frac{\sum_{i=1}^{N} \sigma_i t_i}{t_{total}} \qquad (2.25)$$

whereby σ_i and t_i stand for the individual intrinsic stress and thickness of the i^{th} layer and t_{total} represents the total thickness of a N-layered membrane. [40]

2.2.4 Bistabilty

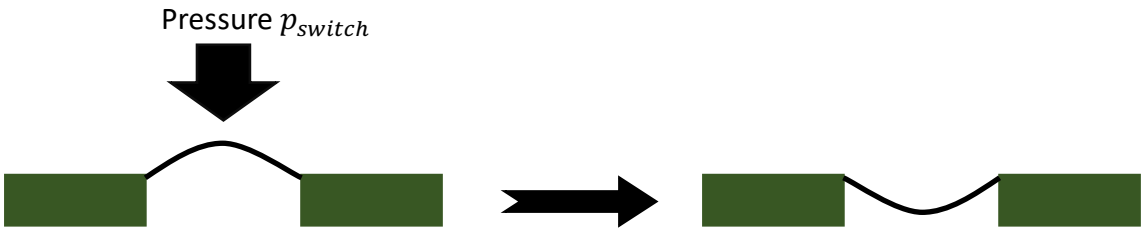

Figure 2.8: Switching sequence of a bistable membrane initiated by an external switching pressure p_{switch}.

Buckled membranes described and used in this work are distinguishable from other membranes by their bistability (see Figure 2.8). This feature describes diaphragms with two stable states, compared with monostable membranes, which are only defined by one stable ground state. With a corresponding load on the membrane, causing differential pressure Δp it is possible to generate enough movement in the membrane to switch from one stable state into the other. A monostable membrane would deflect as well under load, but will move back into its initial position as soon as the stimulating driving force is removed. One of the biggest advantages of bistable membranes is, that no energy will be consumed while the diaphragm keeps one of their ground states. Only for the process of switching, energy is needed. Another huge aspect are the

[1] In this specific case is $\sigma_0 = \sigma_r$.

high displacements, reachable in case of switching the membrane between the ground states. [36][40]

2.2.4.1 Calculating the switching pressure of a bistable membrane

If the differential pressure Δp against a bistable membrane exceeds a specific limit, the membrane will switch from one stable state to the other. By increasing Δp calculated with Equation (2.20), the membrane is forced to change its buckling height, causing a diaphragm deflection $\omega_0(\Delta p)$. The membrane keeps its deflection state until the switching pressure p_{switch} is attained and the membrane subsequently switches into the other stable state. At the moment, when this happens the diaphragm has a deflection of ω_{switch}, which can be calculated by zeroing the first derivation of Equation (2.20) with respect to ω_0 and rearranging the subject to $\omega_0 = \omega_{switch}$.

$$\omega_{switch} = \pm\frac{1}{24}\sqrt{-105\left(3R_M\sigma_r\frac{1-v_M^2}{E_M} - 4t_M^2\right)} \qquad (2.26)$$

Introducing ω_{switch} back into Equation (2.20) leads directly to the pressure needed to switch a diaphragm into its other ground state. [34][36]

2.2.5 Procedures to switch a buckled membrane

This part of the thesis gives an idea of how a bistable membrane can be actuated. Nowadays several actuation principles are applicable in MEMS technologies, though not all will be presented. The choice of which switching procedure will be used is strongly dependent on the available space, cost factors, but mostly on the application itself.

A common actuation principle in microtechnology is to provide energy by heating and cooling cycles. A membrane placed upon a cavity builds up such a setting (Figure 2.9). For example it is possible to increase the temperature inside the chamber with an electrical heater. By slowly heating up the air within a constant volume, the cavity pressure will increase after the law of Gay Lussac and Boyle-Mariotte and the expanding air will escape through a small pressure orifice. If the current is turned off again, the pressure in the cavity will decrease and after reaching the specific switching pressure the diaphragm will switch from the upper to the lower ground state. To achieve switching back in the initial ground state, the cavity is heated up fast, which causes a quickly increasing pressure until the membrane switches back. [36]

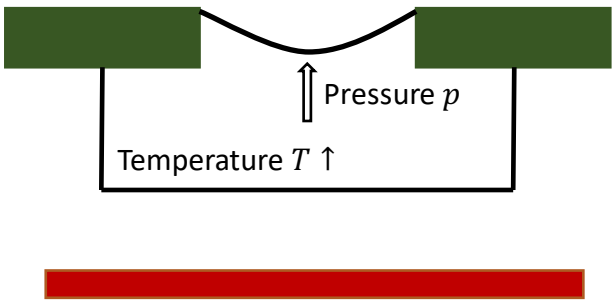

Figure 2.9: External switching pressure p_{switch} created by increasing temperature

The necessary required pressure can also be achieved in a purely pneumatic way (Figure 2.10). Additional gas is inserted through a pneumatic connector into the acting chamber to increase the pressure in order to switch the membrane. By simply pumping gas out of the cavity the reverse effect is achieved. [30]

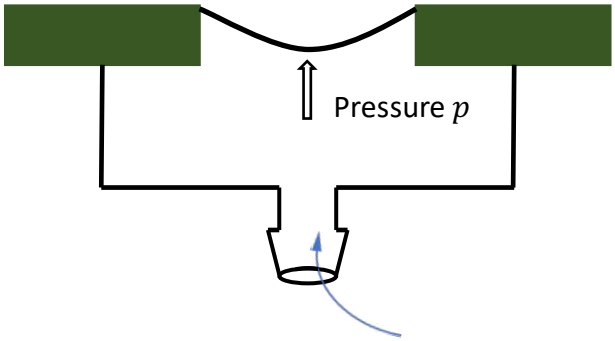

Figure 2.10: Pneumatic way of increasing the pressure to switch a membrane

Both mechanisms have a disadvantage in common, that an acting chamber is crucial to actuate the membrane, which makes only one size of the diaphragm useful, whereby a positive aspect is the simplicity of the actuation principle.

2.2.5.1 The piezoelectric and reverse piezoelectric effect

The membranes characterized and used in this work are actuated on an electrical principle, based on the exploitation of the piezoelectric effect, which involves the big advantage of avoiding a cavity and allows to fully expose the diaphragm into the fluid. The piezoelectric effect is the main transducer mechanism used in this thesis and hence the theoretical description explained in more detail. This effect is defined by an external mechanical load working on certain dielectric materials and therefore creating an electrical polarization and *vice versa*. The load causes a movement of the electrical symmetry and therefore an unsymmetrical material dependent crystal structure, which results in an electrical polarization of $\vec{P}$ (Figure 2.11).

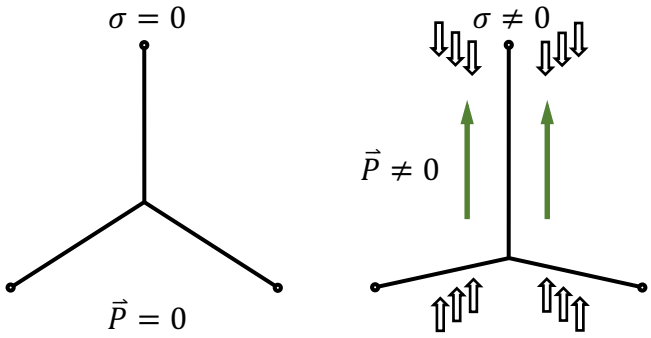

Figure 2.11: Working principle of the piezoelectric effect: polarization through the deformation of material.

Especially important for the bistable membranes investigated in this work is the inverse piezoelectric effect. Due to an anisotropic crystal structure of piezoelectric materials it is possible to generate a rearrangement of atoms within the lattice, by applying an electrical signal to polarize the material, causing small directionally changes of the material's dimensions.

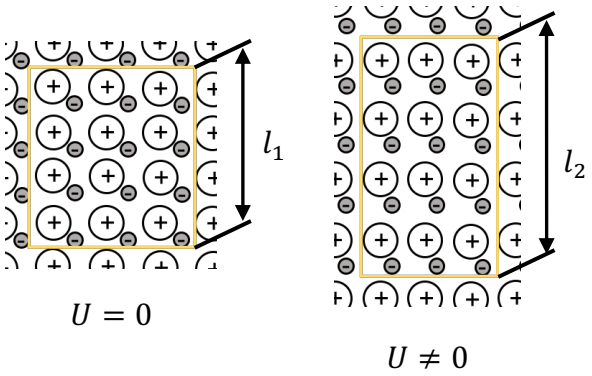

Figure 2.12: Applied voltage U causing a rearrangement of the crystal structure. Doing so, a change in length of $\Delta l = l_2 - l_1$ is generated.

Figure 2.12 shows a typical characteristic length change behaviour of a piezoelectric material, by purposively altering the polarization of the crystal structure due to an applied voltage U. The length change can calculated with $\Delta l = l_2 - l_1$. [37]

The piezoelectric material used in this thesis is aluminium nitride and was chosen because of its good thermal and chemical properties and because it is compatible with the complementary metal-oxide-semiconductor (CMOS) manufacturing process and a promising candidate for applications in MEMS technologies.
To describe the length change behaviour of piezoelectric materials the tensor d is used. In the specific case of deflection Δl in the same direction of the polarization P and an acting force ΔF the possible implications get expressed by the single tensor component d_{33} (Figure 2.13). Despite the good properties of AlN, however, the material has compared to other piezoelectric materials low values for d_{33} ($d_{33.AlN} \approx 5\ pmV^{-1}$; $d_{33.PZT} \approx 215 - 575\ pCN^{-1}$) [38]. [39]
According to [40] an improvement of the piezoelectricity of the acting layer of the membrane can be achieved by using scandium AlN ($Sc_xAl_{1-x}N$). For $x = 42.5$ % a maximum increased value of 27.6 pmV^{-1} was measured and observed near the phase transition from a wurtzite to a cubic type crystal structure starting at 45 %. Between 42 – 45 % the crystal structure is not predictable, if it becomes a wurtzite or cubic type and from 30 – 40% Sc concentration the crystal orientation is assumed to become lower, which leads to drastically decreasing of the piezoelectric constant d_{33} [42]. To avoid a cubic type structure, maintaining most of the good properties of AlN and already generating a strong increase of the piezoelectric constant, a fixed concentration for Sc could be used with $x = 27$ % [40-41]. Because of a possible improvement of the piezoelectric constant by the factor 4 to 5 [42], the necessary voltage U for a switching sequence can be lowered significantly [40].

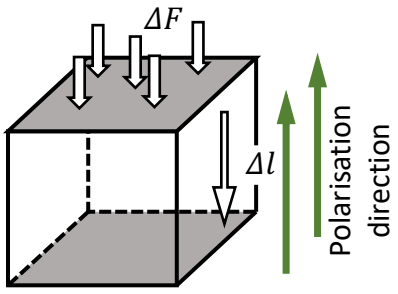

Figure 2.13: Unidirectional external force, length change and polarization are described by the tensor element d_{33}.

2.3 Thin film deposition and etching techniques

The knowledge of processes to create and structure thin films is of utmost importance in MEMS technologies, hence information for the realisation of thin film synthesis, as well as often used terms will be explained in this chapter.

2.3.1 Deposition of thin films

Basically, the deposition of thin films can be divided in two different basic treatments. Depositions are distinguishable, because of their physical state of reaction and will be differentiated between chemical (CVD) and physical vapor deposition (PVD). While the reaction materials for CVD are in the deposition chamber in the gaseous phase, the materials for PVD are in a solid state. CVD is for the generation of thin layers in the range down to a Nano meter scale utmost important and superior compared to PVD in case of covering topographically complex structures, because of its pre-defined directional nature of the impinging particles. [7]

2.3.1.1 Evaporation (PVD)

Physical vapor deposition describes a process, where a material gets deposited in form of a thin layer, while being in a solid state. A pressure chamber creates a vacuum of commonly $p = 10^{-9}\ kPa$, where the basic material, also called target and the substrate are placed inside. A heating process increases the target temperature until it starts vaporising. The temperature is strongly dependent on the basic material and can differ from $500 - 3000\ °C$ for most applications. If the target reaches the critical temperature and the vapor process has started, molecules are dissolved out of the basic material. Due to the high vacuum and therefore a low density of particles, the dissolved molecules will move right away from the target in a straight line. Because of the high linear transition of the molecules the distance between target and substrate can be increased. This causes an almost unidirectional impact of target molecules on the substrate, generating an anisotropic growth of a thin film layer, causing a so-called shadow effect. Also caused by the high vacuum further unwanted side effects like oxidation can be avoided. The specificity of the linear flight trajectory can positively exploited by pre-structuring the substrate in a way, that in defined areas no target material will be deposited. [43]
The heat to necessarily increase the target temperature can be applied in different ways, while every kind has its pros and cons. One simple way is to heat a so-called boat through electrical currents until the inside placed target material starts to vapor. One advantage is the already mentioned simplicity, while on the other hand impurities, caused by the setup itself are the biggest disadvantage.

2.3.1.2 Sputter Deposition (PVD)

Sputter deposition also belongs to the family of PVD processes, although no heat is used to dissolve molecules from the target. The biggest characteristic difference is the movement of target molecules towards the substrate, due to the mechanic working principle. Inside the sputter chamber ions, produced in a plasma are accelerated towards the target, where the impact ejects atoms and particles out of the solid surface. Free target particles get attracted by the opposite

charged substrate and starting there to form a new layer of target material. The vacuum inside the reaction chamber is significantly poorer compared to thermal PVD and therefore target molecules collide several times with other particles, which distracts them from their initial linear trajectory. The changed unpredictable way to the substrate minimises the shadow effect, by which also sidewalls will be coated with target material.
A disadvantage of the sputter deposition process is the relatively low deposition rate compared to other PVD processes. One way to increase the deposition rate is magnetron sputtering. Hereby the original sputter process gets enhanced by adding magnetic fields of permanent magnets behind the target. The applied field achieves a cycloidal flight path of electrons, what increase the collision probability with ions close to the target. This effect causes a higher ionisation rate and furthermore a higher deposition rate of up to 1 µm/min. [44]
Another variation of sputter deposition is reactive sputtering. In this case the plasma undergoes a special treatment by adding an additional gas, which reacts in its gas phase with the travelling target molecules and therefore a new layer is synthesized out of the combination of target and reaction material. This method fits especially well for oxides, nitrides, oxynitrides or carbides, because usually those materials are often unstable and only able to sputter with increased effort. As an example for reactive sputtering shall in relation to this work, the end product AlN be mentioned in Equation (2.28). [43][45]

$$2Al + N_2 \rightarrow 2AlN \qquad (2.27)$$

2.3.1.3 Plasma Enhanced Chemical Vapor Deposition (PECVD)

Plasma enhanced chemical vapor deposition describes an advanced process of CVD. As already mentioned, the target material in the deposition chamber is not in its solid or liquid phase available, but in its gas phase. In addition to conventional CVD processes, where a substrate is placed inside a reaction chamber and the target materials called precursors gets inserted in gas phase, the PECVD differs as the name says, due to an additional plasma functioning as energy source to keep the necessary reaction tempereature low, though the concept itself stays the same. One advance of PECVD over conventional LPCVD (low pressure chemical vapour deposition) or APCVD (atmospheric pressure chemical vapour deposition) is the reduced process temperature. The CVD process is rather straightforward and a simplification can give an overview broken down to three steps:

1. Target gases have to enter the reaction chamber
2. Reactions have to take place on the substrate
3. Unwanted by-products need to be removed

Thus, one or several gases enter the reaction chamber through gas inlets by mass transport, where the actual reaction takes place and the wanted reaction product starts to form a thin film on the substrate. The chemical reaction also creates by-products, which need to be transported out of the reactor [7]. Sufficient temperatures inside the chamber, where a reaction is initiated can significantly decreased by the plasma, which is usually a RF steady glow discharge in the precursor gas mixture [7], from $T_{CVD} = 1000\,°C$ to $T_{PECVD} = 200 - 500\,°C$. The lowered temperatures expand the range of materials, which means that also substrates which would not withstand the high CVD temperatures can now be covered with PECVD layers. The advantages of PECVD are a high grade of purity of the deposited reaction products and the advanced control of the build-up process of the layer on the substrate.[43][45]

The deposition during a CVD process depends on the diffusion through the layer described by Fick's law

$$F = -D\frac{\partial c}{\partial x}, \tag{2.28}$$

whereby F is the material's flux, D stands for the diffusivity of the gas and the concentration coefficient normal to the substrates surface is described by the fraction $\partial c/\partial x$. In a next step ∂x can be substituted with

$$\partial x = \delta = \frac{2L}{3\sqrt{Re}}, \tag{2.29}$$

where δ represents the thickness of the boundary layer, L is the length of substrate where the material is supposed to get deposited on and Re is the Reynolds number. After Equation (2.30) was inserted in Equation (2.29) the result

$$F = -D\frac{\nabla c\sqrt{Re}}{L}\frac{3}{2} \tag{2.30}$$

gives information about the growing behaviour of the film, because since Re is proportional to the gas velocity parallel to the substrate, the growth rate is inclining with the gas velocity in a reaction chamber, where the volume stays constant.[43]

In this thesis several different a-SiC:H layers were deposited with different parameters, which will be introduced in the Subsection 2.5.6. A formation of an a-SiC:H thin layer starts with a chemical reaction of methane (CH_4) and silane (SiH_4) inside the plasma enhanced reaction chamber of a CVD plant. The ideal gas phase reaction is given by

$$SiH_4(g) + CH_4(g) \rightarrow SiC(s) + 4H_2(g) \tag{2.31}$$

whereby g and s stand for gaseous and solid as the physical state of the participatory materials during the reaction [47]. However, an actual reaction within the scope of a PECVD will not result in ideal gas-phase reactions, but will vary in different reaction products (*e.g.* SiH_x, CH_x, $SiCH_x$) causing a typically amorphous a-SiC:H thin layer due to low substrate temperatures. Within this thesis a-SiC:H is used for nomenclature for *hydrogenate amorphous silicon carbide.* Though, the plasma enhanced CVD process does not only come along with benefits. Some possible triggered disadvantages are near surface defects caused by high-energetic particles due to ion bombardment, trapped charges and the more difficult controllability of the deposition due to the RF plasma [48]. Especially the ion bombardment can be significantly reduced by switching from a more common standard parallel-plate reactor performing a capacitively-coupled PECVD (CCP-CVD) to an inductively-coupled PECVD (ICP-CVD) process [49]. [7]

The a-SiC:H layers deposited within this thesis are realized with an *Oxford Instruments PlasmaLab 100 ICP-CVD* reactor (Figure 2.14), which differs from other ICP-CVD reactor due to its two plasma power sources (ICP and table power). Figure 2.14 also reveals the separated gas inlets for Argon (Ar) and the reactive gases Methane (CH_4) and Silane (SiH_4).

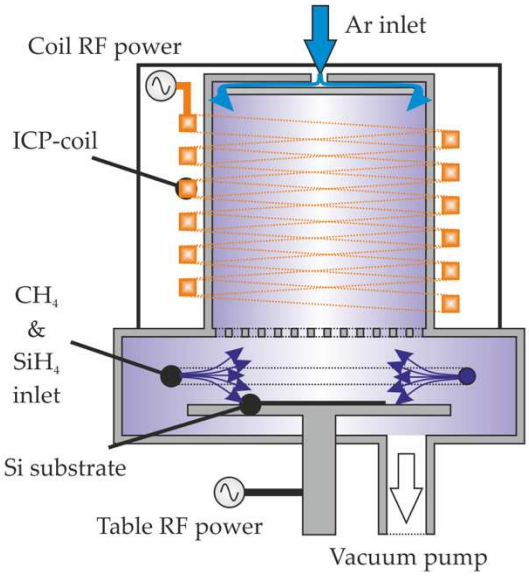

Figure 2.14: Schematic illustration of the *Oxford Instruments PlasmaLab 100 ICP-CVD* reactor used for the deposition of different a-SiC:H layers. [7]

2.3.2 Etching processes

In general etching processes are used to pattern thin layer arrangements by removing material, remove sacrificial layers or bulk material and can vary from physical processes like milling, cutting or laser supported patterning, to chemical etching which is distinguishable in two different processing techniques [43]. Wet etching techniques describe structuring processes, where liquid etchants are deployed, while dry etching is based on media which are gaseous. Both processes unite characteristics which can be described with common parameters as the selectivity S and the anisotropy factor A calculated by

$$S = \frac{R_1}{R_2} \qquad \text{and} \qquad A = 1 - \frac{R_h}{R_v}, \tag{2.32}$$

whereby R_1 and R_2 describes the etching rates of two different materials, of which one is desired to be ablated, while the other is not. The anisotropic factor A gives information about the alignment of the etching process, where R_h is the horizontal and R_v the vertical etching rate of the same material. [45]

2.3.2.1 Deep Reactive Ion Etching (DRIE or BOSCH-etching)

DRIE is a technique for high anisotropic etching. The fundamental working principle is the alternation of etching, ablation and passivation sequences, where ratios of diameter to depth up to $1/50$ are achievable. One processing cycle can be divided into three sub-sequences building up on each other. The first step is the acceleration of ionized gas particles generated in a plasma, to a substrate, where the impact detaches single atoms or bigger molecules from the solid surface (physical dry etching). Also the fact that in case of DRIE the plasma is formed by reactive gases should be mentioned. In a second step the bombarded and unstable surface of the substrate will be processed with dry chemical etching by radicals, which effect the material

isotopically and are already contained in the plasma. In most practical applications the gas sulphur hexafluoride (SF_6) is used. The first two steps happen simultaneously and are also known under the name reactive ion etching (RIE). The third step extends the process sequence to DRIE. For that, the gas mixture of the plasma is completely changed in order to achieve a passivation layer, whereby Octofluorocyclobutane (C_4F_8) is often used as passivation gas. Once the gas is inserted into the reaction chamber, the plasma turns the gas into a reactive gas, which impinges on the surface of the substrate causing a reaction leading to polymerization and forming of a Perfluorocarbon (PFC) passivation layer [46]. After a specific time, the layer has build-up and the gas in the chamber will be changed back to the initial SF_6 composition. The aggressive ionized gas gets again unidirectionally accelerated by a difference of potential towards the substrate and will now impinge the passivation layer in an anisotropic way. The bombardment with high kinetic energy ions destroys the passivation layer and furthermore the structure underneath. The chemical reaction in phase two of the DRIE process can only take place at locations where phase one already resolved the passivation layer (Figure 2.15). [46]

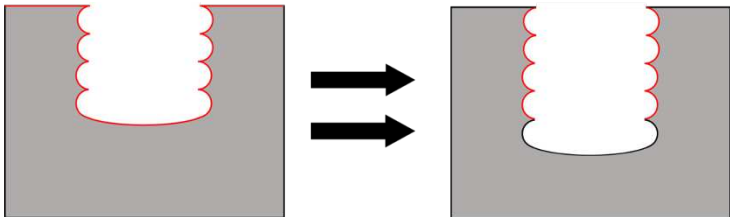

Figure 2.15: Schematics illustrating the DRIE process. The red boarder represents the PFC passivation layer.

To finish the second cycle the gas is changed to the passivation gas, which will again form the PFC layer. Repeating cycle per cycle creates highly anisotropic etching holes of a prior given shape and is stopped when the desired etching depth is achieved. Due to the process sequence itself, the remaining passivation layer needs to be removed in a final step. In most cases chemical wet etching is used for that purpose. The biggest advantage of DRIE is the creation of perpendicular deep structures with huge ratios of depth to diameter, manifesting in values close to 1 for the anisotropic factor A and convinces with a high degree of selectivity S. The production time for structures created by DRIE on the contrary is rather high, compared to other anisotropic etching techniques, ending in a low throughput and high facility costs. [43][45]

2.3.2.2 Wet Chemical Etching

Processes classified under the name of wet chemical etching have in common that the removal of material is triggered by liquid etchants like acids or leaches. As long as the diffusion process is not disturbed, which can be ensured by purity and agitation of the etchant, it results usually in a higher etching rate compared to dry chemical etching. Another notable feature is the high selectivity of materials, which is why the procedure was used in this work for the removal of SiO_2 layer with hydrofluoric acid (HF) without harming any SiC film structures. The exact approach of an HF release is described in Subsection 2.5.5, though the wet chemical reaction will be already displayed here:

$$SiO_2(s) + 6HF(aq) \rightarrow H_2SiF_6(aq) + 2H_2O(l), \quad (2.33)$$

whereby (aq) and (l) stands for aqueous solution and liquid and hexafluorosilicic acid as the resulting chemical reaction product written as $H_2SiF_6 \cdot H_2O$ [51]. Further advantages are the

cleanliness and the low costs of equipment compared to dry chemical etching. On the other hand the disadvantages are represented by mostly isotropic etching facility, except for materials with single crystalline lattice structures and the sanitary, environmental and personal endangerment of using those materials. Another disadvantage are the tough controllable etching rates, which could be compensated by natural etching-stop layer structures. [43][45]

2.3.3 Photolithography

The former described depositing and etching techniques can be applied on whole surfaces or just on particular parts of them. The process of photolithography is one very common and often used way to select specific areas which will get affected by the applied treatment. This step in the production cycle gives the possibility to create thin films in a specific pattern. A wafer gets completely coated by a photoresist, which can be structured by exposure to an UV-light source, in order to change the chemical composition of exposed parts of the resist. A photoresist contains components called sensitizers, which are the photosensitive part and change the chemical structure of the light exposed parts into soluble acid groups to get converted and removed in a development bath. To select which parts get exposed by the light source and which not, a glass mask with the desired pattern printed on, is introduced in several possible ways, like contact printing, proximity printing or projection printing. Each way to send light through the mask onto the wafer has its pros and cons, though only the high resolution of the used method of contact printing, especially hard contact printing, shall be mentioned in this thesis. After exposure and development, the desired structure of the resist will remain on the surface of the wafer and can be used for upcoming deposition or etching steps. [43][50]

2.3.3.1 Photo resist technologies

The most common and also in Subsection 2.5 used way to deposit a photoresist on a wafer is by the wet physical method of spin coating, showed in Figure 2.16. Here, the wafer is placed in the middle of a base (technical jargon: *chuck*), fixed through a vacuum and get to turn with several thousand rounds per minute, depending on the targeted resist thickness. A syringe gets loaded with the necessary amount of photoresist and while the wafer is spinning, unloaded again in the middle of the wafer, whereby due to the centrifugal forces the wafer gets evenly thick coated.

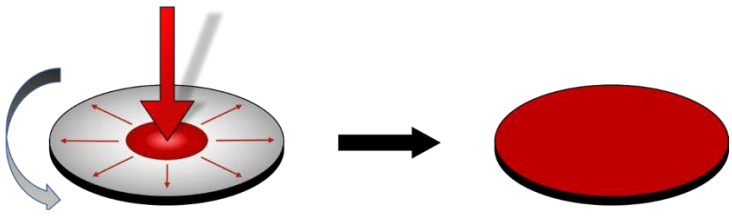

Figure 2.16: Resist is placed with the help of a syringe in the middle of a spinning wafer, from where it spreads evenly over the whole surface.

Different kinds of photoresists are available to achieve specific structures adapted to follow-up processing steps and related materials. All of them can be summed up in two main characteristic resist groups named positive or negative resists. The advantages and disadvantages of each group are listed in Table 2.1. [45]

Table 2.1: Comparison of advantages and disadvantages of positive and negative resists. Despite their differences, both resists get spin coated on the wafer in the same way, as well as exposed through a mask to UV-light, though the emerging effects will be different and express themselves after the development. Figure 2.17 shows the differences of the remaining resist structure.

Positive resist	Negative resist
Exposed structures get **soluble**	Exposed structures get **insoluble**
+ no swelling during development	- swelling during development
+ high resolution	- lower resolution
+ can be removed by leaches	- harder to remove
+ high resistive in case of plasma etching	- low thermal stability
- only conditionally resistive against acids	+ more resistive against wet chemical etching
- bad attachment	+ very good attachment
- expensive	+ cheap
	+ high sensitivity of light exposure

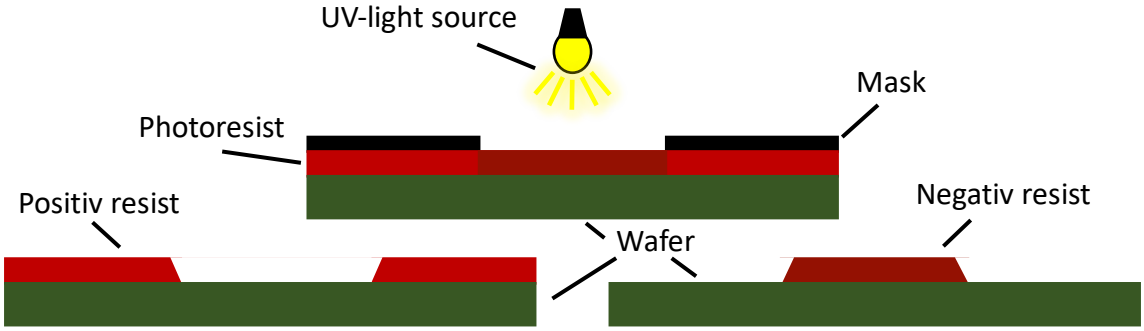

Figure 2.17: Difference between positive and negative resist after developing the same light exposed area. Bottom left: remaining resist structure of positive resist. Bottom right: remaining structure of negative resist

For the development and resolving of photoresist, different solvents can be used depending on the kind of resist. Starting with positive resists aqueous solutions like sodium hydroxide, potassium hydroxide or tetramethylammonium hydroxide can be used to remove material, which got exposed by an UV-light source before, whereas negative resists require more problematic organic solvents in terms of environmental and health safety, like xylenes, which resolve structures that were not exposed to light.
A special kind of resists is introduced by image reversal (IR) resists, which exist for both, positive and negative resists. Hereby, an additional step needs to be carried out during the development process sequence to change the chemical structure of an initial positive resist into a negative one and vice versa. Overhanging sidewalls are now achievable with IR positive or negative resists (Figure 2.18), which can be greatly used to create the already mentioned shadow effect, which is required for the lift-off process, specified in Subsection 2.5. [45][50]

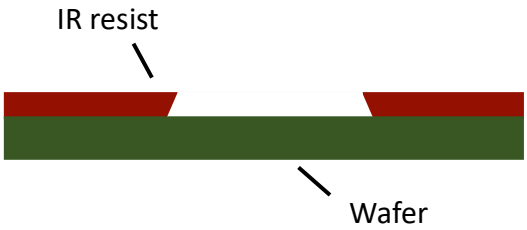

Figure 2.18: Remaining structure of positive IR-resist after development.

2.4 Techniques for thin film characterization

This section of the thesis reveals methods to quantify stress levels in thin films, since they cannot be measured directly like electrical current with an amperemeter. Equivalent quantities can be determined and converted in stress values by several methods, which differ from each other in complexity and usability. Also, a method to quantify the actual amount of carbon in an a-SiC:H thin layer will be presented.

2.4.1 Waferbow

The waferbow measurement is a non-destructive and easy tool to measure the stress level of thin films, though it does not give any information about the structure of the layer itself. The stress will be calculated with the Stoney Equation (2.35), which takes the arising bow of a substrate after depositing a thin layer in account, depending on the thickness. Thus, two measurements are required, whereby once the radius of the bow of the wafer without coating is measured and once with the interested deposited layer on it. The dimensions are determined by capacitive proximity sensors, placed for high resolution over the whole wafer surface [34] and the average thickness by a Filmetrics© F20-UVX thin film analyser based on altered wavelengths, after being reflected off a film [52]. Introducing the results of the measurements into the Stoney equation, leads to a value for the wanted stress level σ with

$$\sigma = \frac{E d_S^2}{6(1-v)d_F}\left(\frac{1}{R} - \frac{1}{R_0}\right), \qquad (2.34)$$

whereby E is the Young's modulus, d_S and d_F are the thicknesses of the substrate and film, v stands for the Poisson's ratio, R_0 is the curvature radius of the wafer before and R after deposition of a thin film. [30]

2.4.2 Laser-Doppler-Vibrometer

The Laser-Doppler-Vibrometer is an instrument to measure small deflections and high frequent vibrations and belongs to the kind of optical and contactless measuring devices. The working principle of an LDV is the optical interference of two laser beams with known wavelengths, which are coherent to each other. While one beam is used for the actual measurement, the other works as a reference.

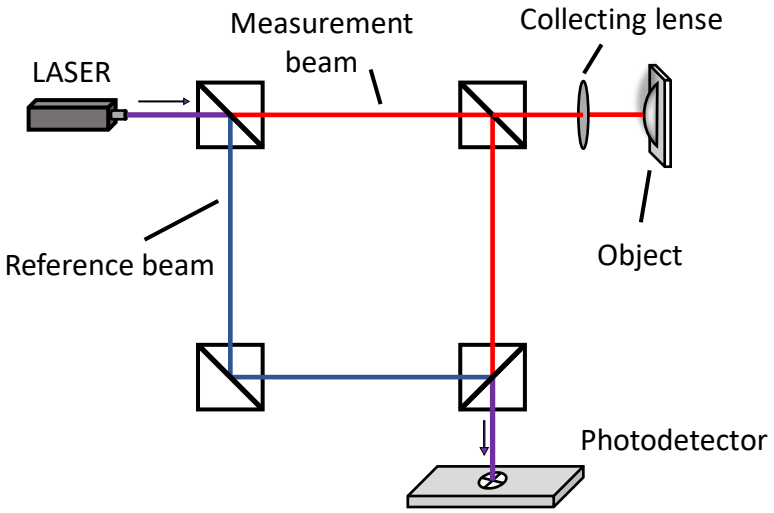

Figure 2.19: Working principle of a LDV.

As it can be seen in Figure 2.19 a beam splitter divides an initial laser beam into measure and reference beam, resepctively. The measure beam is directed to the surface of an object, gets reflected and altered in phase and frequency depending on the movement due to the Doppler effect. Both beams get superimposed and imping at a photo detector, which records a modulated intensity signal

$$I_{tot} = I_1 + I_2 + 2\sqrt{I_1 I_2 cos\left[\frac{(r_1 - r_2)}{\lambda}\right]}, \qquad (2.35)$$

where I_1 and I_2 are the single initial intensities of the laser beams and the term $\frac{(r_1 - r_2)}{\lambda}$ represents the phase shift for a specific wavelength λ. Because of the modulation of the signal's intensity, Equation (2.36) enables the possibility to directly draw a conclusion on the amplitude and velocity of a deflection. [53]

2.4.3 White-Light-Interferometry (WLI)

White-Light-Interferometry is often used in the field of three-dimensional measurement of structured microsystems and belongs also to optical-contactless measurement techniques (Figure 2.20).

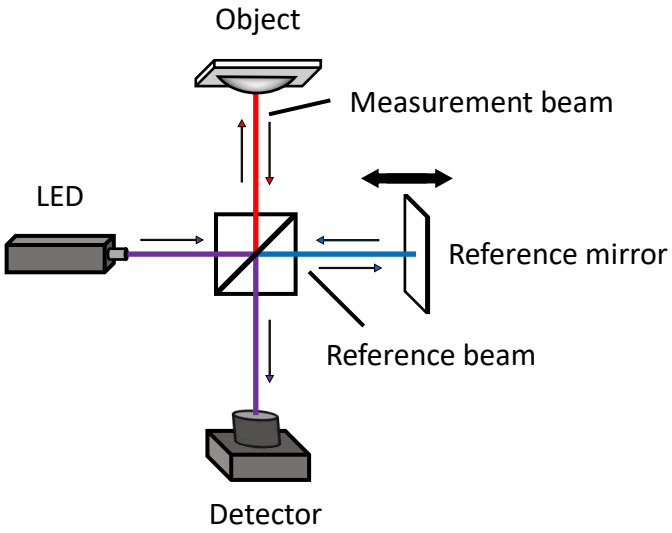

Figure 2.20: Working principle of a WLI.

Again, a laser beam will be split up in a measurement beam, which hits the desired object, where it gets reflected and a reference beam, which gets reflected by an adjustable mirror. After the two beams are superimposed again, the interference output signal is measured by the detection system. If the length of the measurement arm and the reference arm is coherent, the according pixel results in a maximum intensity. Every point of the object, which does not correspond to this condition, results in a lower intensity. Thus, the detection system records all pixels of the same height. Significant values can only be generated in the range of wavelengths of the applied laser. Differences in the length of the pathway of measure- and reference beam can reach a maximum of 1.5 µm in case of white light. The main advantage of WLI over LDV is the measurement of static deflections. [54]

2.5 Fabrication process of biocompatible bistable membranes

This subsection of the thesis will briefly describe the manufacturing of the used bistable membranes. The processing steps and specific settings of the production parameters are close to those reported in [11] and [55].
A 4-inch SOI wafer with 350 µm thickness and a 2 µm device layer above a 1 µm buried oxide (BOX) layer served as substrate for membrane fabrication (Figure 2.21 a). By increasing the thickness of the device layer, the likeliness of a membrane to show switching behaviour will decrease [55], which is why in the scope of this work no other substrates were used.

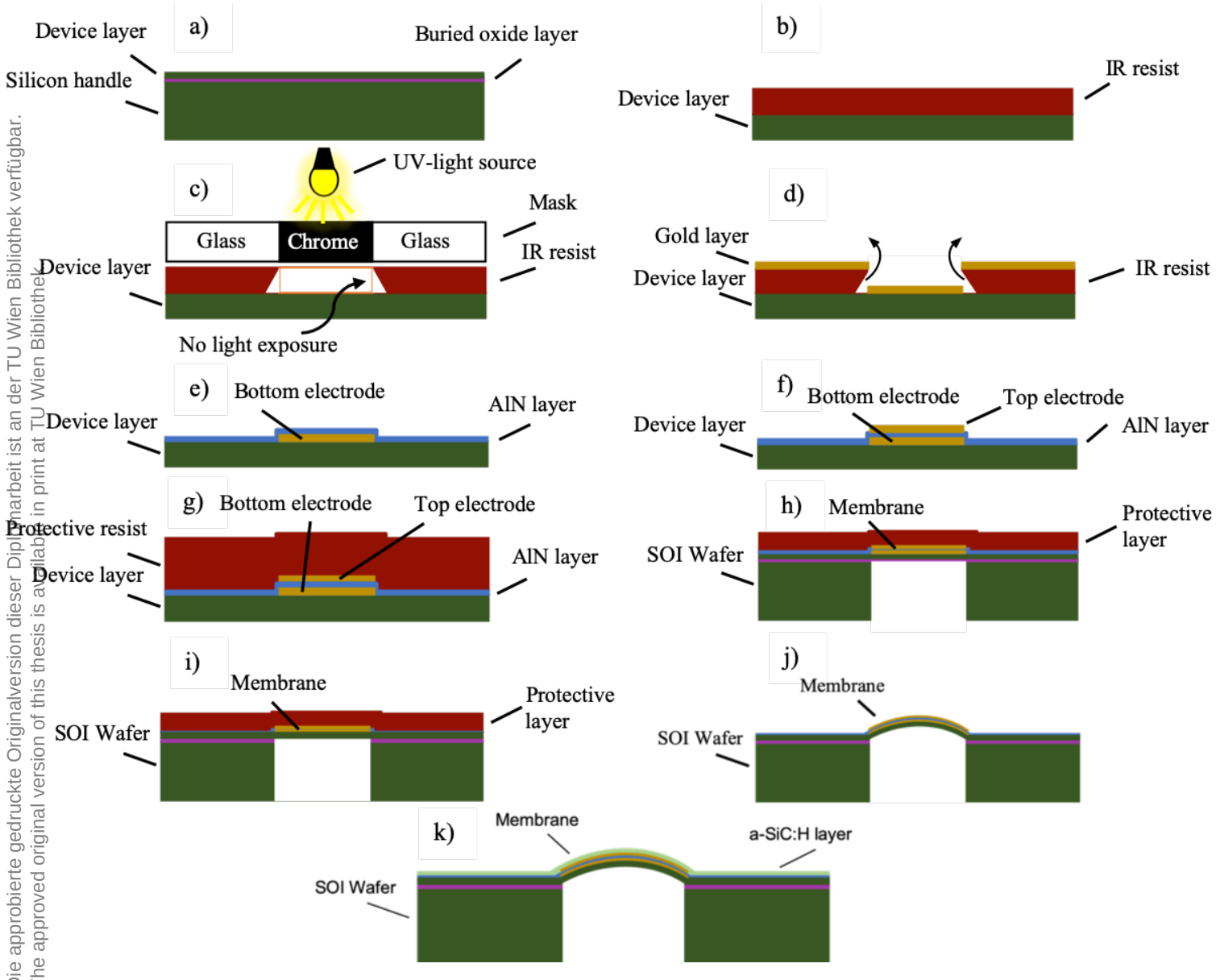

Figure 2.21: Fabrication steps of an a-SiC:H coated bistable piezoeletric membrane
a) SOI-wafer with 350 µm handle, 1 µm BOX and 2 µm silicon top layer. b) Lift-off step 1: spin coating of 1.8 µm positive IR photoresist. c) Lift-off step 2: UV-light exposure through a patterned mask and subsequently development. d) Lift-off step 3: thermal PVD of the bottom layer and removment of the residual resist to achive the desired structre. e) 400 nm AlN layer by DC-sputtering and liftoff process. f) Top electrode. g) 18 µm protective resist by spray coating. h) 1500 cycles of DRIE-etching, naturally stopped by the SiO_2 layer. i) 15 min HF-bath to remove the BOX layer. j) Resolving the protective resist. The membrane shows first buckling behaviour. k) SiC coating with a gasflow ratio of Methane to Silane of r_{CH4} of 0.05.

2.5.1 Bottom-electrode

Before the first layer on top of the device layer could be deposited, the wafer needed to be cleaned. Therefore, the wafer underwent an HF-dip, got washed up with de-ionised (DI) water and cleaned with a wafer cleaner. The bottom electrode was deposited by lift-off process, which included the following steps. To begin the process the wafer got pre-baked in order to get rid of water residuals. The positive IR resist AZ5214 was spin-coated on the wafer to achieve a continuous 1.8 µm thick resist layer. The wafer got soft-baked to dry the resist for the subsequent hard contact photolithography and light exposure of 2 seconds (Figure 2.21 b). The follow-up reverse-bake turned the resist from positive to negative and by flood exposure and spray development (using AZMIF726 development), the structure pictured in Figure 2.21 c) was achieved. As the material of choice for the electrodes, functioned gold in combination with a pre-layer of chrome as adhesion promotion agent, whereby the chrome layer got deposited first by electron beam evaporation, while the gold layer deposition was conducted by direct heating evaporation. The final step of the lift-off process structured the arisen 200 nm thick Au/Cr layer by ablating the residual resist with acetone, whereby the on-top metal layer was removed as well (Figure 2.21 d). Since acetone does not dry without remains, a subsequent cleaning by isopropanol and a wafer cleaner was needed.

2.5.2 Aluminium nitride layer

On top of the bottom-electrode the AlN layer got deposited, which will work as the active layer inside the membrane (Figure 2.21 e).
The layer was deposited by reactive DC sputtering and also due to a lift-off process for the contact pads, in order to let them remain uncovered of any other material for further contacting and bonding. Subsequently the wafer were cleaned again as described in 2.5.1.

2.5.3 Top-electrode

The top-electrode was deposited in the same way as the bottom electrode by thermal heating and a lift-off process to structure the electrode in the desired way, though some parameters had to be changed, since an AlN layer covers the wafer. By increasing the light exposure times of the photoresist the possibility of imperfections in the developed resist layer were minimized. Also the resists thickness was increased, while the PVD processing parameters for Cr and Au stayed unchanged. A final cleaning cycle completed the top-electrode manufacturing step (Figure 2.21 f).

2.5.4 Bosch- or DRIE-etching

This step contains the treatment of the back side of the wafer, which is why the front side with the already deposited layer structure got protected from mechanical and chemical wear with an 18 µm spray coated resist layer (Figure 2.21 g). The purpose of this process sequence was to release the created membrane structure from the bulk material by high anisotropic Bosch-etching of the handle layer. The back side got structured with an 8 µm thick layer of AZ6632 positive photoresist, light exposed and developed by AZ726MIF developer. The wafer was

placed inside the Bosch-plant and processed with 1500[1] cycles as described in 2.3.2.1. In [56] only 1200 cycles were used for the same handle layer thickness, though the same results were achieved, because of the BOX-layer, which works in case of the high selectivity for organic materials of DRIE-etching as natural etching stop layer. The achieved structure can be observed in Figure 2.21 h.

2.5.5 HF-treatment

To finally release the membrane, the buried oxide layer was removed by wet chemical etching. Due to the high selectivity of hydrofluoric acid to organic materials, the wafer is treated with a 12.5 % buffered HF-bath for several minutes, to remove the BOX layer directly underneath the diaphragms, without harming any other structures (Figure 2.21 i).

2.5.6 Cutting and bonding

The diaphragms, including connection pads and pathways, were designed to fit a housing for wafer parts with dimensions of 6 x 6 mm^2. Thus, the wafer was cut in 124 pieces by a diamond wafer saw with 40000 rpm and a feed of 4 mm/s. The single wafer parts were held together by blue-tape[2], wherefrom they needed to get detached by hand and cleaned with acetone and isopropanol to remove the protective resist layer. This is the first time the membrane shows buckle behaviour, caused by the pre-set stress of the previous deposited thin layers (Figure 2.21 j). The chip can now be inserted into the housing and be bonded with a very thin gold wire by an ultrasonic induced welding process [57], though only a few promising membranes got a housing for further tests, while the rest remained unbonded.

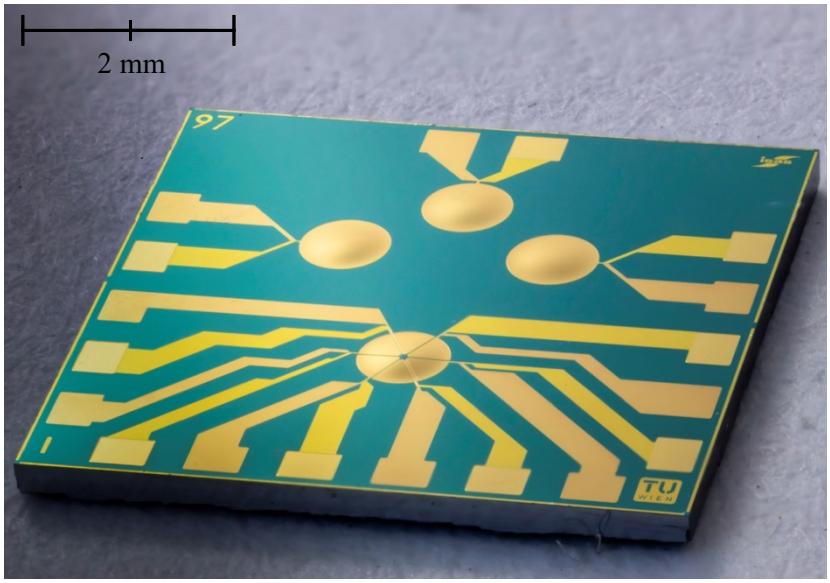

Figure 2.22: Example for a possible 6 x 6 mm^2 sample, comprising of four 700 µm membranes.

[1] One cycle contains of 3 s etching and 2 s of ablating and creating a new passivation layer
[2] Special sticky wafer foil, 125 µm thick

3 Biocompatible a-SiC:H layers

This part of the thesis is new compared to [11] and [55], which is why it will be described in a more detailed way in order to understand the chosen deposition parameters for an additional a-SiC:H membrane layer (Figure 2.21 k).

3.1 Different silane to methane ratios

This layer has two main tasks, which both can only be controlled together by the settings of the following production cycle. The first part is to ensure the biocompatibility by coating the whole chip with a SiC layer. The layer needs to be thick enough to serve this purpose, but also thin enough, not to influence the behaviour and structure of the prior deposited layers in a negative way. The second part is to control and set the total stress level. In case of this membrane the stress level of the a-SiC:H -layer should be as close to zero as possible or even better slightly compressive.

A layer of a-SiC:H can be deposited under different conditions with PECVD. Depending on the substrate temperature, reactive gas flow variation, plasma power, chamber back pressure und processing time, the layer will result in different thicknesses and stress levels. Since the electrochemical potential of carbon is comparable to the one of living tissue, a gas flow ratio with low content of silane would be preferred in case of a likely higher biocompatibility, though the hydrophilicity decreases with an increasing carbon content of the SiC layer. As reported in [7] the resulting stress level of the a-SiC:H layer can be set as close to zero as possible by choosing the right values for the deposition parameters seen in Table 3.1.

Table 3.1: PECVD constant parameter settings.

Substrate temperature [°C]	Plasma power [W]	Chamber back pressure [mTorr]
25	800	30

25 four-inch silicon wafer were processed by holding these parameters constant, but changing the processing time and gas flow variation in order to find the best symbiosis of thickness and stress level of a deposited a-SiC:H layer. The goal was to achieve a layer which is as thick as possible, while holding the stress level as close to zero as possible. The gas flow consisted of 50 sccm Argon and a combined amount of 20 sccm of methane and silane. The gas flow ratio of CH_4 and SiH_4 can be varied from $r_{CH4} = 0 \dots 1$, while values around 0 and 1 are the most promising for a resulting preferably neutral stress value, according to [7]. Different gas flow ratios were processed once with 10 min processing time and once with 5 min.
Table 3.2 lists the most extreme stress values, depending on the altered processing parameters.

Table 3.2: Most extreme stress values of different a-SiC:H coated Si-wafer.

Wafer name	Processing time [min]	Gas flow ratio r_{CH4}	Layer thickness [nm]	Layer stress [MPa]
MO_25	5	0.05	74	-192
MO_24	5	0.1	62.4	-235
MO_16	5	0.9	15.8	-875
MO_15	5	0.95	13	-1002
MO_14	10	0.05	106.5	-141
MO_13	10	0.1	103.5	-187
MO_07	10	0.9	45.5	-505
MO_06	10	0.95	39.8	-714

Plotting the results of the measured stress and thickness values depending on the processing time over the gas flow ratio r_{CH4} ends in a high controverts diagram compared to the expected one, predicted in [7]. While the deposition rate and hence the thickness was as expected (Figure 3.1), the resulting stress values differed strongly from values of $r_{CH4} > 0.6$ (Figure 3.2, blue and orange line). The difference between the predictions of [7] and the measured results was most likely, because of the combination of altered parameters, also the comparison of stress levels of layers with varying thicknesses is complicated to interpret.

Using the known parameters of the previous measurements another 13 wafers were coated with different r_{CH4} ratios, while the processing time was altered in order to achieve a constant layer thickness of all different coatings of 70 nm (Figure 3.1, grey line). The stress values of the deposited layers (Figure 3.2, grey line) corresponded better with the ones in [7].

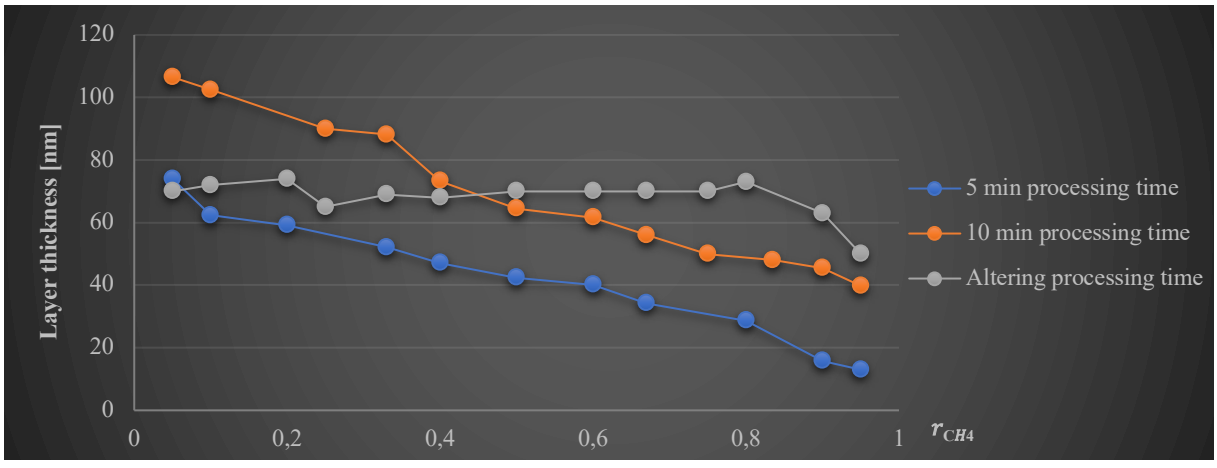

Figure 3.1: Resulting layer thickness depending on altered r_{CH4} and processing time parameters.

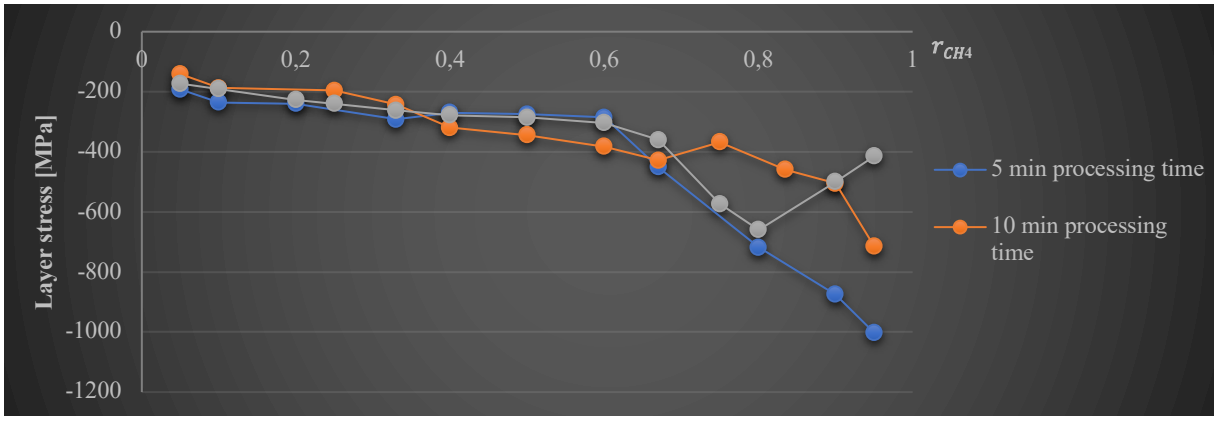

Figure 3.2: Resulting layer stress depending on altered r_{CH4} and processing time parameters.

3.2 Altered membrane behaviour

These stress pre-measurements were used to figure out the possible best settings of parameters for the actual coating process with a-SiC:H of the membranes, for which four different parameter sets were chosen according to Figure 3.1 and Figure 3.2. While the substrate temperature with 25 °C, the plasma power of 800 W, the chamber back pressure with 30 mTorr and the gas flow of Argon with 50 sccm stayed the same, the processing parameters of time and gas flow ratio r_{CH4} were altered (Table 3.3).

Four membrane arrays were processed with four different parameter sets, to receive values helping to figure out which parameter set would be the best in terms of not changing the membrane's behaviour. Pre- and post-measurements were executed, while in between the a-SiC:H layer was deposited. Therefore, 30 so far processed diaphragms were loaded with an electrical sinusoidal signal of 5 V amplitude between top and bottom electrode and the responding vibrational behaviour was measured optically with a LDV. After the membranes got coated with different a-SiC:H layers, the same measurements as just described took place to compare the altered behaviour of the membrane through an additional tensile stress layer. The results can be seen in Table 3.3.

Table 3.3: Altered displacements of membranes after different SiC composition coatings.

Name	Processing time [min]	Gas flow ratio r_{CH4}	Remaining amplitude after SiC [%]	
			Each	Average
W17_16_105 W17_15_39 W17_17_60 W17_17_85	10	0.05	100 93.33 92.72 95	95.26
W17_17_35 W17_17_105 W17_18_15 W17_18_57	10	0.25	96.47 98.88 85.65 92.30	93.33
W17_18_21 W17_18_65 W17_18_41 W17_18_3	5	0.05	94.20 100 95.81 100	97.50
W18_22_111 W18_22_21 W17_15_65 W18_22_90	5	0.25	100 91.37 93.25 97	95.41

According to Table 3.3 a set of parameters with a gas flow ratio r_{CH4} of 0.05 and 5 min processing time will affect the membranes the least. This stands in good contrast to a maximum reachable thickness of the SiC layer, which guarantees a more continuously processed layer and hence less chance of small areas without a biocompatible SiC coating. This set of parameters was chosen for further coatings of membranes and the characterization of their vibrational behaviour in air and fluids addressed in Chapter 5.

4 Deposition of living cells

This chapter reveals the interaction of living cells with different a-SiC:H layer compositions to find a relation between cell attachment and varying ECMs. In Subsection 3.2 13 Si-wafer were coated with different r_{CH4} ratios with the same thickness and got defined over their occurred stress level. Those wafers were cut in 6 x 6 mm^2 parts with the described treatment of 2.5.6 and used for the follow-up cell planting and measurements.

4.1 Influence of different silicon carbide layer compositions on living cells

To achieve quantitative and statistically correct results many measurements and different repetition cycles would have been required and since such expenses would have exceeded the limits of this work, the intended results can only give a tendency for further measurements. However, the possible distinguishable outcomes of the cell attachment and proliferation behaviour on different a-SiC:H substrates will be interpreted and set in correlation of the layer's stress level.

4.1.1 Cell planting setup

The proliferation of cells is not only depending on temperature, time and a nutrient solution, but also on the direct contact to the extra cellular matrix. In order to clarify the impact of different a-SiC:H ECMs on cells, six sets of different pre-treatments were used for the cell planting, while each set consists of the 13 a-SiC:H compositions of 3.2, resulting in 78 different samples (Figure 4.1).

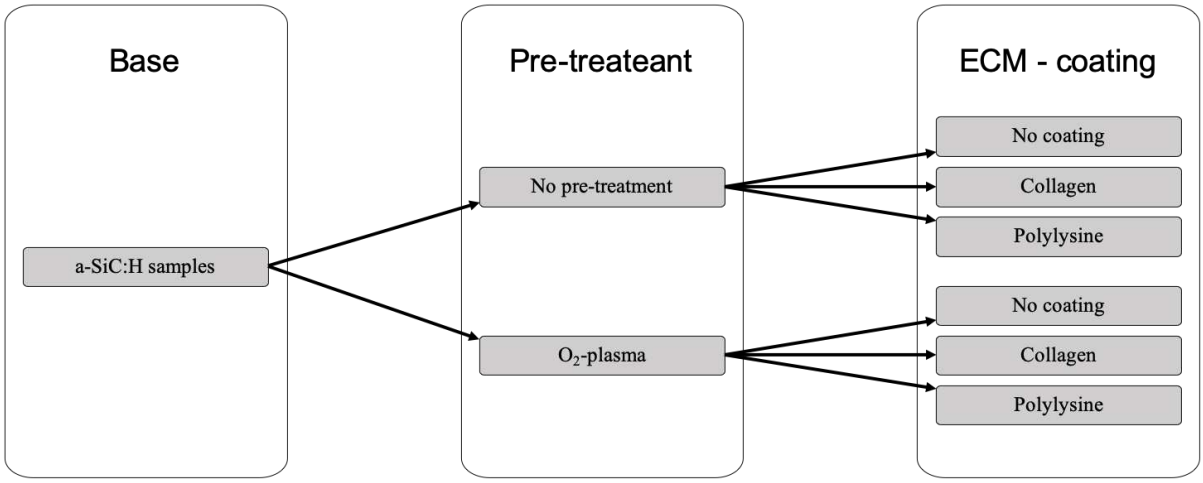

Figure 4.1: Overview of the different substrate pre-treatments and coatings.

Those samples were supposed to give information about the cell attachment and a comparison of the proliferation on different coated substrates after a specific number of days. For the purpose of containing the specimens nine 24-well arrays were used. Furthermore, additional samples were planted to gain also information about the growth rate, whereby the cells of the

same substrate would be counted on day $X-2$, $X-1$ and day X. Since this additional task would require another two complete planting sets of 78 samples each, this part was not conducted in the full extend, however, an educated selection of samples was processed to investigate a possible tendency of different growth rates of cells on different substrates (Figure 4.2).

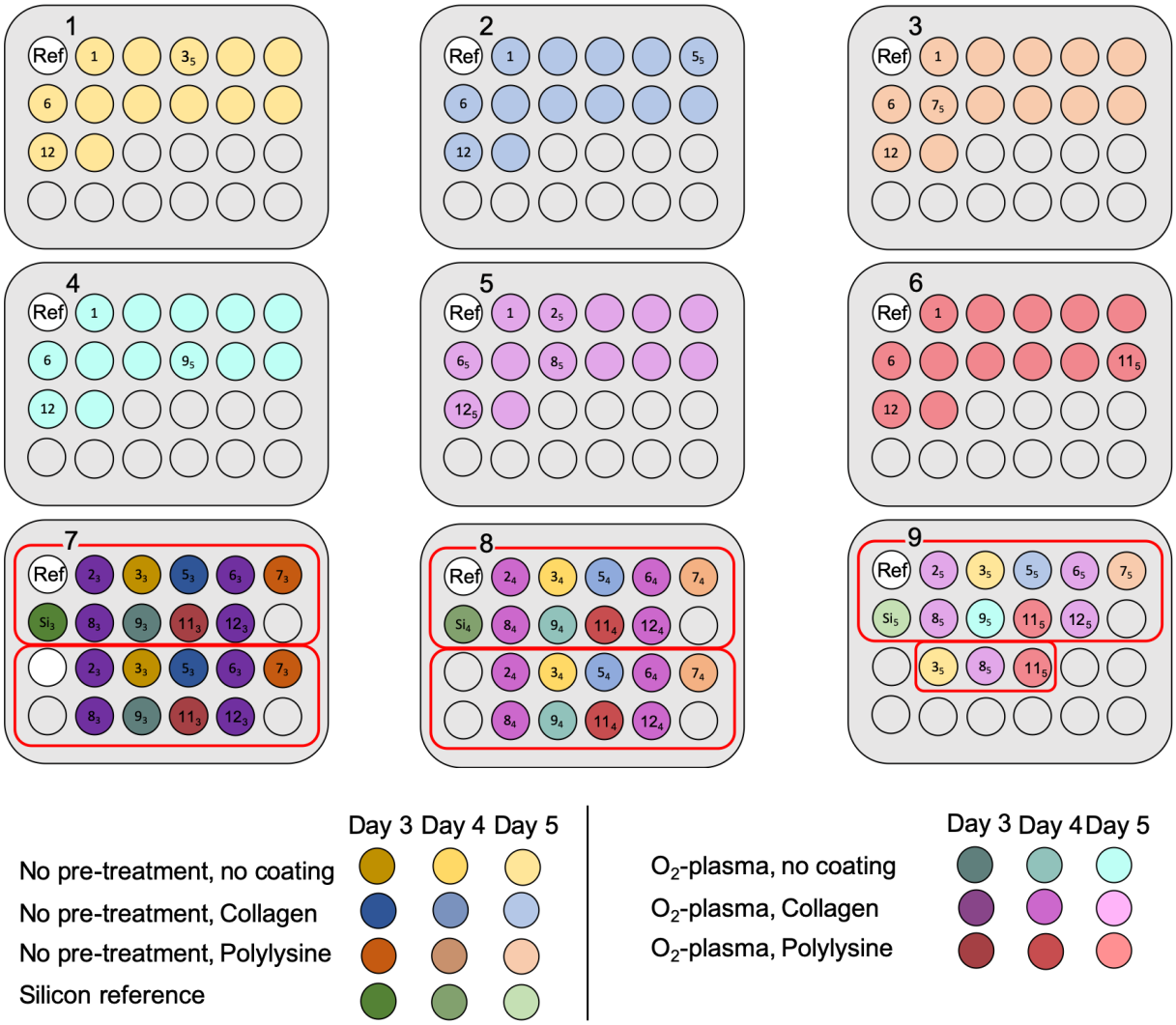

Figure 4.2: Organisation of different prepared specimens for the subsequent cell cultivation. Well plates one to six were counted on day five. The upper red marked part of the well plates seven and eight was counted on day three and four, respectively. The lower red marked part of well plate seven and eight as well as the upper part of well plate nine was photographed on days three to five. SEM pictures were taken of the three red marked samples of well plate nine on day five. The capital numbers stand for the r_{CH4} value, introduced in Table 4.1, while the subscripted numbers stand for the counting day.

To compare the growth rates, the proliferation and the cell attachment of another two different reference samples were included in the measurements. One is simply the bottom of a single well, while the second is a pure silicon specimen, which will also be present in triplicate. They were chosen as reference, because proliferation values of those surfaces might be interesting, if set in contrast to the rest of the samples.

Table 4.1: The blue marked fields in the most left column give an overview of which r_{CH4} compositions were counted on day three to five and imaged as well. Green and purple coloured fields mark the exact sample and related SiC-number of each substrate. The O_2-plasma treated and collagen coated samples are marked purple to highlight the increased number of investigated samples.

r_{CH4}	untreated, uncoated	untreated, Collagen	untreated, Poly-D-Lysine	O_2-plasma, uncoated	O_2-plasma, Collagen	O_2-plasma, Poly-D-Lysine
0.05	1	1	1	1	1	1
0.1	2	2	2	2	2	2
0.2	3	3	3	3	3	3
0.25	4	4	4	4	4	4
0.33	5	5	5	5	5	5
0.4	6	6	6	6	6	6
0.5	7	7	7	7	7	7
0.6	8	8	8	8	8	8
0.66	9	9	9	9	9	9
0.75	10	10	10	10	10	10
0.8	11	11	11	11	11	11
0.9	12	12	12	12	12	12
0.95	13	13	13	13	13	13

4.1.1.1 CaCo-2 cells

The cells used in this work are declared under the name CaCo-2 cells and are used in this work, because of their property to form a confluent monolayer instead of clusters. These cells are derived from a colon carcinoma, but if cultured under the right conditions they change their morphological und functional properties in a way, that their altered phenotype resembles the cells lining the inner wall of the small intestine. The quality to form a cell monolayer has been taken advantage of, in order to measure the area covered by cells after specific time intervals and furthermore the likeliness of the cells attaching not to each other, but side by side on the provided substrate. [59]

4.1.2 Proliferation and growth phase

The experimental part started with the preparation of the 132 specimens as pictured in Figure 4.2. The O_2-plasma was conducted by a STS© 320PC plasma generator for five minutes[1], in order to create an oxygen terminated SiC surface. The O_2-plasma treatment increased the hydrophilicity, which was measured by the associated contact angle (Figure 4.3 and 4.4). To ensure a viable surrounding for living cells, the pre-treated specimens needed to get sterilized, whereby a wet chemical procedure with 70 % ethanol was chosen, since many samples could be treated at once. Next, the specimens got coated with collagen and Poly-D-lysine as ECM and were placed in wells, which will be filled afterwards with 1 ml of a nutrient solution called MEM (Minimum Essential Medium) with 20 % FBS (Foetal Bovine Serum), 1 % of Penicillin and Streptomycin working as antibiotics, 1 % Sodium Pyruvate and 1 % L-Glutamine to provide aliments for the cells to fulfil their proliferation purpose. To finish the setup an amount of 50.000 CaCo-2 cells was added to each sample and as well to the reference wells. All nine

[1] With 150 W power, 150 mTorr chamber back pressure, 50 sscm of O_2 gas flow and 25 °C of substrate temperature.

24-well plates were placed inside a BINDER incubator at constant 37 °C for five days. On day three and four the relevant samples were taken out of the incubator to determine the increased number of cells at this point. On day five, the remaining cell cultures were removed from the incubator and counted individually.

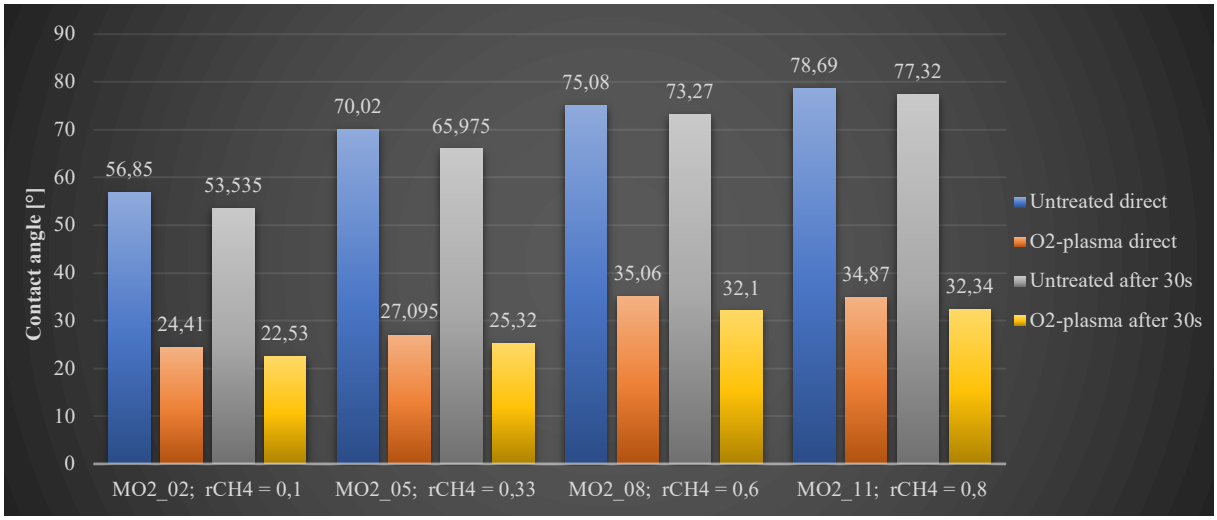

Figure 4.3: Altered contact angle of four different representative a-SiC:H coatings

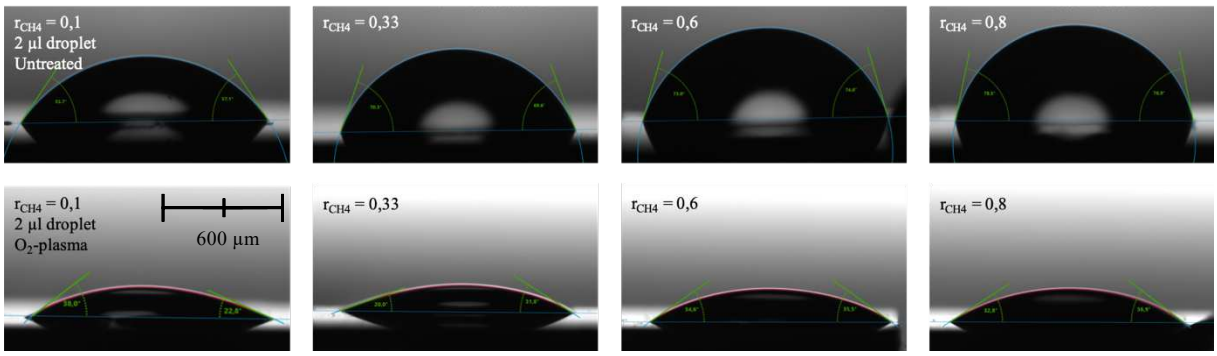

Figure 4.4: Visual impression of the decreasing contact angle on all substrates and therefore increasing hydrophilicity, because of a 5 min O_2-plasma treatment.

4.1.2.1 Detaching cells from substrates and cell counting

The first batch of cells was removed from the incubator on day three and counted with a PerkinElmer© EnSpire 2300 plate reader. This device does not count the exact cell number in the first place, but measures the changed fluorescence of a solution prior added to the cells called PrestoBlue, which gets partly absorbed and digested, depending on the number of cells. 50 µl of PrestoBlue were added to 500 µl of MEM and after half an hour analysed by the plate reader. Cells measured by this procedure remain unchanged and can be used for further tests as detaching and counting of single cells.
Despite many existing, physical and chemical well working ways of cell detachment, only one specific was used in the scope of this work. To dissociate adherent cells from their substrate, integrins can be broken down by the process of trypsinisation using the proteolytic enzyme trypsin. This enzyme can naturally be found in the digestive tract and once added to a cell culture it basically starts to digest the connective proteins of cells to their surrounding ECM.

Detached cells can be differentiated according to their shape, because the more integrins are broken down, the rounder the cells appear. Completely detached cells are floating in the suspension close to the substrate's surface. Trypsinisation needs to be stopped after a specific time depending on the substrate, cell type and amount, otherwise the digesting process goes on until cleaving the cells surface, which would make them invalid for further cell counting. [60] The process of cell counting started by replacing the well, because only cells attached to the surface of the samples were supposed to be counted. By adding 500 µl of trypsin for 5 minutes at 37 °C to the well, cells were detached from the surface, rather bad or good depending on coating and pre-treatment. The ongoing trypsinisation was stopped by 1 ml of MEM and cells floating in the solution were subsequently extracted with a syringe. 100 µl of cell suspension was added to 10 ml CASY TON and counted by a CASY© cell counter, which distinguish cell fragments from single cells and cell clusters by size and extrapolates to the actual number of cells. On day four and five cells of the appropriate batches underwent the same treatment.

4.1.3 Imaging of cells

Cells counted on day three and four grew on the same kind of substrate to compare the measurements. A third sample of every kind of these counted samples existed for another counting on day five. To give an example, a specific SiC layer processed with a methane to silane ratio of *e.g.* $r_{CH4} = 0.8$, was cultured three times with cells for counting measurements on day three, four and five as described in 4.1.2.1. Which SiC compositions were chosen to be measured on all three days shows Table 4.1. All of those just described samples were cultured two times, once for counting and once for imaging purposes. Cell cultures, which were imaged got stained with Fluorescein Diacetate (FDA) and Propidium Iodide (PI). While PI just diffuses through cell membranes of dead cells, FDA is only absorbed by living cells and gives a good contrast of viable to dead cells. The pictures were taken through a fluorescence filter by a reflected light microscope (DM6000) and a LEICA camera system.

As already mentioned, the time dependency measurements are only supposed to give a possible tendency of a change in cell proliferations on differently pre-treated substrates. Further and more precise results can be achieved by conducting more samples. However, the O_2-plasma pre-treated and collagen coated sample line (Table 4.1, purple marked fields) was intentionally chosen to be investigated closer in order to find a possible time dependency of cell proliferation on different composed a-SiC:H layers. Additionally, if there is no difference in the growth rates of the other samples the dependency of a collagen coating can be neglected.

On day five three samples were fixed with PFA/GA (Paraformaldehyde/Glutaraldehyde) for SEM recordings of single cells. After fixing the cells on the substrate, the whole water content needed to be extracted by the use of ethanol baths of increasing concentrations. This process ended by three 100 % ethanol baths to ensure the absent of water and subsequently drying the samples with HDMS (Hexamethyldisilane).

4.2 Outcome

The outcome of a cell experiment is often hard to interpret. Performing an experiment on one day and repeating it after some time could produce very diverging results. That is why the usual way of starting a cell experiment is to carry out the whole experiment in triplicate. Since this work was not conducted at a biological institute, the experiment was just performed a single time, taking into account that the results cannot give precise and correct predictions, though could be able to confirm presumptions and give tendencies for further and more biologically correct experiment setups.

4.2.1 Cell growth on pre-chosen substrates

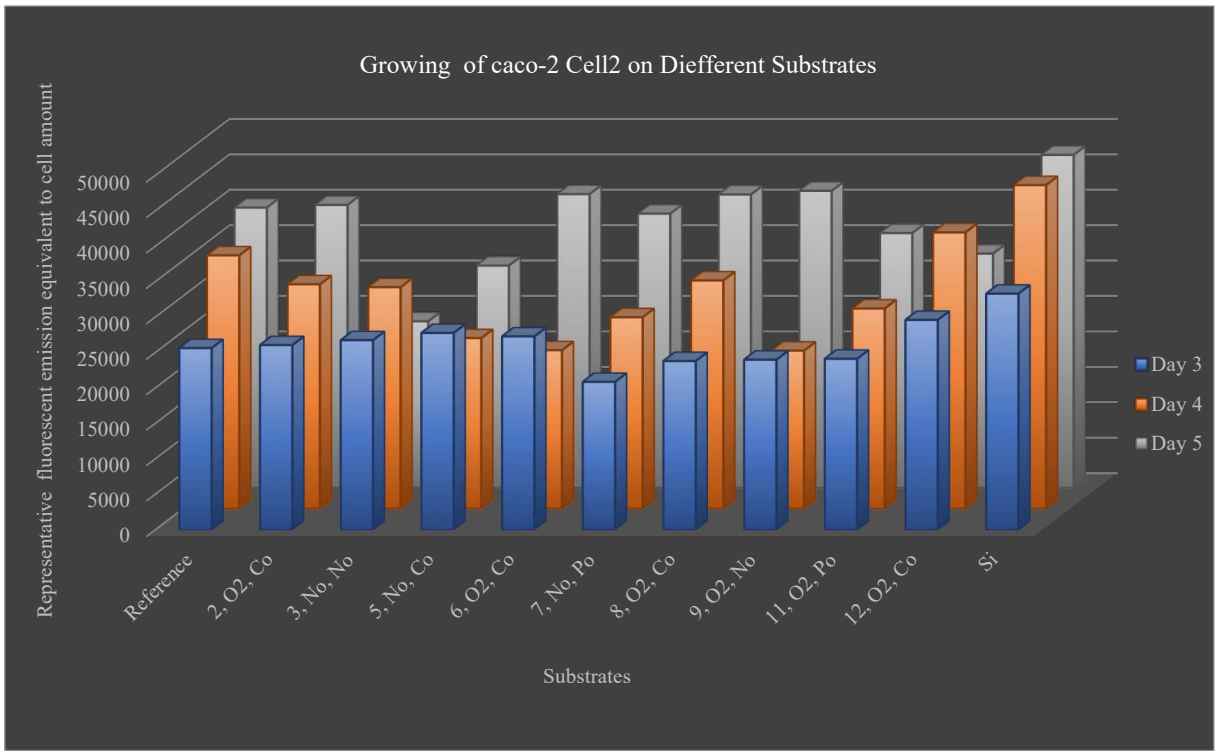

Figure 4.5: Cell count with fluorescent emission method on three consecutive days of the same pre-chosen substrates addressed in Table 4.1.

Three different batches of different substrates (including r_{CH4}, O_2-plasma treatment and coatings) were cultivated with the same number of CaCo-2 cells at the same time under the same conditions and counted after 72, 96 and 120 hours. Figure 4.5 shows the outcome of the cell count. This part of the experiment was performed because of the presumption for an exponential cell growth. The first notable point is the unstable cell proliferation of cells planted at the same time on some of the chosen substrates. While the cells planted on silicon and a single well plate working as reference samples, showed the expected growing behaviour, most of the other samples proliferated different from batch to batch resulting in the need of a repetition of the experiment to determine whether the results will always come out unpredictable or just in this specific case. However, the tendency that cells grow especially well on collagen coated surfaces can be clearly seen in Figure 4.5.

4.2.2 Proliferation images

The second set of samples was stained and photographed as described in 4.1.3 with the same time intervals as the first set was counted. The left column of Figure 4.6 shows the cell population on day three on the different substrates (Table 4.1). Every picture shows the smallest density of cells on each specimen to generate a visual impression of population differences. The investigation under the microscope of the cell confluence on day four showed an already almost completely populated sample, which is why another technique was used. Instead of taking almost the same pictures of every specimen, the cells were tried to be washed off the specimen with four repetitions of 100 µl of medium by a syringe. The boarders of the remaining cells on the chip are pictured in the right column of Figure 4.6 as well as the percentage of the area, which was still covered with cells. After 120 hours the last set of samples was photographed in the same way as on day three and pictured in the middle column of Figure 4.6. Again, the least covered areas were photographed for a proper comparison.

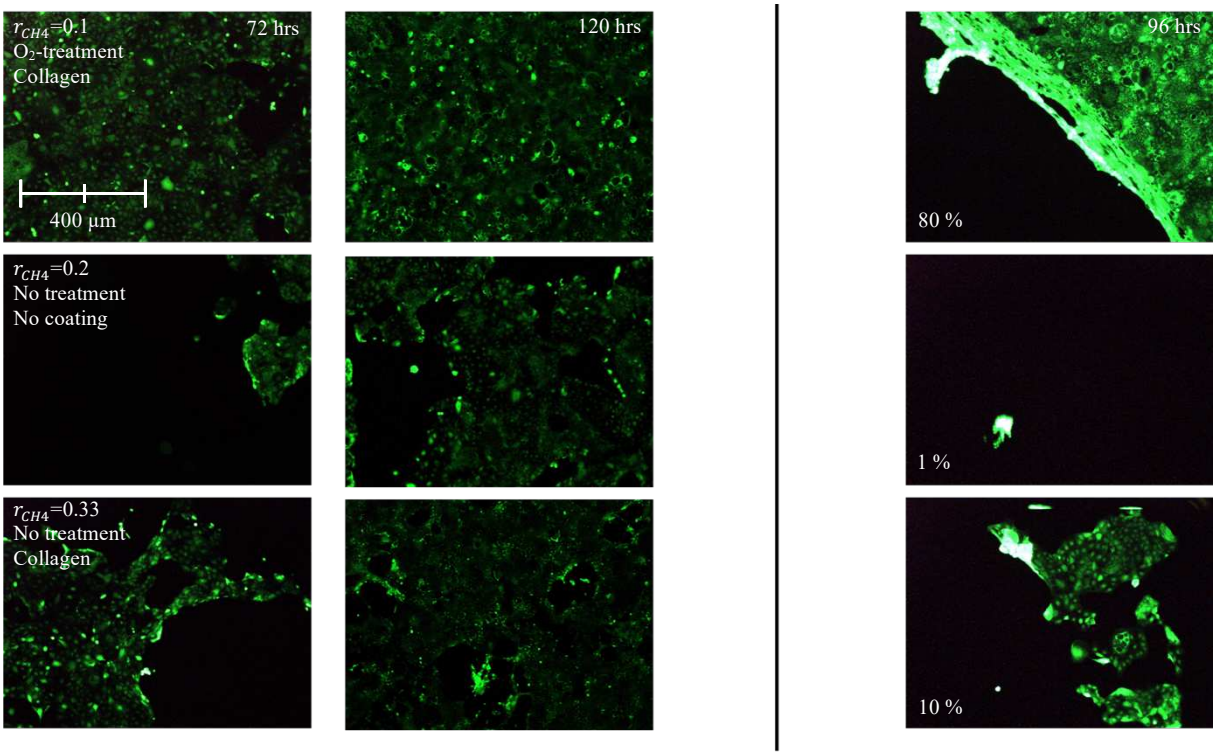

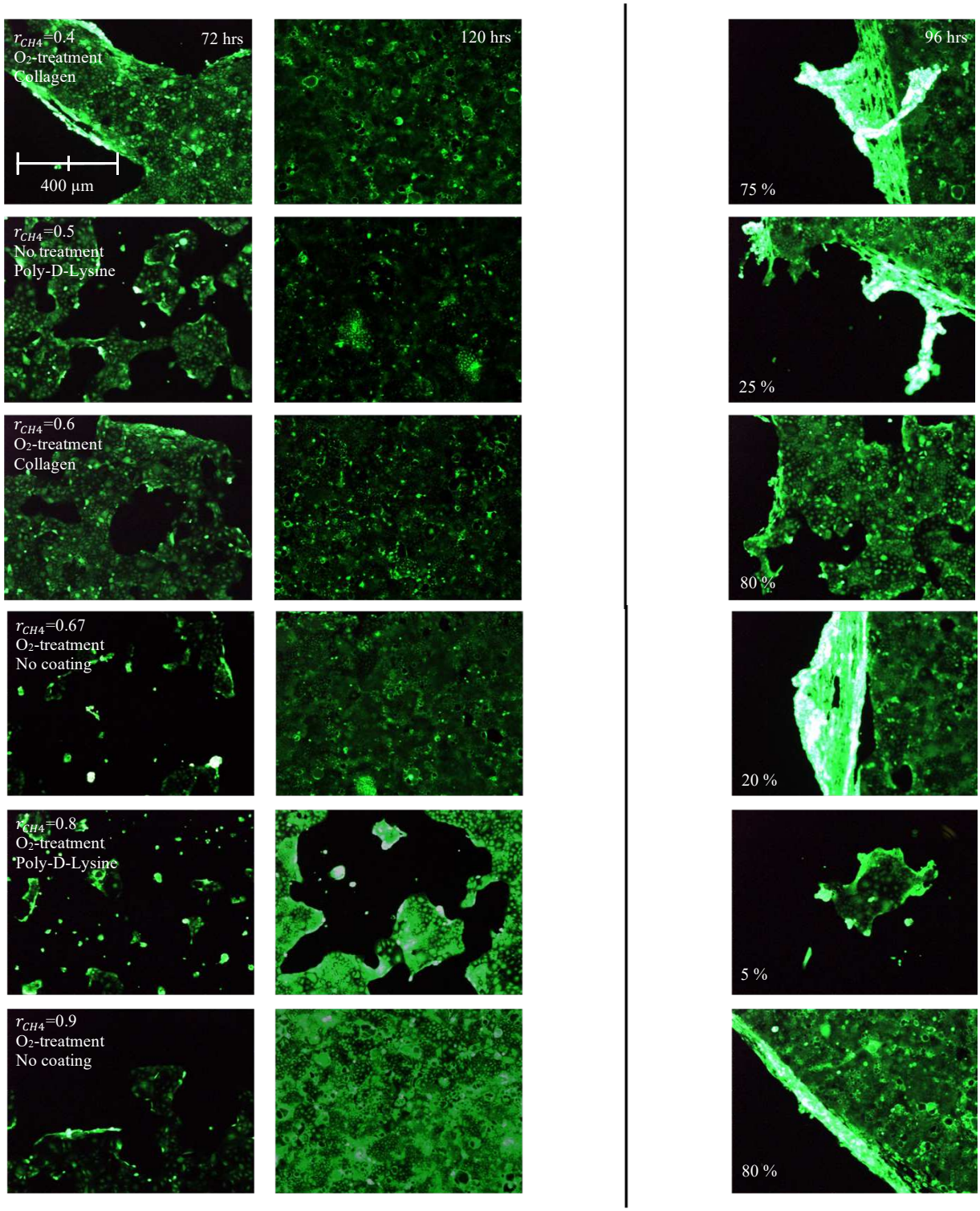

Figure 4.6: Cell growth photographed after 72 (left), 96 (right) and 120 (middle) hours. Every single green dot represents a living cell, while the dark areas are uncovered substrate The left and middle column show the least covered areas of cell, respectively. The right column pictures the percentage of still covered area and the boarder of the remaining cell film after a wash assay.

4.2.3 CASY cell count and imaging of remaining cells

The counted samples summed up in Figure 4.5 were subsequently treated with trypsin for 5 min and counted with a CASY© cell counter (Figure 4.7). A major problem appeared during the process of trypsinisation, because depending on the SiC layer, pre-treatment and coating the cells adhered sometimes better, sometimes worse. This made an estimation of an actual cell number on the sample almost impossible. If both cell counting methods are compared, it can be clearly seen, that both results show almost no agreement, which leads to the assumption that the counted absolute cell values cannot be accurate in most cases.

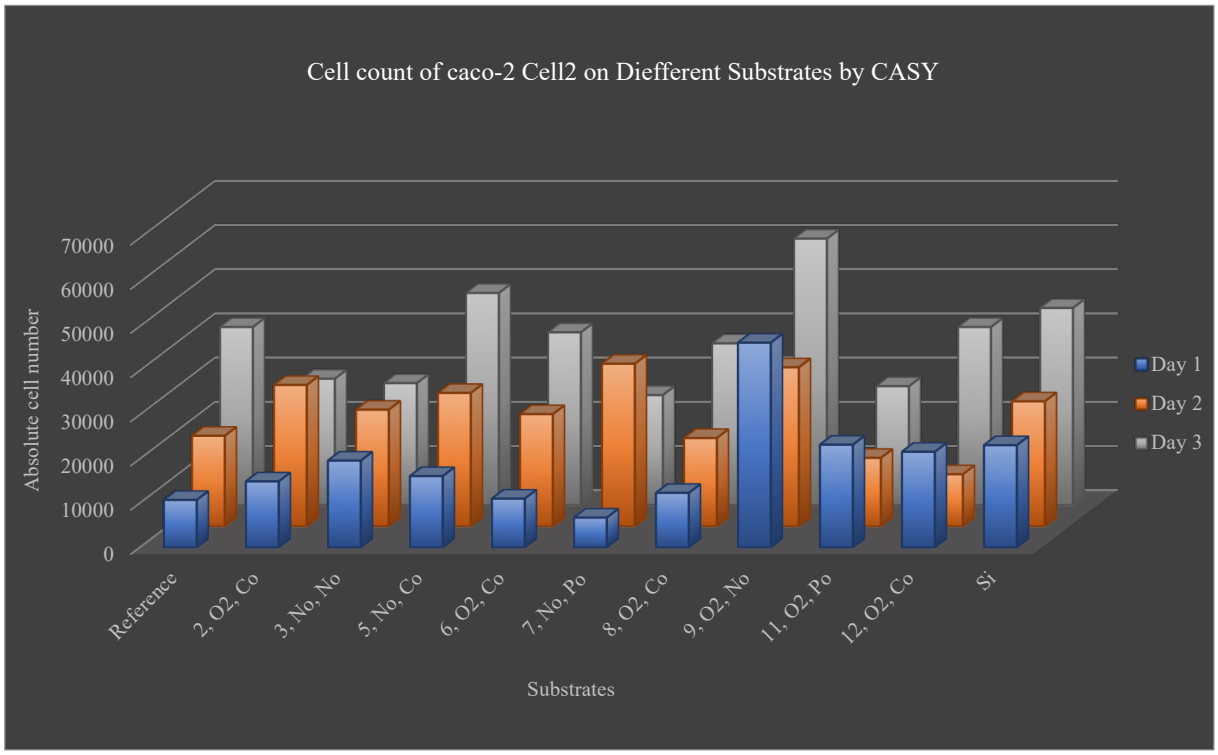

Figure 4.7: Cell count with a CASY cell counter. The number of cells of the reference is pictured with a factor of l/10.

The remaining adherent cells on the substrates' surfaces were also stained and photographed after the actual counting to show the major influence of different pre-treatments and coatings to the adhesiveness and the cell count in a broader sense. Figure 4.8 shows an increasing amount of remaining cells on the substrate over time, which was induced by the working principle of trypsinisation, since the more confluent cells attach to each other, the harder the trypsin containing fluid is able to reach the integrins to break them down. The pictures were taken from those regions on the specimens of the highest remaining cell density. Particular striking is the amount of cells still adherent to the surface of all O_2-plasma treated and also collagen coated samples, independent of the r_{CH4} ratio. Also noticeable is that the untreated samples regardless of the coating showed a comparable very low number of remaining cells, which stands also in good agreement with Figure 4.6.

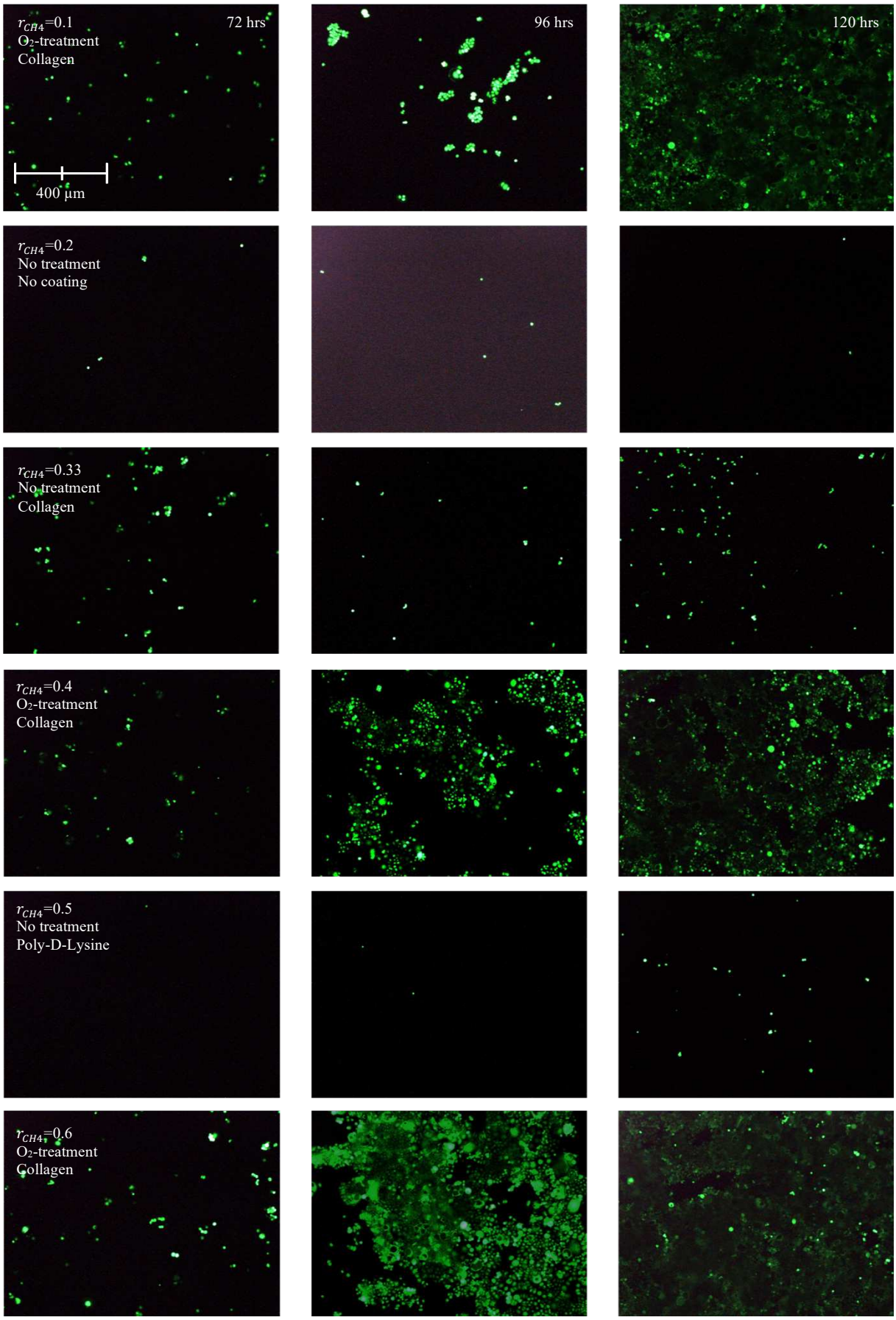

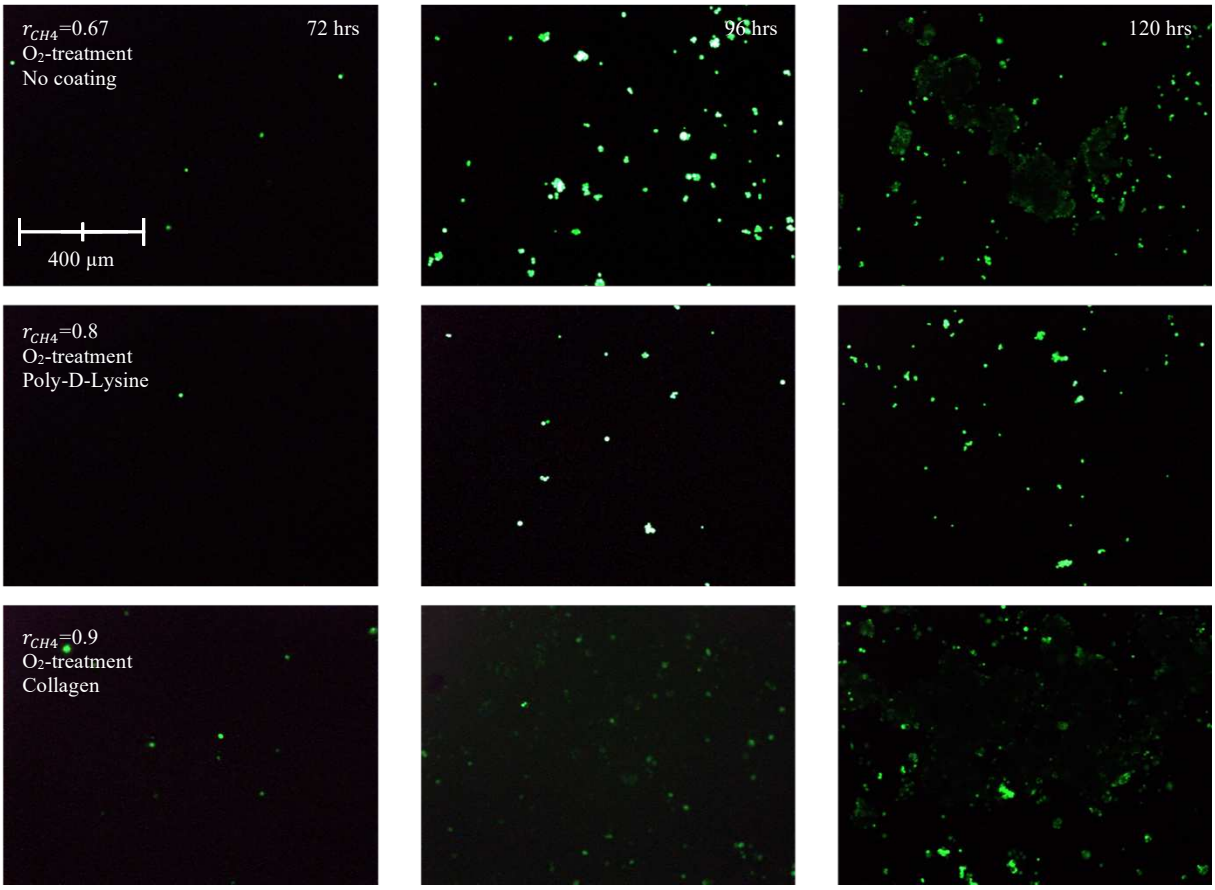

Figure 4.8: Images of remaining cell on samples, after five minutes of trypsin treatment, photographed after 72 (left), 96 (middle) and 120 (right) hours of proliferation. The most covered areas of remaining cells are pictured.

4.2.4 Total cell count

On day five after a total development time of 120 hours the well plates 1 – 6 were counted. The cells grew under the same conditions on 78 different surfaces, in order to confirm or deny presumptions given by [2]. The cells were counted with the PrestoBlue plate reader, without the additional CASY counting process. The outcome of this part of the experiment is presented as 3-dimensional graphical image (Figure 4.9) to point out common features of the different samples represented in local maxima or minima. The graphic reveals several things, which corresponds very well with the relevant literature. Looking at the substrates with the smallest r_{CH4} value of 0.05 the cell numbers of all different treated surfaces resulted in high values. This might be caused by the higher hydrophilicity of the almost pure silicon, only slightly affected by different surface finishes. Increasing the carbon content by raising the r_{CH4} results in a common minimum, again regardless of pre-treatment or coating. By further increasing of r_{CH4} to the range of 0.4 to 0.67 a local maximum can be observed depending on the different surface treatments. By raising the carbon content of the substrate, the electrochemical potential increases, which seems to be liked by CaCo-2 cells, if the surfaces are additional treated with an O_2-plasma and with or without a collagen coating. Particularly noticeable are the surfaces that were treated with an O_2-plasma and coated with collagen in the r_{CH4} range of 0.4 to 0.75. Here, an almost constant plateau of high cell number values can be observed. This can be caused by the higher carbon content, the increased hydrophilicity through the O_2-treatment and the raised adhesiveness of CaCo-2 cells on additionally collagen coated surfaces. If the carbon

content is further raised, the hydrophilicity of the surfaces further decreases and cells proliferated worse again. Surfaces finished with a Poly-D-Lysine coating showed not the expected behaviour of an increased cell number comparable to the ones of collagen.

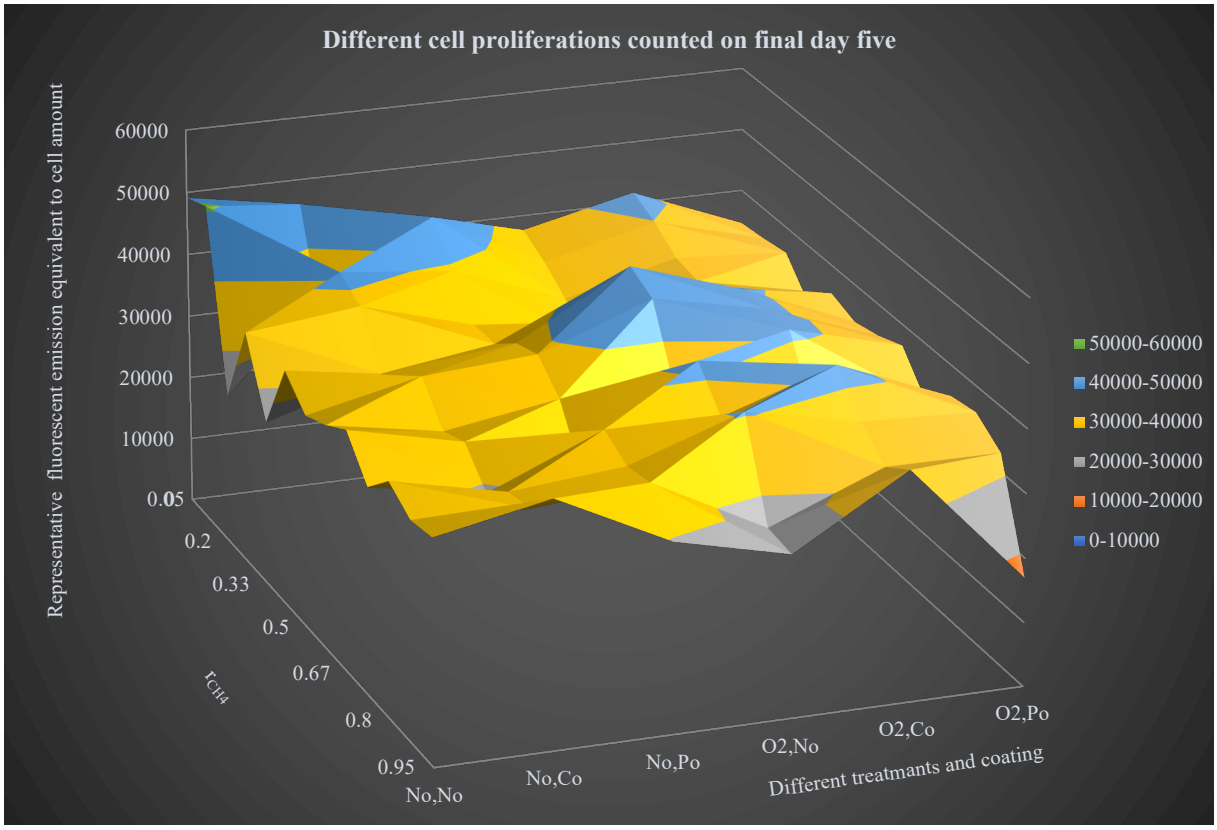

Figure 4.9: Final cell count on day five of all planted cells on 78 different substrates differing through the silane to methane ratio r_{CH4}, the pre-treatment and coating.

The experiment confirmed some tendencies of presumptions as the likeliness of cells to grow on hydrophilic surfaces or adhere especially well on collagen coated surfaces, but also left room for interpretations, which can be only clarified by further and more specific experiments.

5 Membrane measurements

This chapter contains the measurements of bistable biocompatible membranes, fabricated as described in 2.5 and 3. To characterize the switching behaviour of such membranes several significant properties were investigated by the application of different kind of electrical signals. The vibrational behaviour was conducted by small electrical loads in order to define deflection amplitudes and the related characteristic resonance frequencies, before and after the biocompatible SiC layer was integrated on the membranes. The most promising diaphragms with the highest deflection under the load of small electrical excitations were bonded and tested for a possible bistable switching behaviour. The latter measurements were conducted in air and in different viscous fluids.

5.1 Measurement setups

The experimental part splits up in two different setups, while one obtained the results of small signals impinging on the membranes and the other gained knowledge of the reaction of bistable membranes to signals of higher amplitudes in order to get switched from one stable ground state into the other.

5.1.1 Small deflections setup

This section can also be seen as pre-measurements for a proper selection of promising membranes, which might show a switching behaviour in the next step. Diaphragms exceeding a specific deflection level, when excited with a 5 V 2000 Hz sinusoidal signal [55] were chosen for further bonding fabrication steps described in 2.5.6. However, those pre-measurements were also used to investigate the influence of a SiC layer on top of the diaphragms to their vibrational behaviour and furthermore the tendency of showing switching behaviour.
For this purpose, the membranes of the un-bonded samples were placed centrally under the laser beam (Figure 5.1 a) of a LDV (Figure 5.1 b). The bonding pads of the associated membrane were contacted with two needles (Figure 5.1 c and d), which act as an extension of two adjustable blocks (Figure 5.1 e), where the electrical connections are located. The electrical signal was applied over these connectors and set over the by-standing PC via the program POLYCON. The display (Figure 5.1 f) shows the magnified[1] live image of the sample placed underneath the laser.

[1] Five times magnification

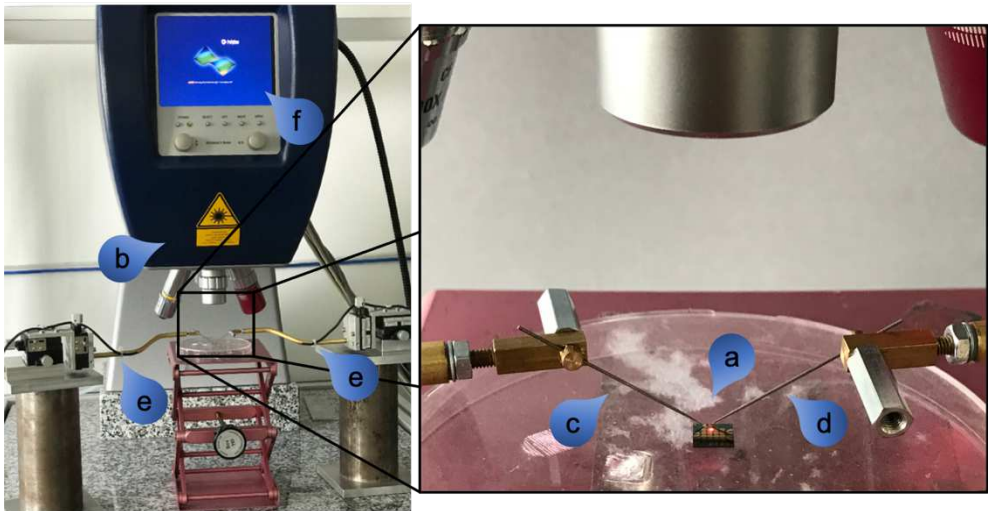

Figure 5.1: Measuring setup: a) Laser beam pointing at the centre of one membrane. b) Laser-Doppler-Vibrometer. c) and d) Contact needles connected to the bonding pads of the associated diaphragm. e) Mountings and connectors for applied signals. f) Screen for monitoring

5.1.2 Membrane switching setup

The setup to determine the switching ability of a membrane consisted of an Agilent© 33521A waveform generator, a TREK© 2100HF amplifier with a x50 gain, a Tektronix© TDS2024 oscilloscope to display the output and trigger signal of the waveform generator, a x10 probe to monitor the actual amplified signal as reference signal and a LDV to record the movements of the membranes as in 5.1.1 (Figure 5.2). The waveform generator created an initial low voltage signal as well as a trigger signal, which both were connected to the oscilloscope. The low voltage signal was also directed to the amplifier, subsequently amplified and applied to both the membranes held by an IC-package holder and via the probe[1] to the reference input of the POLYCON hardware-software interface.

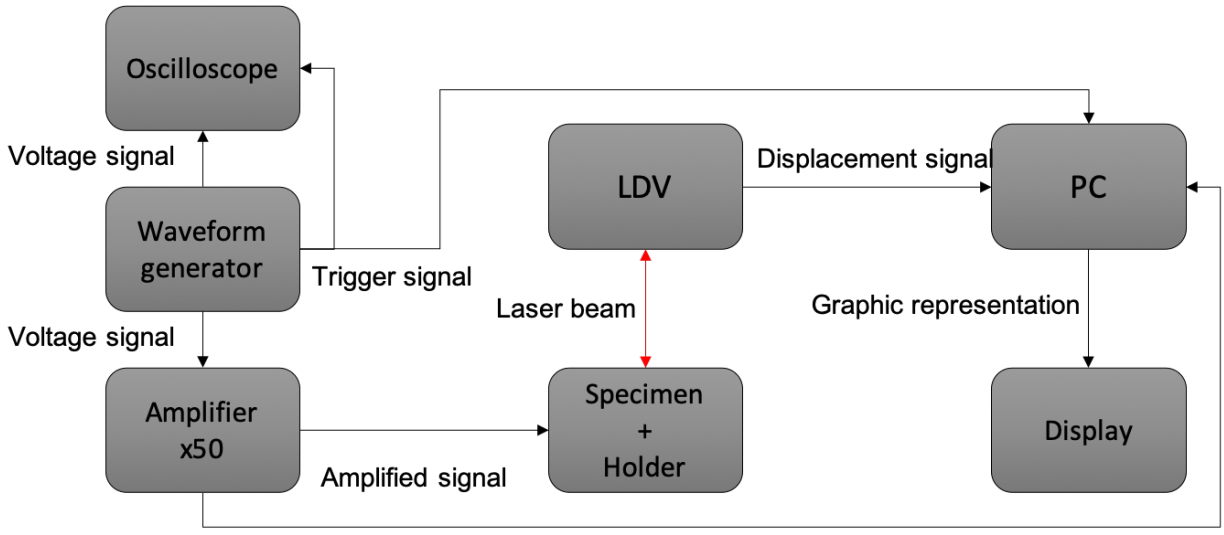

Figure 5.2: Graphic illustration of the membrane switching setup.

[1] The signal will arrive the input ten times lower

5.2 Results

Following the setup of 5.1.1 and the recommendation for the voltage parameter of [55], the pre-measurements to characterize the vibrational behaviour and determining the characteristic resonance frequencies took place with the chosen signals pictured in Table 5.1. All membranes were loaded with the same signals in order to compare differences.

Table 5.1: Applied low voltage signals

Signal	Amplitude	Frequency	Resolution
Sinusoidal	5 V	2 kHz	1 mm/s/V
Periodic Chirp	0.3 V	1 – 350 kHz	5 mm/s/V

Both signals were subsequently applied to the electrodes of the membranes, causing an appropriate deflection depending on the quality of the piezoelectric layer, the cumulated layer stress of the membrane and the diameter.

5.2.1 Amplitude of the membranes

By loading the membranes with the sinusoidal signal of Table 5.1 each membrane will directly react with a deflection depending on their properties. The diaphragms followed in a nearly perfect manner the given signal with the same frequency and a corresponding deflection height directly related and linear to the applied voltage level [55-56]. To give an overview over the 60 tested membranes the highest and lowest deflection values are displayed in Table 5.2.

Table 5.2: Overview of the highest and lowest deflection amplitudes sorted by different diameters

Diameter [µm]	Wafer name	Membrane number	Deflection [nm]
600	W17_18	84	190
	W17_15	61	185
	W17_18	80	172
	W17_17	110	110
	W17_18	66	110
	W17_15	110	100
700	W17_17	49	260
	W17_17	50	258
	W17_17	29	200
	W17_17	91	120
	W17_15	12	120
	W17_15	23	102
800	W17_17	60	275
	W17_15	39	270
	W17_18	15	258
	W17_18	21	138
	W17_16	105	130
	W17_18	57	130

The deflection differs partially by a factor of two from each other, which gives only information of the inconsistency of the fabrication process, since the other parameters were held constant. However, the membranes with the highest deflections seems to represent the best candidates, as the quality of the piezoelectric layer and a most homogeneous layer structure is needed for high deflections [55-56].

5.2.2 Characteristic resonance-frequency

The deflection of a membrane out of its stable state is always caused by an energy input. The eigenfrequency of a resonating system, based on a spring-mass combination, is the frequency, at which the system starts oscillating after a one-time excitation. If a single excitation frequency is selected which matches the eigenfrequency of the system, the amplitude is amplified with respect to the non-resonant case. A membrane typically possesses more than one resonance frequency associated with different mode shapes, whereby the highest peak is called the dominant characteristic resonance frequency. [61]
To determine those frequencies the membranes were loaded with a sinusoidal periodic chirp signal[1] (Table 5.1) and the corresponding frequency level of the initiated velocities was recorded in air. Figure 5.3 shows an example of a typical resonance frequency pattern of a membrane. Although the first peak has the lowest displacement velocity, the following Figures 5.4 and 5.5 will show its importance.

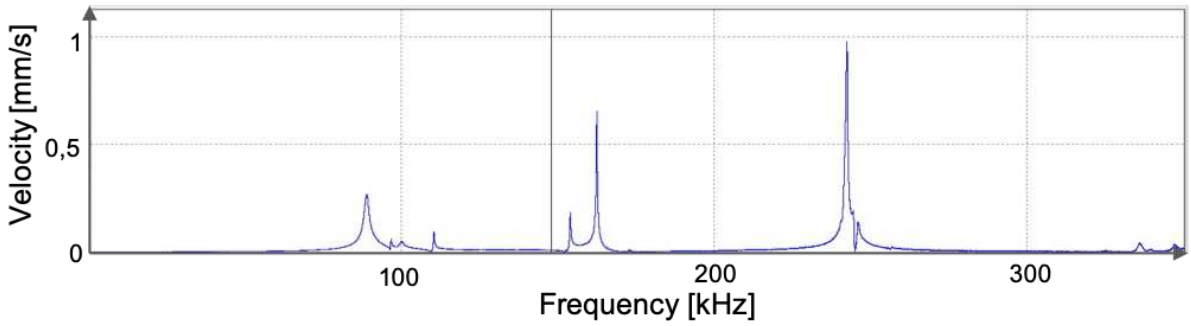

Figure 5.3: Example for a possible pattern of characteristic resonance frequencies

All membranes were measured with the same procedure and were described by their vibrational behaviour and characteristic resonance frequencies. According to [55] those values can be set in relation to show their importance.

[1] The excitation frequency of the signal sweeps through a desired frequency band.

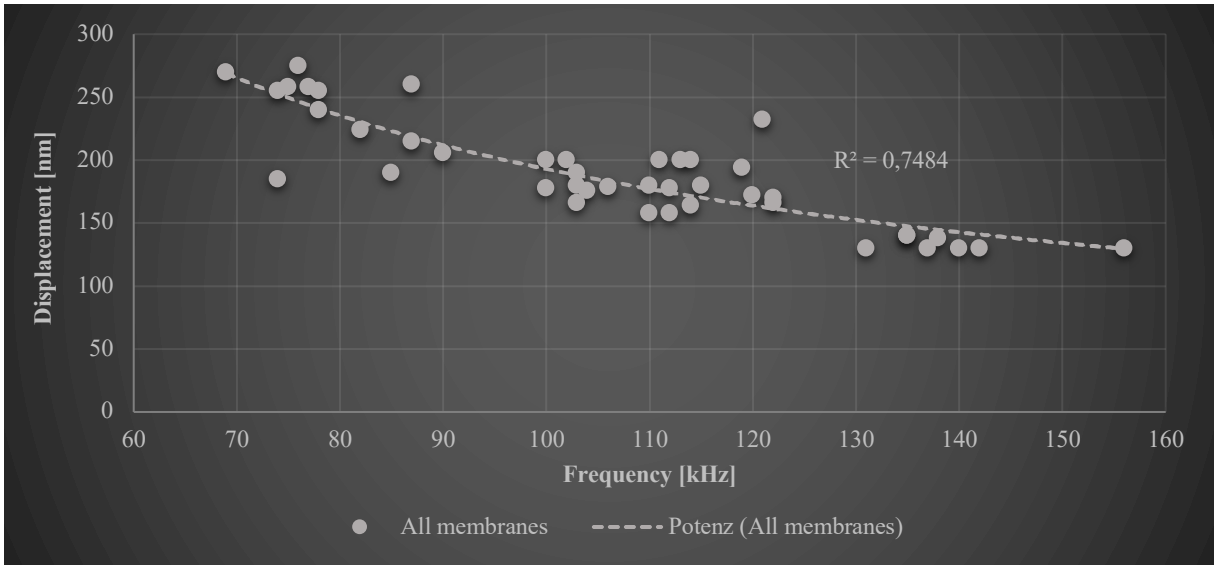

Figure 5.4: Deflection of every measured membrane over their *first* characteristic resonance frequency f_{res1}. The green arrows mark membranes with uncommon values.

Figure 5.4 shows the most import aspect of the pre-measurements. In 2.5.7 the coating of the membranes with SiC was described, those membranes were characterized before and after adding the additional layer and were treated as new membranes subsequently. It can be seen that most membranes align very well with their common potential line calculated with the Pearson function, though some membranes showed a strong deviation (Figure 5.4, green arrows). These membranes also looked different under the microscope and appeared more even and smooth compared to the others (Figure 5.6). Most of the measured diaphragms had their dominant resonance frequency as fourth characteristic frequency f_{res4}, though no characteristic correlation to other recorded parameters or graphic patterns could be found (Figure 5.5) [55]. This leads to the conclusion that even though the fourth (and mostly dominant) characteristic resonance frequency f_{res4} has the highest velocities, it can be neglected for further characterizations. Measurements addressed in 5.2.3.1 will prove that assumption.

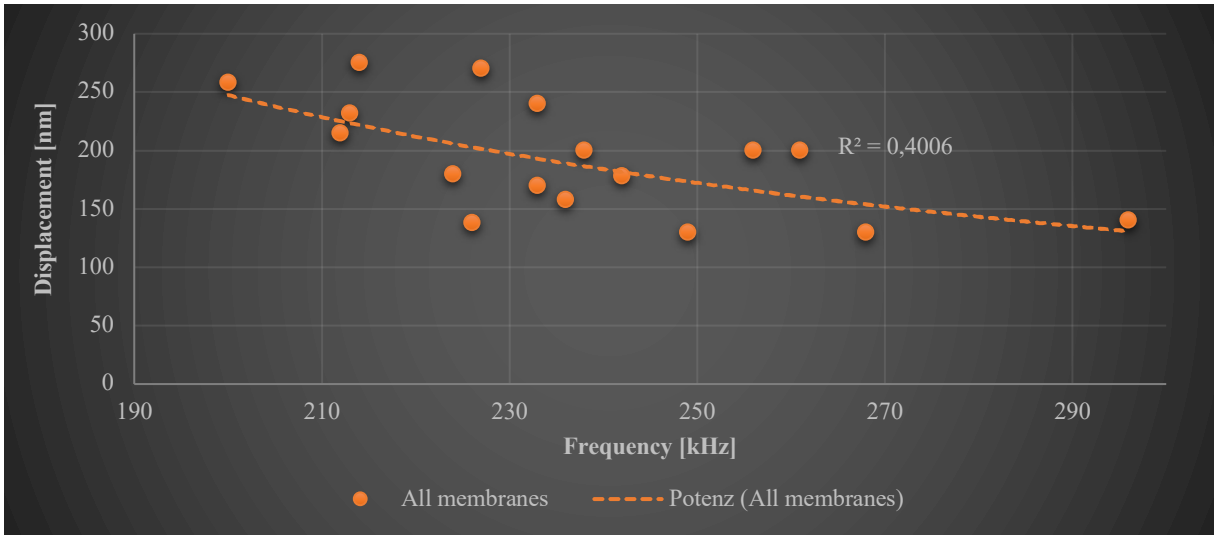

Figure 5.5: Deflection of every measured membrane over their *fourth* characteristic resonance frequency f_{res4}.

The pre-measurements were meant to figure out which membranes might be able to show switching characteristics and since not every membrane had the same mechanical properties caused by manufacturing intolerances, a pattern of characteristics must be found to select the right ones. According to [55] and proved with Figure 5.4 the membranes with the lowest *first* resonance frequency tends to have the highest deflection. Furthermore, by increasing the low voltage sinusoidal signal the deflections will rise linearly and with a higher slope the lower f_{res1} is [55].
In conclusion membranes with a diameter of 800 µm and a f_{res1} lower than 80 kHz, a diameter of 700 µm and f_{res1} lower than 100 kHz and a diameter of 600 µm and f_{res1} lower than 120 kHz will have the best tendencies to show switching behaviour under the right circumstances. In total 30 membranes including each diameter were bonded (Subsection 2.5.6) and chosen for further characterization.

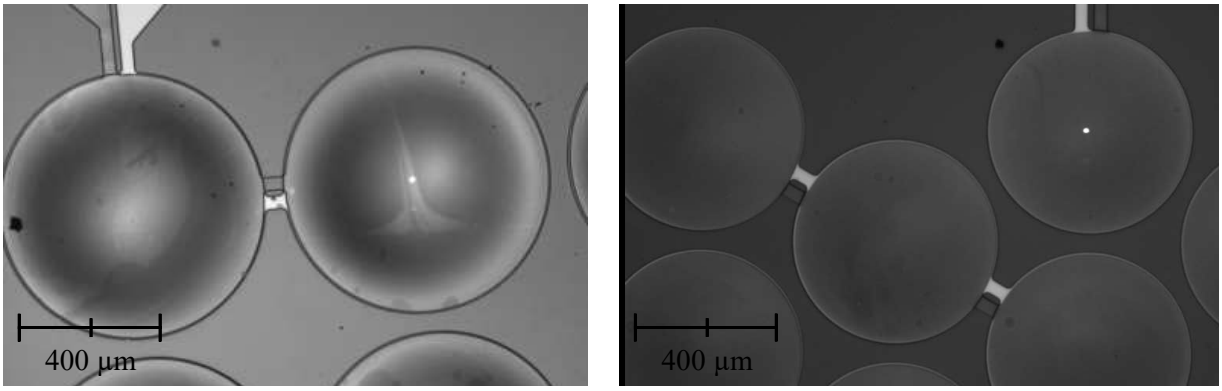

Figure 5.6: Different pattern of a "normal" 800 µm (left) and more even and smooth 600 µm (right) membranes, while the latter achieved much higher deflections, caused by the same electrical excitation.

5.2.3 Bistable switching in air

For the process of switching a bistable membrane by exploitation of the inverse piezoelectric effect a particular voltage[1] signal and level is required. The following voltage generation based on recommendations of [62] and was altered in order to find the best working parameters to create deflections high enough, that a membrane will switch in its second ground state and remain there. This task requires the measuring setup of 5.1.2 and an electrical signal from the waveform generator as source. A rectangular pulse signal with a peak-to-peak voltage of 30 V_{pp} and an offset of 15 V was applied to a single membrane. The reaction of the diaphragm to the applied signal was recorded with the LDV and displayed on the monitor. In the meantime, it should be obvious that every membrane is different and a particular adjusted signal, which is able to switch one membrane, will not switch another membrane without changing the signal's parameter, hence a procedure of stepwise changing the parameter settings of the signal was designed to guarantee a switching, if the membrane is initially able to be switched. Thus, the first step is to change the rectangular signal from continuous to burst mode, since only very few pulses are necessary to generate enough movement in the membrane for sufficient deflections. An increased number of pulses would inhibit the build-up of the oscillation, which is why the number of bursts is initially set to three pulses. In the scope of this theses no automation of changing the parameter was used, which is why the initial voltage was set as already mentioned

[1] No number can be given at this point, since every membrane requires a different voltage level.

to 30 V_{pp} and an offset of always half of the amplitude. The next step is to set the frequency to 10 kHz[1] below the first resonance frequency of the relevant membrane [62]. Unusually, this is an absolute value, though it fits most diaphragms very well. By applying these pulses to the membrane, the LDV already recorded high deflections. It was also possible that the parameter settings were exactly right for this particular membrane and the membrane switched. If that was not the case, the parameters for voltage level and burst number were hold constant, while the frequency was changed around the set point and the altering vibrometer signal of the displacement was monitored. A certain frequency must be found where one displacement peak of the recorded curve increases to a maximum value. Next, the number of burst pulses was changed, while monitoring the peak *after* the highest peak. If the peak decreases, the additional pulse inhibits the build-up of oscillation and the initial setting was more beneficial for this membrane. On the other hand, if the peak exceeded the level of the initial highest peak, this burst count was set as new pulse value. This step was looped until no increasing could be observed. By changing the burst pulses also the ideal frequency, set before had slightly shifted and needed to be reset again by maximizing the highest peak. The last step is to stepwise increase the voltage level while holding frequency and burst pulses constant until the membrane switches.

5.2.3.1 Possible outcomes

Following the just described steps will lead to three possible outcomes depending on the purity and homogeneity of the layer structure and the position of the sample on the wafer before cutting.

No switching
The first option is that the membrane will not switch, because the manufacturing process was not even and homogeneous enough to achieve the required layer structures. In this case the membrane oscillates with the exciting frequency, also builds up its deflection, but will not reach sufficient displacements for locking in the second ground state.

Monostable switching
In the second scenario the necessary displacements are achieved by applying the right voltage loadings, which leads to the switching of the membrane, though it is not able to maintain the position of the second ground state (Figure 5.7). This is a typical behaviour of a monostable membrane. As soon as the excitation is gone, the membrane switches back into its initial ground state.

[1] This value is only appropriate for the membranes manufactured with the production cycle of Subsection 2.5 and Chapter 3.

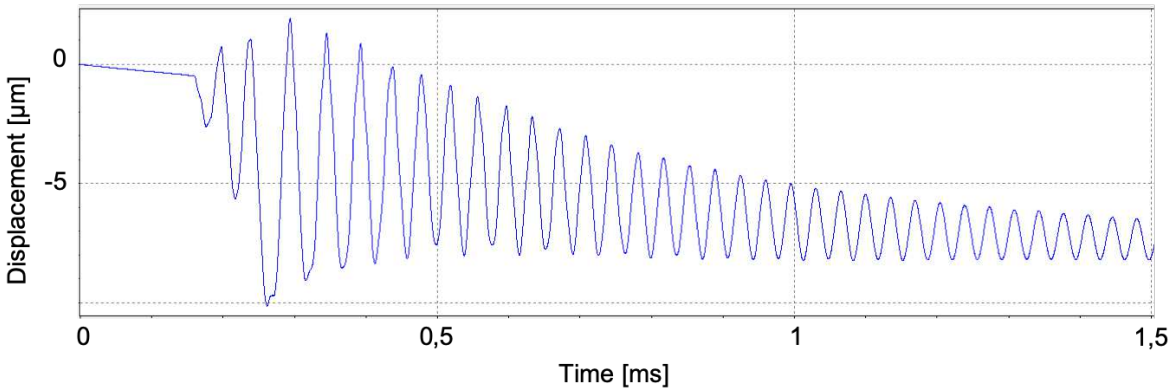

Figure 5.7: Monostable switching of a membrane. The third peak reached the needed deflection, though the membrane could not maintain the position and switched back after a minimal delay of 20 µs in this case (green arrow).

Bistable switching

If the membranes were fabricated with the required quality and excited with proper electrical signals, the LDV will record a typical displacement curve of a switching event. Depending on the original ground state the curve will also show different patterns, whether the diaphragm switches from the first into the second stable state (Figure 5.8) or *vice versa* (Figure 5.9). Under five times magnification the changed light reflections on the membrane's surface can be monitored on the screen (Figure 5.10).

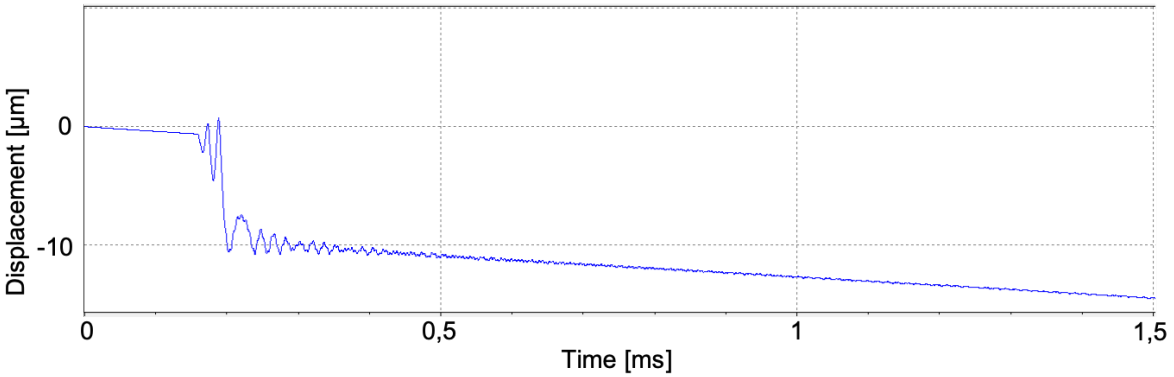

Figure 5.8: Pattern of the displacement curve of a membrane, while switching from the upper to the lower position.

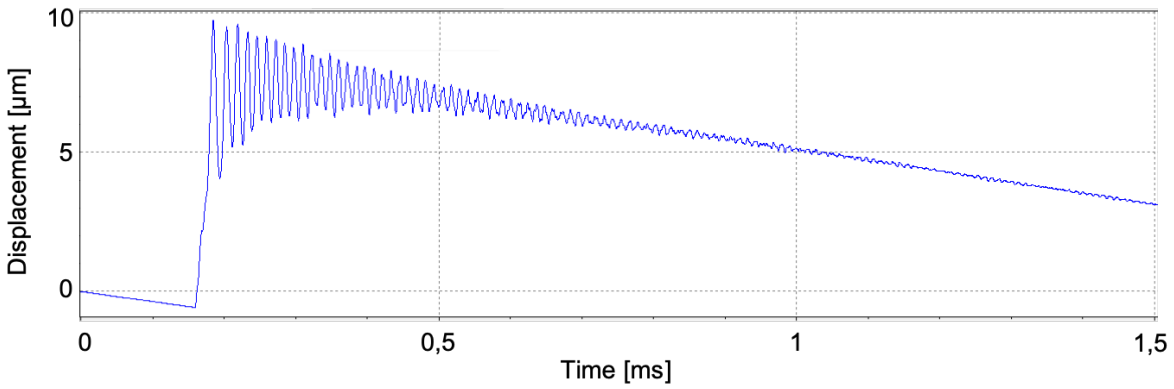

Figure 5.9: Displacement curve of the same membrane, while switching back from the lower ground state to the upper.

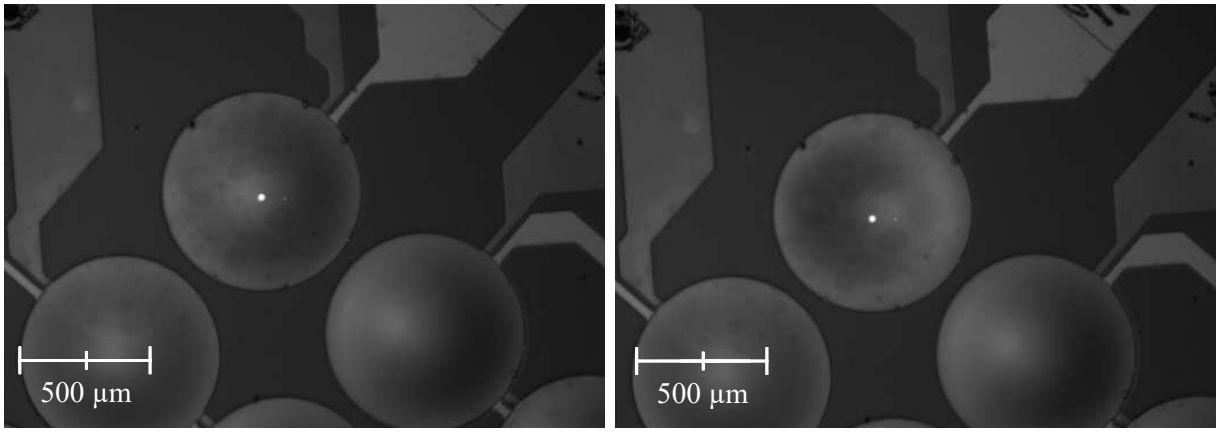

Figure 5.10: Changed light reflexions, caused by switching from upper (left) to lower (right) ground state of an 800 µm membrane.

As it can be seen in Figures 5.8 and 5.9 the displacement curves strongly differ from each other. This is because of another characteristic of the here presented bistable membranes. Those bistable diaphragms have a preferred ground state, which results from the asymmetric membrane architecture, caused by the integrated piezoelectric transducers. Almost every membrane is initially in its *upper* ground state after completion of the fabrication process, which hampers the switching from the upper to the lower state and will consume more energy during this process. [62]
If the membrane switches from up to low, the LDV records a snap in like behaviour and once a membrane stays in its lower state, switching back can be achieved more easily, mostly with the same or slightly lower frequency (Figure 5.11). If switching back to the membrane's preferred stable state, a strong wobbling of the membrane could be monitored (Figure 5.9). Figure 5.11 also shows the predicted tendency of the frequency range, where membranes were able to be switched, depending on the first resonance frequency and diameter.

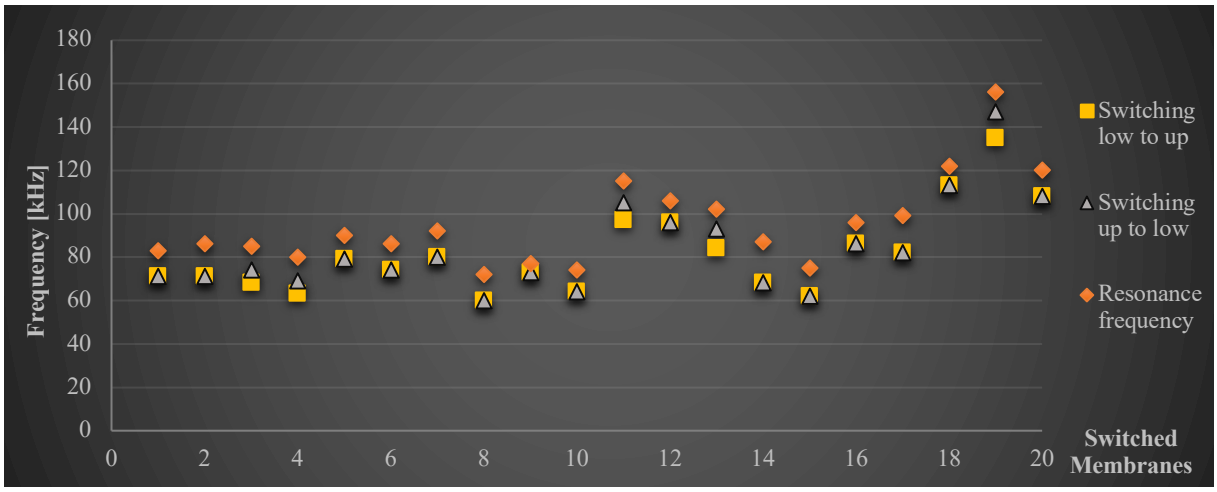

Figure 5.11: First resonance frequency and switching frequencies of every membrane, which was able to achieve required switching displacements. Membranes 1 – 10: 800 µm diameter; 11 – 17: 700 µm diameter; 18 – 20: 600 µm diameter.

Another phenomena was discovered by looking for other possible switching frequencies of one membrane, since also more than one characteristic resonance frequency exists. If the same scheme of 5.2.3 was adopted to the mostly fourth dominant resonance frequency almost no

build-up of deflections could be observed, despite the much higher velocities at those frequencies. However, this stands in good agreement with Figure 5.5 and the statement that only f_{res1} has an influence for a possible switching procedure.

In Subsection 5.2.2 were already membranes mentioned, which deflections diverged strongly from the common potential line, depending on f_{res1} (Figure 5.4). Even though these membranes showed high displacements and very low f_{res1} *no* switching could be achieved as opposite to the expectation. This leads to the conclusion that those membranes must have been stiffer, which results in high deflections through small voltages and low resonance frequencies [62], but also in a suppression of the switching potential.

5.2.3.2 Ejection of particles by bistable switching

An additional task was carried out with membranes in air. The potential of bistable membranes to eject settled particles on the surface of the membrane as a cleaning process by the switching procedure itself was investigated. Particles, which settle down over time on the membrane's surface will change the resonance frequencies and further decrease the sensing potential of such a device. By getting rid of the particles without removing the device out of its application area, the sensing quality could be maintained over longer periods.

Dry conditions
An unspecific amount of 10 µm round shaped SiO_2 microbeat particles was added onto the membrane's dry surface and by measuring the altered f_{res1}, a switching was subsequently induced at f_{switch}.

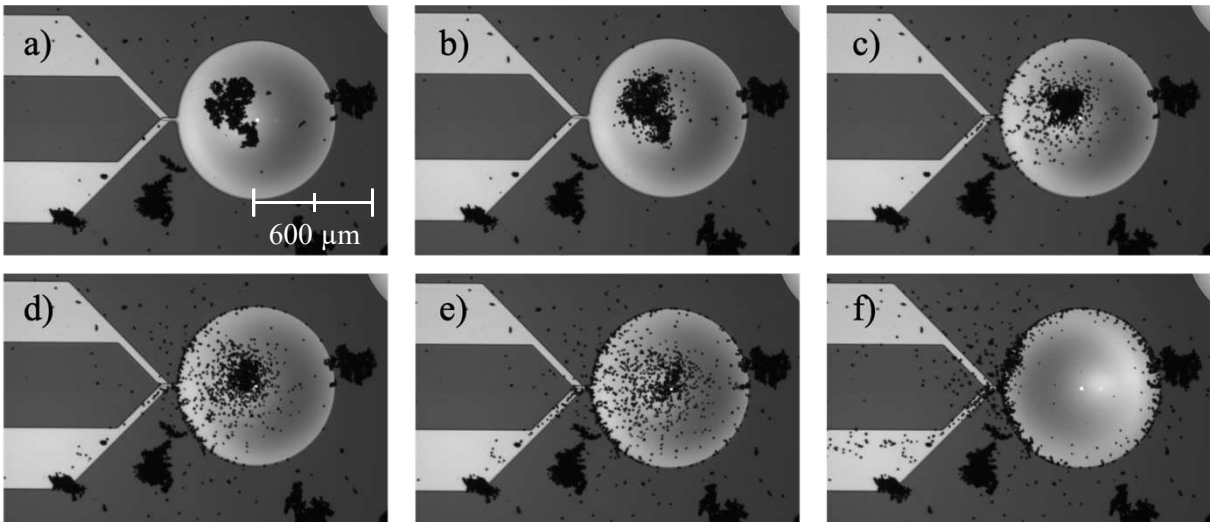

Figure 5.12: Removing particles during a cleaning cycle of a 800 µm membrane by switching between the two ground states. The pictures were taken after a) zero, b) one, c) five, d) 15, e) 25 and f) 45 switching procedures.

During each switching cycle it could be monitored, that the particles were slung away from the membrane, while the better distributed the particles were over the surface, the more effective and faster the membrane was cleaned (Figure 5.12).

5.2.4 Switching in fluids

By placing a not electrically conductive fluid (Table 5.3) on top of the membrane the characteristic switching behaviour investigated in air will change significantly. The key parameter to induce a switching mechanism is still the first characteristic resonance frequency, though the value for f_{res1} altered through the changed medium around the membrane. Fluids with different dynamic viscosity values were added subsequently onto the diaphragm's surface and with the procedure of 5.2.2 the according resonance frequencies were measured, respectively. Six different viscosity calibration fluids were used to determine commonalities between f_{res1} and the fluid's properties. To measure f_{res1} several droplets of the fluid were dropped onto the device, covering not only the membrane, but the whole chip. It is very important that no surface tensions arise, while measuring the resonance frequencies. Bubbles in the fluid, surface tension, movements of the fluid or fast evaporation will cause a drift of f_{res1}, which was observed by testing different amounts of fluid added onto a membrane's surface. The right amount of approximately 200 – 250 µl will result in stable resonance frequencies, leading to conditions where a switching procedure could be possible. Figures 5.13 and 5.14 show the first resonance frequency of 17 membranes in six different fluids compared with the fluids' viscosity and density. It can be clearly seen that f_{res1} is only dependant of the density of the fluid and not the viscosity.

Table 5.3:Properties of fluids used for this thesis.

Fluid	Temperature		Viscosity		Density		Root products	
ISO	20	°C	2.19	mPa·s	0.785	g/ml	0.385	m²·√s/kg
D5	20	°C	5.51	mPa·s	0.840	g/ml	0.465	m²·√s/kg
N10	20	°C	17.53	mPa·s	0.846	g/ml	0.260	m²·√s/kg
D35	20	°C	71.96	mPa·s	0.855	g/ml	0.127	m²·√s/kg
N100	20	°C	286.10	mPa·s	0.866	g/ml	0.064	m²·√s/kg
D500	20	°C	713.40	mPa·s	0.872	g/ml	0.040	m²·√s/kg

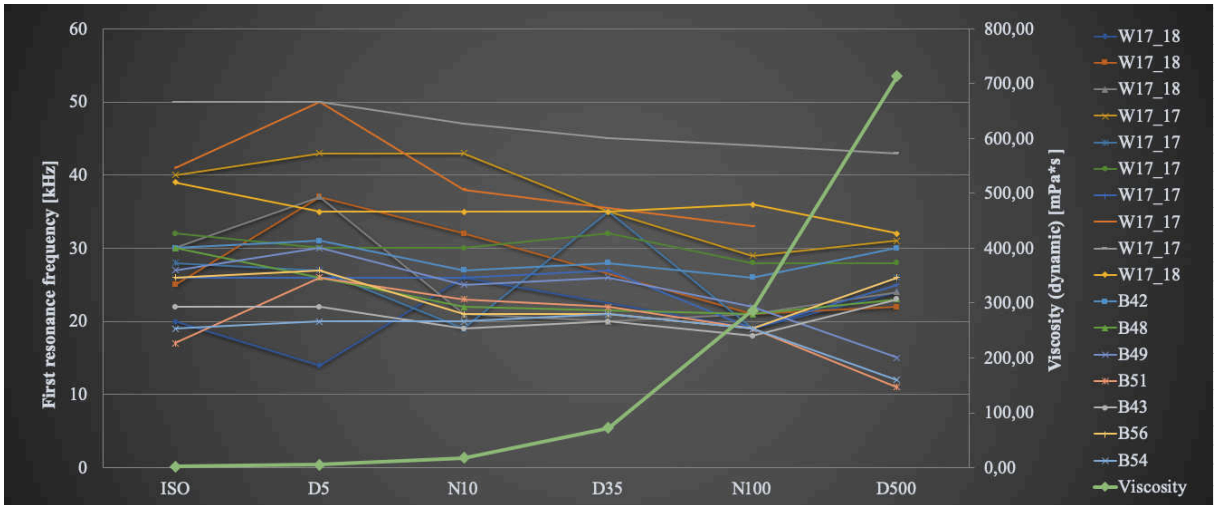

Figure 5.13: Altering f_{res1} depending on different fluids compared with the viscosity values.

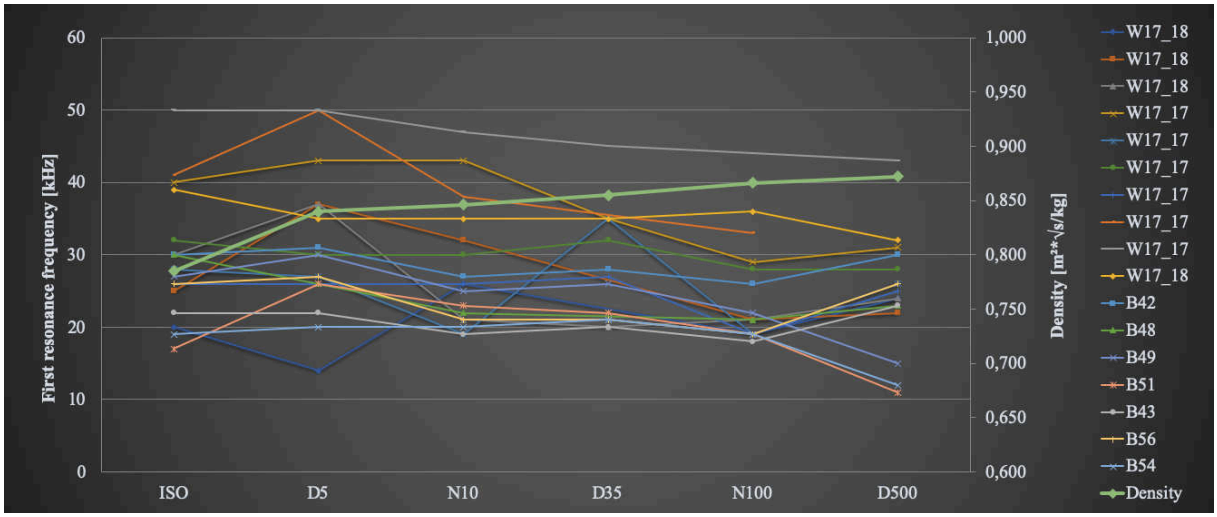

Figure 5.14: The first resonance frequency fitting the pattern of the fluids' densities (Green line).

Once the first resonance frequency is known, the same switching procedure as in air can be conducted. The extended process for switching in fluids is listed below:

- Finding of f_{res1} in air
- Adding of 200 – 250 µl fluid and finding the new f_{res1} depending on the fluid's density
- Starting the process of 5.2.3
- Cleaning the device with acetone, isopropanol and air drying.

Before adding another fluid onto a membrane, which was already tested before with a different fluid, the initial f_{res1} in air must be determined again to guarantee the absence of residuals. The switching frequencies f_{switch} were recorded and set in relation with the according f_{res1} of one membrane (Figure 5.15). There is no impact of the different fluids recognizable, since all frequencies were in the same bandwidth or rather had randomly distributed distances between those two frequencies. Two membranes were switched above f_{res1}, which could have been induced by the frequency drift caused by too much time passed between finding f_{res1} and f_{switch}. f_{res1} is stable for about 1 – 2 min[1], but will start after that time gap to drift towards its initial f_{res1} in air. The experiment showed that f_{switch} rises with f_{res1} once it started to drift, which is why in case of a time gap exceeding the stable frequency phase, f_{switch} can be recorded with a higher value than f_{res1}.

[1] depends on the fluid, device size and fluid amount; the time values for isopropanol are much smaller.

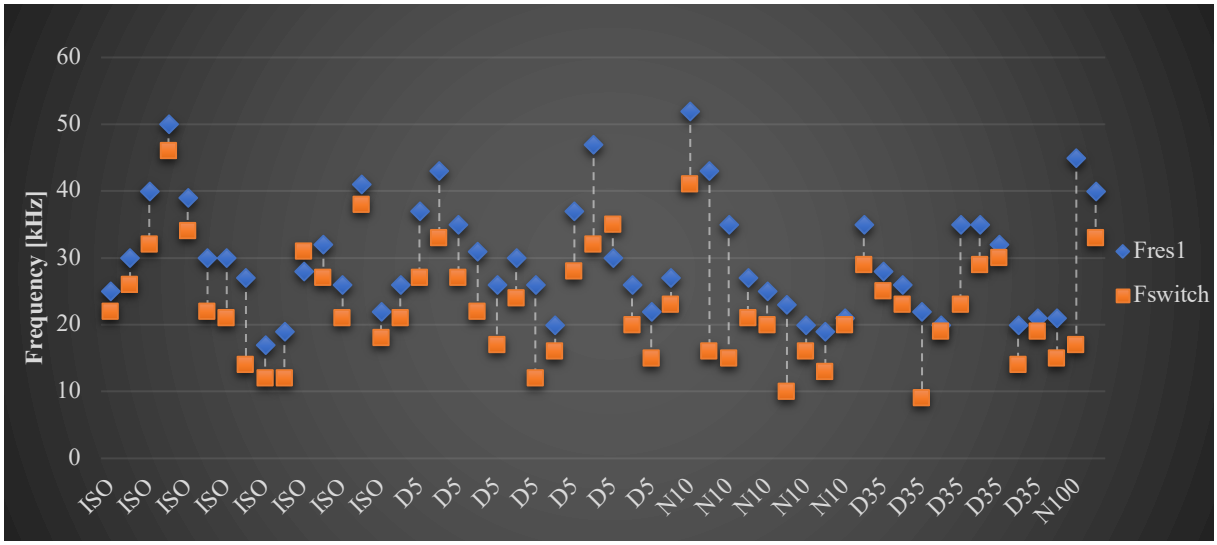

Figure 5.15: The image shows f_{res1} and the corresponding switching frequency f_{switch} of a membrane depending on the fluid. Only membranes are pictured, which reached sufficient switching deflections.

In total 30 membranes were chosen by pre-measurements for further experiments in order to get switched in air and fluids. Figure 5.16 shows the course of membranes, which were able to reach sufficient deflections to switch into the other ground state. The green part of each bar represents the membranes, which showed a bistable switching behaviour, while the yellow part stands for membranes, which reached the second ground state without maintaining it. By increasing the viscosity of the fluid, the proportion of membranes, which were not able to be switched increased and is represented by the red part of each bar. It is worth mentioning that only membranes, which were able to accomplish bistable switching in one specific fluid or in air, also had the potential to perform bistable switching, if the viscosity was increased. This also applies to membranes, which only showed monostable switching behaviour. These membranes were never able to achieve bistable switching again by increasing the fluid's viscosity.

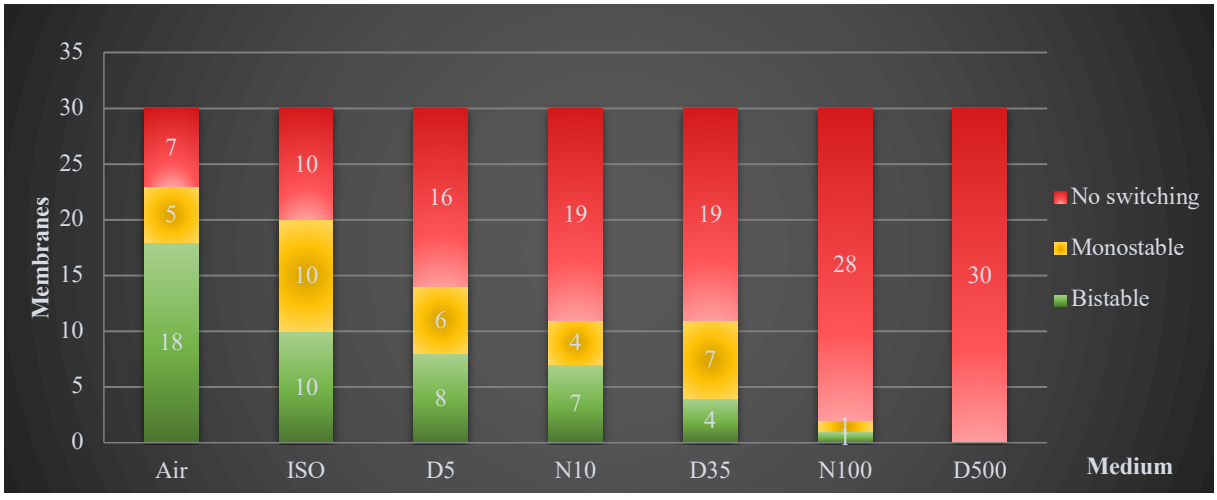

Figure 5.16: 30 Membranes were selected to get switched first in air and fluids subsequently. The higher the viscosity of the fluid was, the less membranes were able to switch.

The tendency, if a membrane will switch in a specific medium could not be predicted with 100 %, but guessed in a more or less precise way. The switching parameters of the average voltage and burst count (Table 5.4) were increased for each medium until a maximum deflection was reached and a switching was approached. These parameters showed, if the membrane had difficulties to achieve sufficient deflections for switching and gave an indication, if the same membrane will also be able to perform a switching in higher viscosities or not. The here presented membranes usually started to switch at 30 V and three bursts. Difficulties of a membrane were first noticeable, if the necessary voltage was increased towards the 40 V mark. Also, the average burst count was higher to even attain monostable switching performances. The comparable low voltage of 30 V in N10 and D35 of monostable switching resulted out of the experience gained by the measurements before. The initial presumption was, that even though a diaphragm reached the point of monostable switching, it could be possible to expand this behaviour to bistable switching by further increasing of the voltage. This assumption could be neglected by increasing the voltage until the membranes burst without changing their behaviour. This led to the conclusion that once a membrane reaches sufficient deflections and shows monostable switching, this behaviour cannot be changed by increasing of the switching voltage.

Table 5.4: Average switching voltage and burst counts depending on different mediums.

Medium	Bursts for *bistable* switching	Bursts for *monostable* switching	*Bistable* switching voltage [V]	*Monostable* switching voltage [V]
Air	3.3	4.6	32.8	38.5
ISO	3.9	4.6	32.5	40.15
D5	3.2	4.2	31.5	35.8
N10	3.7	3.5	32.1	30
D35	4	3.4	33.5	30
N100	4	4	40	45

Also, the pattern of the displacement curve gave indications for further predictions of the behaviour in fluids with increased viscosity. In Figure 5.17 a) and c) show the switching process from the upper to the lower ground state of the same membrane in isopropanol and D5, respectively. The graphics c) and d) picture the switching curve from the lower to the upper ground state. If both switching processes are compared, an additional peak in D5 during switching can be observed, which indicates an increased difficulty of the membrane to achieve switching. This is a typical sequence of patterns, which would lead to the assumption that this specific membrane will not achieve bistable switching again, after further increasing of the viscosity.
Also, an increased damping of the deflection was observed, caused by higher viscosities, which, inter alia, can be seen in Figure 5.17.

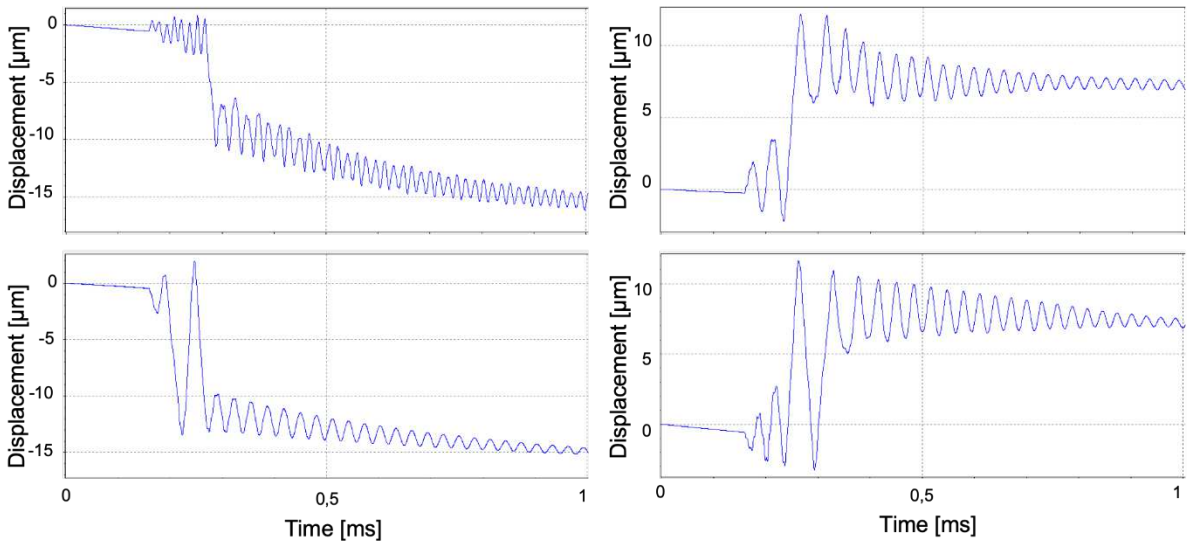

Figure 5.17: Different switching patterns of the same membrane in isopropanol (a + b) and D5 (c + d).

If the viscosity was further increased, membranes changed their behaviour from bistable to monostable, whereby different hold times were observed (Figure 5.18). The shorter the hold time got, the harder it was for a diaphragm to maintain the second ground state, while on the other hand, the longer the hold time was, the more likely it was to achieve bistable switching by changing to more suitable parameters.

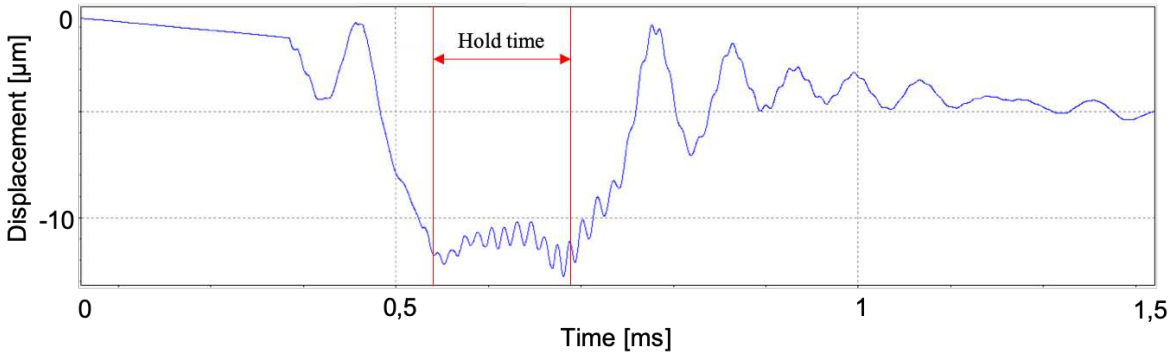

Figure 5.18: Monostable switching in isopropanol with an extraordinary long hold time of 150 µs.

Until this point only a rough prediction could be given by many pre-measurements, if a membrane will switch in a specific fluid or not. To find a parameter, which can be set in correlation with the different viscosities and furthermore the switching behaviour of a membrane, another measurement was conducted to characterize the property of the velocity of a diaphragm at their resonance frequencies. The speed and the associated acceleration might be crucial for a switching prediction in fluids, although it is not in air, where just the frequency level of f_{res1} is significant. The difference is that an added fluid represents an additional mass, which needs to be moved, whereby high velocities can be supportive. The experiment was carried out the same way as the resonance frequencies were determined, while this time not frequency levels, but the velocity at those frequencies was recorded (Figure 5.19).

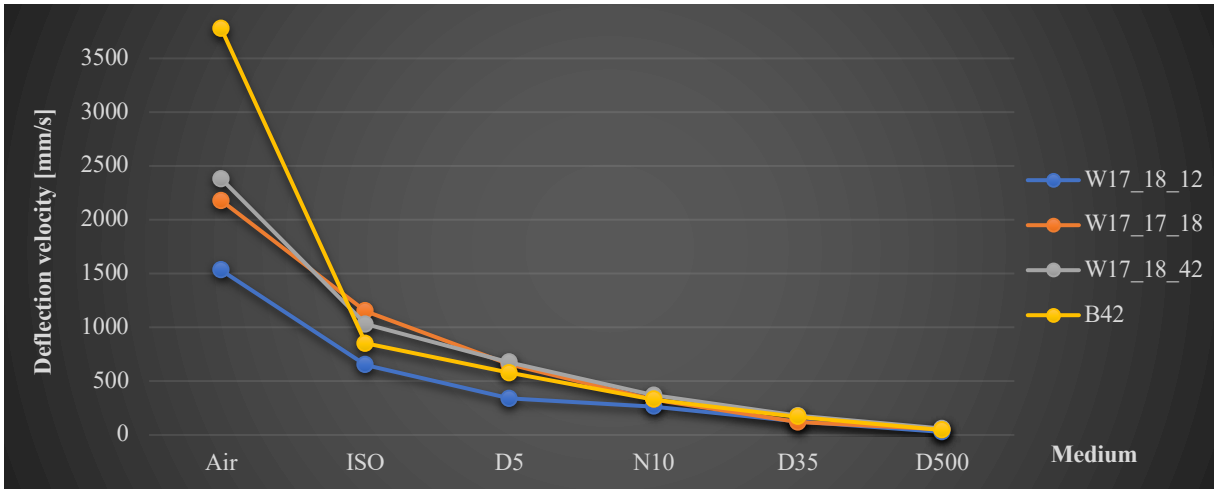

Figure 5.19: Deflection velocities at f_{res1} of four representative membranes depending on different fluids.

It can be seen that in contrast to air, the decrease of the velocities aligns very well with an increase of the viscosity, although no direct correlation with the specific viscosity values could be found. Table 5.5 shows the measured velocities in different fluids, including the property of the switching behaviour of the membrane in the corresponding fluid. While green marked velocities indicate a bistable switching, the membranes with too low values just achieved monostable switching (Table 5.5, orange fields), up until no switching could be measured with further decreasing velocities (Table 5.5, red fields). This gave the idea of a threshold of velocities depending on the fluid's properties.

Table 5.5: Register of velocity values pictured in Figure 5.19 at f_{res1} depending on different fluids. Green markings represent bistable switching, yellow stands for monostable switching and red marked values indicate no switching behaviour.

Sample Name	Deflection velocities at f_{res1} depending on the fluid [mm/s]					
	Air	ISO	D5	N10	D35	D500
W17_18_12	1531	650	340	265	125	28
W17_17_18	2179	1150	654	330	120	52
W17_18_42	2381	1030	675	370	179	60
B42	3778	850	576	330	170	46

5.2.4.1 Cleaning of membrane surfaces in fluids

The last experimental part was carried out in order to make a complete statement of removing particles on a diaphragm's surface not just in air, but also in fluids. Therefore, a membrane was covered in isopropanol[1], after the deposition of an unspecific amount of 10 µm particles as in Subsection 5.2.3.2. As expected, the particles floated within the fluid (Figure 5.20, a), until they settled on the membrane during the fluid dried out (Figure 5.20, b).

[1] Isopropanol was chosen because of its property of fast drying in ambient air, compared with *e.g.* D5, which would have required additional heating.

Dried out conditions
Switching the membranes to sling the particles away was not as effective as in completely dry conditions, because most particles stuck to the surface, caused by drying effects. After ten cycles of switching every movable particle was removed from the surface (Figure 5.20, c) and no further improvements could be observed by additional 15 switching procedures (Figure 5.20, d).

Wet conditions
If the fluid has not dried out and the particles were floating within the fluid, a completely different behaviour could be observed by inducing switching procedures. At first no changes were recognizable, except more disturbances in the movement of the particles. By increasing the time gaps between each switching, the particles had enough time to settle down, before another switching impulse was fired through the fluid. This caused a circular arrangement of the particles around the diaphragm after ten (Figure 5.20, e) switching cycles, whereby only few stayed on the membrane. After 25 cycles almost no particles remained on the diaphragm and a sharper boarder of the circular arrangement could be monitored (Figure 5.20, f).

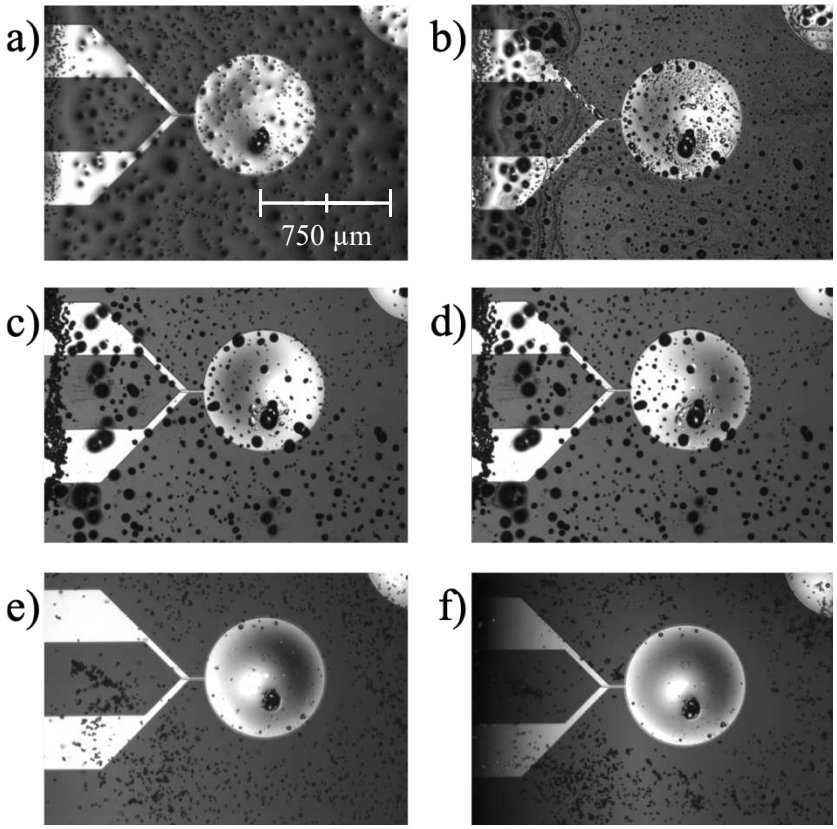

Figure 5.20: a) Surface of a 700 µm membrane covered with isopropanol, polluted with 10 µm particles and already started to dry out. b) Partially dried out membrane with already settled and randomly distributed particles. c) Completely dried out membrane pictured after ten and d) 25 switching cycles, whereby both stable states can be seen. e) The surface was wetted again to induce a wet cleaning procedure and pictured after ten and f) 25 switching cycles.

6 Conclusions and Outlook

This chapter is supposed to provide a basis for the interpretation of the outcome of the cell experiments, as well as the measured results of membranes, fabricated as in 2.5 and loaded with electrical signals, in order to predict their characteristic vibrational and switching behaviour. Also, a precise outlook for further investigations, arisen due to the experiments within this thesis, will be provided.

6.1 Conclusions

This thesis united two main tasks in order to find and declare a connection of biocompatible SiC membranes fabricated with MEMS technologies and the biological aspect of cell proliferation of CaCo-2 cells on different SiC substrates. 13 different SiC compositions were measured with the wafer bow method to determine the stress level of each compositions, which started from –141 MPa and reached with increasing carbon content down to –1002 MPa of tensile stress. Six sets of those substrates were treated differently with O_2-plasma and coatings and prepared for planting 50.000 CaCo-2 cells on each of these samples. The cell count confirmed an expected growing behaviour [2], depending on the a-SiC:H layer, the pre-treatment and coating. The results revealed two main plateau peaks of substrates, where cells grew the best on. This information could be used to select the SiC composition in order to set the stress level of a thin layer to a preferred value depending on the application and additionally choose the cell proliferation by the right treatment. The experiment also contained the process of trypsinisation, whereby enzymes break down the integrins of cells to their surroundings. By photographing the residuals on each sample after 5 min of trypsinisation the pictures showed very diverged amounts of remaining cell, depending on the substrate. A clear tendency of an increased adhesiveness of cells on collagen coated samples could be observed, whereas on uncoated samples almost all cells were removed of the sample's surface. This aspect also can be used for specific medical SiC applications, whereby either strong adherent or easily removable cells are required.
As a part of the cell experiment preparation, the four most promising SiC compositions, depending on a preferred stress level as close to zero as possible, were chosen to figure out possible changes of properties of SiC membranes compared to uncoated ones, described in Chapter 3. All further membranes were coated with a 70 nm a-SiC:H layer produced with a r_{CH4} ratio of 0.05, because the average change of deflections accounted for 97.5 % of the original displacements under the same load. In total 60 membranes were coated and characterized by their vibrational behaviour and resonance frequencies in order to choose the most promising diaphragms to get bonded in an IC-package for further measurements. Only membranes within a specific frequency band depending on the diameter of the membrane were selected for switching purposes.
The aim of the second main task was to switch membranes with the integrated piezoelectric thin film actuator from one stable state into the other in air and fluids of different viscosities, describing this process and characterize the behaviour during a switching performance. The diaphragms were loaded with 2 – 6 rectangular bursts of 30 – 50 V with an adapted frequency, depending on the first resonance frequency of each membrane until one of three possible outcomes of switching behaviours could be determined. 23 of 30 membranes in air switched from one stable state to the other, which supported the designing of a procedure to guarantee a switching performance, if the membrane had the ability in the first place. The average switching

frequency from the upper to the lower ground state was 7 kHz below f_{res1}, while f_{switch} for reverse switching was 10 kHz under f_{res1}.
In a last step six different fluids were subsequently applied onto the membranes' surfaces, in order to characterize the switching behaviour in fluids and measure the changing properties, caused by altered viscosities and densities. At first f_{res1} was determined to assume f_{switch}, which was 8 kHz on average below f_{res1}, whereby no differences showed up depending on the current ground state of the membrane. This was probably caused by a compensation of the asymmetric architecture of the membrane by the fluid working just on the upper side of the diaphragm. The more the viscosity was increased, the less membranes were able to execute a switching, although the resonance frequency f_{res1} maintained almost the same level. This is because of the dependency of f_{res1} not on the viscosity, but on the density, which correlates well with the curve progression of the different resonance frequencies in fluids. Also worth mentioning is the fact that monostable switching behaviour just showed up from the upper to the lower ground state. If a membrane was in the lower ground state, it was always possible to switch back into the upper state. This is because even a compensation of the asymmetry of the membranes took place, the diaphragms still maintained their preferred ground state. Once f_{res1} was known, the electrical signal parameters were altered until one of the three switching outcomes (5.2.3.1) was achieved. The last measurement was conducted to find a correlation between the viscosity and the velocity at resonance frequencies and to determine a common threshold, if a membrane will be able to achieve switching behaviour, whereby only an almost linear decreasing of the velocity curve was observed, compared to the viscosity, which rises exponentially.

6.2 Outlook

The first thing worth mentioning here is the further investigation and repetition of the cell experiment, whereby this subsection shall also give a recommendation of how this would be performed the best. The scope of the whole experiment was too extensive for a biologically correct process, which is why it is advisable to split it in several smaller parts. Every part needs to be done at least in biological triplicates, whereby cell counting with the PrestoBlue method should be additionally carried out in technical triplicates.
This thesis showed an outstanding behaviour of CaCo-2 cells growing on collagen coated samples and the extraordinary adhesiveness, even after an unusual long time trypsinisation. This circumstance could be explained through more precise experiments by investigating the integrins of cells to the substrate, cell-cell connections and the enzymic reaction with trypsin.

The results approached from the membrane measurements led to new views and a lot of potential of further investigations. One aspect could be the automation of the switching process by sensing and controlling a feedback loop based on the changing and development of the switching parameters described in 5.2.3. This would also lead to more precise results and a better characterisation of the membranes.
The origin of the exceptional membranes mentioned in 5.2.2 and pictured in Figure 5.6 is still uncertain. The mere fact that these membranes were fabricated exactly with the same procedure, but had completely different vibrating and switching properties, might give interesting insights in the fabrication process and their behaviour by further investigation of this topic.
The investigation of the switching behaviour in fluids in the scope of this work has raised several questions, which also might be able to explain by further measurements. One reasonable presumption was that once a membrane was manufactured, it would always just achieve either bistable or monostable switching, but measurements showed that the switching behaviour

changed from bistable to monostable by increasing the viscosity of the fluid. The answer to this behaviour could be found by slowly increasing the temperature of the fluid, which changes continuously the viscosity of the fluid as well as the displacement velocities at f_{res1}, whereby a possible threshold for this changing behaviour could be investigated.

To conclude, the cell experiment delivered results which stood in good agreement with the literature and can be used as a base for further measurements, while discovered tendencies of the relation from cell adhesiveness and collagen coatings were revealed. Furthermore, it was the first time that within the scope of this thesis bistable membranes were recorded switching in fluids from one ground state to the other by the electrical stimulation of integrated piezoelectric thin film actuators.

List of Figures

List of references

[1] Jove Graham Ph.D., Jonathan Peck M.E., FDA Regulation of Polyaryletheretherketone Implants, PEEK Biomaterials Handbook, 2012

[2] C. Coletti, M.J. Jaroszeski, A. Pallaoro, A.M. Hoff, S. Iannotta and S.E. Saddow, Biocompatibility and wettability of crystalline SiC and Si surfaces, IEEE Engineering in Medicine and Biology Society. Conference, February 2007

[3] X. Li, X. Wang et al., Micro/Nanoscale Mechanical and Tribological Characterization of SiC for Orthopedic Applications, J Biomed Mater Res B Appl Biomater., Feb 15;72, (2), 353-61 (2005).

[4] A.J. Rosenbloom, D.M. Sipe, Y . Shishkin, Y . Ke, R.P . Devaty and W.J. Choyke, Nanoporus SiC: „A Candidate Semi-Permeable Material for Biomedical Applications", Biomedical Microdevices, 6, (4), 261- 267, 2004.

[5] R.I. Freshney, Culture of animal cells. John Wiley & Sons, Inc., Hoboken, NJ, 2005, pp. 105-113.

[6] G. Cicero, A. Catellani, G. Galli, Interaction of water molecules with SiC(001) surfaces, Journal of Physical Chemistry B, 2004.

[7] Tobias Frischmuth, Hydrogenated Amorphous silicon carbide Thin Films for Microelectromechanical Systems, Technical University of Vienna, 2010

[8] A. Angelescu, I. Kleps, M. Mihaela, M. Simion, T. Neghina, S. Petrescu, N. Moldovan, C. Paduraru, A. Raducanu, Porus silicon matrix for applications in biology, Rev. Adv. Mater. Sci., 5, 440-449, 2003

[9] US Population Mortality Observations, Updated with 2016 Experience, Society of Actuaries, 2018

[10] Donald E. Cutlip, David L. Fischman; Mortality After Percutaneous Coronary Intervention, Circ Cardiovasc Interv.;11:e007008. DOI: 10.1161/CIRCINTERVENTIONS.118.007008, 2018

[11] Manuel Dorfmeister, Michael Schneider, Ulrich Schmid; A Bistalbe Ultrasonic MEMS Device with an Integrated Piezoelectric Scandium-AlN Thin Film Actuator for Switching; 20th International Conference on Solid-State Sensors, Actuators and Microsystems & Eurosensors XXXIII (TRANSDUCERS & EUROSENSORS XXXIII); 2019

[12] A.C. Gelijns; Technological Innovation: Comparing Development of Drugs, Devices, and Procedures in Medicine; Institute of Medicine (US) Committee on Technological Innovation in Medicine; Washington (DC): National Academies Press (US); 1989.

[13] Sagvolden, G.; Giaever, I.; Pettersen, E.O.; Feder, J. Cell adhesion force microscopy. Proc. Natl. Acad. Sci. USA 1999, 96, 471–476

[14] Huang, W.; Anvari, B.; Torres, J.H.; LeBaron, R.G.; Athanasiou, K.A. Temporal effects of cell adhesion on mechanical characteristics of the single chondrocyte. J. Orthop. Res. 2003, 21, 88–95.

[15] A. A. Khalili, M. R. Ahmad; A Review of Cell Adhesion Studies for Biomedical and Biological Applications; Int. J. Mol. Sci. 2015, 16, 18149-18184; doi:10.3390/ijms160818149

[16] Saif, M.A.T.; Sager, C.R.; Coyer, S. Functionalized biomicroelectromechanical systems sensors for force response study at local adhesion sites of single living cells on substrates. Ann. Biomed. Eng. 2003, 31, 950–961.

[17] Dembo, M.; Torney, D.; Saxman, K.; Hammer, D. The kinetics of membrane-to-surface adhesion and detachment. Proc. R. Soc. 1988, 234, 55–83.

[18] Shen, Y.; Nakajima, M.; Kojima, S.; Homma, M.; Kojima, M.; Fukuda, T. Single cell adhesion force measurement for cell viability identification using an AFM cantilever-based micro putter. Meas. Sci. Technol. 2011, 22, 115802.

[19] Hong, S.; Ergezen, E.; Lec, R.; Barbee, K.A. Real-time analysis of cell-surface adhesive interactions using thickness shear mode resonator. Biomaterials 2006, 27, 5813–5820.

[20] Christ, K.V; Turner, K.T. Methods to measure the strength of cell adhesion to substrates. J. Adhes. Sci. Technol. 2010, 24, 37–41.

[21] Garcia, A.J.; Gallant, N.D. Stick and grip: Measurement systems and quantitative analyses of integrin-mediated cell adhesion strength. Cell Biochem. Biophys. 2003, 39, 61–73.

[22] Werner Karl Schomburg, *Introduction to Microsystem Designs*, Springer Verlag, 2011

[23] Milton Ohring, Materials Science Of Thin Film Deposition and Structure, Academic Press, 2002

[24] Stephen Timoshenko, Theory of Plates and Shells, 1958

[25] E. Chason, B. W. Sheldon, and L. B. Freund, ``Origin of Compressive Residual Stress in Polycrystalline Thin Films," *Physical Review Letters*, vol. 88, no. 15, p. 156103, 2002.

[26] R. W. Hoffman, ``Stresses in Thin Films: The Relevance of Grain Boundaries and Impurities," Thin Solid Films, vol. 34, pp. 185-190, 1976.

[27] K. Cholevas, N. Liosatos, A. E. Romanov, M. Zaiser, and E. C. Aifantis, ``Misfit Dislocation Patterning in Thin Films," Physica Status Solidi (B), vol. 209, no. 10, pp. 295-304, 1998.

[28] R. Koch, The intrinsic stress of polycrystalline and epitaxial thin metal films, Journal of Physics, Condensed Matter, 6(45):9519, 1994

[29] Georg Hass, Maurich H. Francombe, Richard W. Hoffman, Physics of thin films: Advances in Research and Development, Elsevier, 2013

[30] Christian Kirsch, Entwicklung, Herstellung Charakterisierung eines bistabilen mikromechanischen Schaltaktors in Siliziumtechnik, 2014

[31] A. Braun, K.M. Briggs, P. Böni, Analytical solution to Matthew´s and Blakeslee´s critical dislocation formation thickness of epitaxially grown thin films, Journal of Crystal Growth, 241(1-2):231-234, 2002

[32] Christian Köpf, Modellierung des Elektronentransports in Verbindungshalbleiterlegierungen, TU Wien, 1997

[33] Bernhard Gottwlad, Grundlegende Ansätze zur Modellierung und Simulation von Beschichtungsprozessen am Beispiel von PVD-Kupfer, 2006

[34] Isaac James Phelps, Mechanical characterization of MEMS bi-stable buckling diaphragm, University of Louisville, 2013

[35] S. Krylov, B.R. Ilic, D. Schreiber, S. Seretensky, H. Craighead, The pull-in behavior of electrostatically actuated bistable microstructures, J. Micromech. Microeng. 18 (2008) 055026

[36] W. K. Schomburg, C. Goll, Design optimation of bistable microdiaphragm valves, Sensors and Actuators A 64, 259-264, 1997

[37] Gerhard M. Fasching, Werkstoffe für die Elektrotechink, Mikrophysik, Struktur, Eigenschaften, Springer Verlag, 2005

[38] Michael Schneider, Einfluss der Schichtdicke und Substratvorbehandlung auf die elektromechanischen Eigenschaften von gesputterten Aluminiumnitriddünnfilmen, Verlag Dr. Hut, 2014

[39] Richard M. Martin: Piezoelectricity, Physical Review B. Jg 5, Nr. 4, 1607–1613, 1972

[40] M. Dorfmeister, M. Schneider, U. Schmid, Static and dynamic performance of bistable MEMS membranes, Sensors and Actuators A 282, 259–268, 2018

[41] P. M. Mayrhofer et al., "Circular test structure for the determination of piezoelectric constants of ScxAl1−xN thin films applying Laser Doppler Vibrometry and FEM simulations", Sensors and Actuators A: Physical, vol. 222, no. Supplement C, pp. 301-308, Feb. 2015.

[42] M. Akiyama et al., "Enhancement of Piezoelectric Response in Scandium Aluminum Nitride Alloy Thin Films Prepared by Dual Reactive Cosputtering", Advanced Materials, vol. 21, no. 5, pp. 593-596, 2009

[43] Marc J. Madou, Fundamentals of microfabrication: the science of miniaturization, CRC Press, ISBN 9780849308260, 2002

[44] Georg Hass, Maurich H. Francombe, Richard W. Hoffman, Physics of thin films: Advances in Research and Development, Elsevier, 2013

[45] Franz Keplinger, Skriptum Sensorik und Sensorsysteme, TU Wien 2012

[46] Yoshinori Matsumoto, Makoto Ishida, The property of plasma-polymerized fluorocarbon film in relation to ch 4/c 4 f 8 ration and subtrat temperature, Sensors and Actuators A: Physical, 83(1):179 185, 2000

[47] R. A. Marra and J. S. Haggerty. Synthesis and Characteristics of Ceramic Powders Made from Laser-Heated Gases, Chapter 2, pages 3–19. John Wiley & Sons, Inc., Hoboken, NJ, USA., 2008.

[48] Graziella Malandrino, Sergei E Alexandrov, Michael L Hitchman, Mohammad Azad Malik, Paul O'Brien, Susan P. Krumdieck, Anthony C Jones, and Michael L Hitchman. Chemical Vapour Deposition. Precursors, Processes and Applications. Edited by Anthony C. Jones and Michael L. Hitchman. WILEY-VCH Verlag GmbH & Co. KGaA, 2009.

[49] Daniel Dobkin and M.K. Zuraw. Principles of Chemical Vapor Deposition. Springer Netherlands, 2003.

[50] Titus Rinke, Christian Koch, Fotolithoithografie: Grundlagen zur Microstrukturierung, MicroChemicals GmbH, 2017

[51] A. Somashekhar and S. O'Brien. Etching SiO2 films in aqueous 0.49% HF. Journal of The Electrochemical Society, 143(9):2885–2891, 1996.

[52] Filmetrics, Thin film measurement, https://www.filmetrics.com/technology, 2019

[53] Grundlagen der Virbometrie:

http://www.polytec.com/de/loesungen/schwingungen-messen/grundlagen-der-vibrometrie/, 2016

[54] Grundlagen der Weißlichtinterferometrie:

http://www.polytec.com/de/oberflaechenmesstechnik/technologie/weisslichtinterferometrie/, 2020

[55] Philipp Moll; Entwicklung, Herstellung und Characterisierung eines piezoelektrischen MEMS-Membran Arrays; ISAS TU Wien, 2017

[56] Georg Marschick, Fabrication and Characterisation of bistable piezoelectric Actuators, 2016

[57] Wolfgang Scheel, Baugruppentechnologie in der Elektronik: Montage, Verlag Technik, 1997

[58] Pinto M; Enterocyte-like differentiation and polarization of the human colon carcinoma cell line Caco-2 in culture. *Biol Cell*. 47: 323–30, 1983

[59] Hidalgo IJ; Characterization of the human colon carcinoma cell line (Caco-2) as a model system for intestinal epithelial permeability. *Gastroenterology*. 96 (3): 736–49, 1989

[60] Huang, H. L.; Hsing, H. W.; Lai, T. C.; Chen, Y. W.; Lee, T. R.; Chan, H. T.; Lyu, P. C.; Wu, C. L.; Lu, Y. C.; Lin, S. T.; Lin, C. W.; Lai, C. H.; Chang, H. T.; Chou, H. C.; Chan, H. L. "Trypsin-induced proteome alteration during cell subculture in mammalian cells". Journal of Biomedical Science. **17** (1): 36. 2010

[61] Stefan Plagg & Martin Pobitzer, Eigenfrequenzen – Eigenmoden, Resonanzfrequenzen – Raummoden, 2011

[62] M. Dorfmeister, B. Kössl, M. Schneider, G. Pfusterschmied, U. Schmid; Switching performance of bistable membranes activated with integrated piezoelectric thin film transducers, Journal of Micromechanics and Microengineering; 29 (10); 2019

[63] T. Goettsche et al., "Novel approaches to microfluidic components in high-end medical applications," TRANSDUCERS '03. 12th International Conference on Solid-State Sensors, Actuators and Microsystems. Digest of Technical Papers (Cat. No.03TH8664), Boston, MA, USA, 2003, pp. 623-626 vol.1.

[64] https://www.merriam-webster.com/dictionary/toxicity

[65] https://www.omicsonline.com/bioinert-materials/leading-journals.php

[66] https://www.azom.com/article.aspx?ArticleID=2630

Declaration of Authorship

I hereby declare that the thesis submitted is my own unaided work. All direct or indirect sources used are acknowledged as references. This paper was not previously presented to another examination board and has not been published.

Eidesstattliche Erklärung

Hiermit erkläre ich, dass die vorliegende Arbeit gemäß dem Code of Conduct, inbesondere ohne unzulässige Hilfe Dritter und ohne Benutzung anderer als angegebenen Hilfsmittel angefertigt wurde. Die aus anderen Quellen direkt oder indirekt übernommenen Daten und Konzepte sind unter Angabe der Quelle gekennzeichnet.
Die Arbeit wurde bisher weder im In- noch im Ausland in gleicher oder ähnlicher Form in anderen Prüfungsverfahren vorgelegt.

Vienna, 15 January 2020